Materials Science and Engineering B 263 (2021) 114849

Contents lists available at ScienceDirect

Materials Science & Engineering B

journal homepage: www.elsevier.com/locate/mseb

Sensor applications based on AlGaN/GaN heterostructures

Kavita T. Upadhyay [a,b], Manju K. Chattopadhyay [c,*]

[a] Department of Electronics and Communication Engineering, IPS Academy, Institute of Engineering and Science, Indore 452012, India
[b] Department of Electronics and Telecommunication Engineering, Institute of Engineering and Technology, Devi Ahilya University, Indore 452017, India
[c] School of Electronics, Devi Ahilya University, Khandwa Road, Indore 452017, India

ARTICLE INFO

Keywords:
GaN HEMT
2DEG
Radiation sensors
Mechanical sensors
Chemical sensor
Bio-sensor

ABSTRACT

Gallium Nitride (GaN) belongs to III-N family of compound semiconductors, which albeit new, is well-established material system in the fields of high power, high temperature electronics and optoelectronics. Also, its properties such as high mobility, surface sensitivity, non-toxicity, thermal endurance, low power consumption make it an ideal material for realizing sensors. This paper provides a review on the significant research work done in the field of GaN based sensor technologies. We classified the work done so far, according to the applications and the different types of parameters being measured. The challenges faced by the current sensing systems and future opportunities are also briefly explained for a variety of applications *viz.* radiation sensors, mechanical sensors, gas sensors, biosensors, chemical sensors and high temperature Hall-effect sensors *etc*. Additionally, the sensing mechanism of various sensors is explained. This paper can supply initial reading material for beginners and research students working on GaN heterostructure based sensor applications.

1. Introduction

In year 2020, High Electron Mobility Transistor (HEMT) celebrates its four decades of existence. During these years, a wide portion of nano-electronics based sensor industry has been massively occupied by III-V compound semiconductor family. Large surface sensitivity, high electron transport properties, and ready accessibility of heterostructures make III-V compound semiconductors perfect material for producing sensors. III-N based technologies have been extensively investigated for chemical and biological sensor for gases, pH, ions, liquids and biomolecules. In particular, Gallium Nitride (GaN) and Aluminum Gallium Nitride (AlGaN), including their combinations in heterostructures, are attractive material for sensors due to additional features, *viz.* non-toxicity, chemical stability, biocompatibility, and high temperature endurance [1-3].

2. Properties

Conventional Silicon based sensors do not perform well in harsh environment parameter such as high temperature, high pressure or corrosive ambient. In such environments, GaN based HEMTs are better option for sensors to be deployed *in-situ*. Comparison of material properties of GaN with other semiconductor are summarized in Table 1.

1) Exceptional chemical and physical stability allows GaN to immobilize biomolecules and find utility in liquid-phase sensors [4-7].
2) Very high two-dimensional electron gas (2DEG), due to high polarizations *viz.* spontaneous (P_{sp}) and piezoelectric (P_{pz}) in the AlGaN/GaN heterostructure, results in high sensitivity [7]. The electron gas is quite responsive to the surface states as it does not intermingle with the analytes. Work on functionalizing the gate electrode of a GaN HEMT for various analytes, *viz.* polyimides, heavy metals, enzymes; sensitivity to H_2, NO_2, NH_3, methane (CH_4), pH, urea, glucose, chloride ion, heavy metal, DNA etc., has been reported in the literature. [8-18]
3) Optical transparency of GaN allows simultaneous microscopic and electronic detection of biochemical and biophysical processes [19].
4) Intrinsic carrier concentration and large band gap, enables GaN-based sensors to operate at extreme temperature above 600 °C. On the other hand, Si-based device operations are limited to temperatures less than 350 °C [20].
5) Environment-friendly and bio-friendly with non-toxic surface content, for interaction between the living cell and the surface. GaN materials perform well in this condition [21].
6) It's small sensing response time of range of milliseconds. A GaN-based sensor does not need surface passivation and hence, has instantaneous and effective response to distinguish polar molecules

* Corresponding author.
E-mail address: mkorwal@yahoo.com (M.K. Chattopadhyay).

https://doi.org/10.1016/j.mseb.2020.114849
Received 3 January 2020; Received in revised form 1 August 2020; Accepted 27 September 2020

Table 1
Comparison of material properties at 300 K [1-3].

Property	Si	GaAs	4H-SiC	GaN	Ga_2O_3
Bandgap E_g (eV)	1.12	1.42	3.25	3.4	4.85
Breakdown Field ($MVcm^{-1}$)	0.3	0.4	2.5	4	8
Electron Mobility ($cm^2V^{-1}s^{-1}$)	1500	8500	1000	1300	300
Maximum Drift Velocity v_d (10^7cm. s^{-1})	1	2	2	3	2
Thermal Conductivity (W cm^{-1} K)	1.5	0.5	4.9	2.3	0.23
Relative Dielectric Constant	11.8	12.9	9.7	9	10

and ions, although the passivation does improve the HEMT performance [22,23].

3. Common devices for sensors

A number of devices appertaining to GaN material system, together with Schottky diodes, metal oxide semiconductor (MOS) diodes, HEMTs and nanowires have been fabricated for speedier and responsive sensor uses [24-26].

3.1. Schottky diodes

Si based Metal–insulator–semiconductor (MIS) and $p - n$ diodes usually block the free charge current which delays the response of piezoelectric (PE) charge. Contrasting this, in GaN Schottky diodes, free charge carriers move rapidly. Symbolic Schottky diodes on *n*-GaN are shown in Fig. 1 (a), with their huge reverse differential resistance, the time of persistence may be of the order of a few seconds.

Inside the GaN MIS diode, PE bound charge, formed at the oxide interface, causes a dc-strain, leading to steady-state shift in the electrostatic surface potential. In turn, this shift causes a change in the diode capacitance. In this manner, GaN MIS diodes can work as conventional capacitive strain sensors with higher resolution. The schematic of MIS diode is shown in Fig. 1 (b).

3.2. Heterojunction bipolar transistor

The Heterojunction Bipolar Transistors (HBT) can operate at elevated temperatures (>500 °C). Fig. 2 shows its fundamental construction consisting of a p-SiC base on an n-SiC collector. Then-GaN emitter is prepared as a heterojunction with the base.

3.3. Light emitting devices and LASER diodes

Nakamura *et al.* developed GaN LED using GaN PN junction with Zn

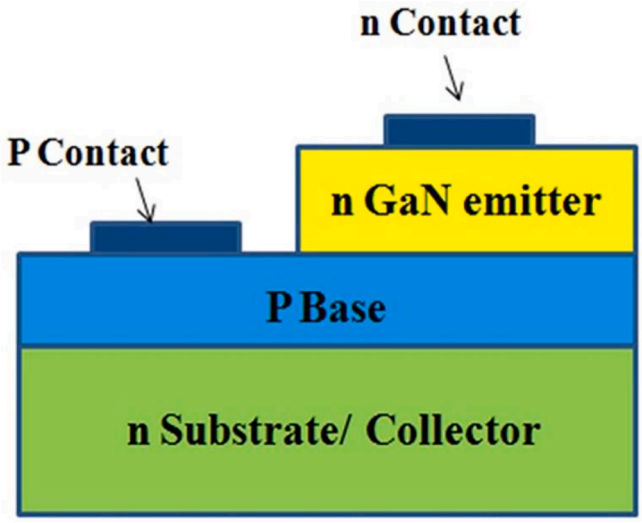

Fig. 2. Structure of GaN heterojunction bipolar transistor.

doped well. The rationale behind creating the well is to retain the carriers in a diminutive volume. Zn introduces a proficient blue or green radiant core. Eventually, the well was substituted by multiple quantum wells (QWs) (as shown in Fig. 3) to envisage laser diodes. These small wavelength lasers are used to accumulate optical data on CDs [19].

In December 1997, S. Porowski *et al.* developed a GaN sample by growing Ga solution at high temperature and pressure. Its response improved by three orders of level. The reason for this behaviour was described by J I Pankove in ref. [27]. Later, S. Nakamura developed a sample of GaN grown by Metal-Oxide Chemical Vapour Deposition (MOCVD) [28].

It is observed that if energy of photon or particles is larger than the GaN bandgap, it produces large number of electrons. GaN based radiation-hard detector maintain their low temperature which makes it useful for space applications [20].

At temperature upto 827 °C, efficient photoluminescence (PL) spectra are observed by C. Prall from GaN layers with high dynamic resolution and low noise. Lot many exhaustive spectral features in the photoluminescence were directly related to physical properties of epitaxial growth layer. This method is recommended as an *in situ* checking tool during epitaxial growth of nitride laser and LED structures [29].

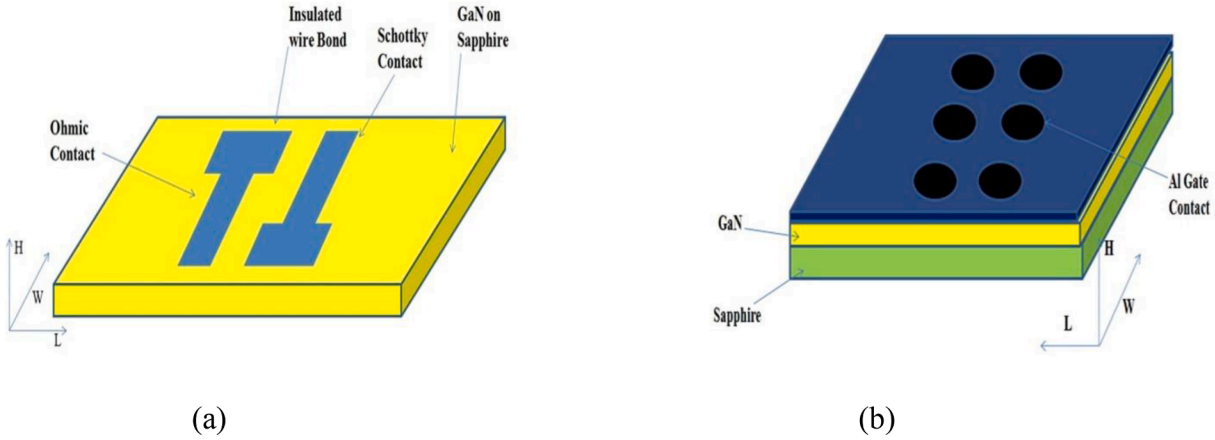

Fig. 1. (a) Schottky Diode, (b) MOS diode.

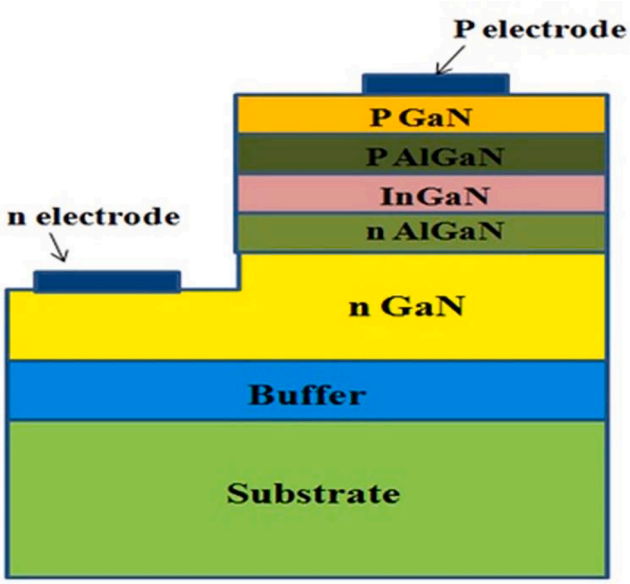

Fig. 3. Structure of III-Nitride light emitting diodes (LEDs).

3.4. High electron mobility transistors (HEMT)

HEMTs are also known as Modulation Doped Field Effect Transistors (MODFETs) and Two Dimensional Electron Gas FETs (TEGFET). Fig. 4 (a) depicts a conventional D-mode GaN HEMT device structure. The drain and the source metal connections enable the Ohmic contacts and the gate metal provides a Schottky contact. As voltage V_{ds} is applied, a lateral electric field is generated and the charge carriers, flow along the heterointerface of AlGaN/GaN layers as current. Unless gate voltage crosses the threshold voltage (V_T), device remains in off condition.

Though HEMT is most reliable transistor for high frequency and high-power applications, it lately has found immense potential for biological, chemical and gas-sensing applications. In real time, AlGaN/GaN HEMT-based biosensors have shown reliable detections of biological agents. Now days, semiconductor fabrication techniques have realized small sized sensors, with high sensitivity, and are even responsive to small amount of samples.

3.4.1. Working of HEMTs

Fig. 4 (b) shows energy band-diagram of a GaN MODFET. Electrons from the boundary region of the higher bandgap doped AlGaN layer move into the GaN layer and collect in the QW formed in the GaN at the junction. Greater size of channel length and width in addition to the small size of QW, cause the distribution of the electrons to be two-dimensional. The charge density formed is hence, termed 2DEG [26]. It is characterized as a sheet charge density. The 2DEG is accumulated in the u-GaN layer. As the carriers are now separated from donor ions, scattering effect is diminished and higher carrier mobility is achieved. 2-DEG has the advantage that there are no impurity atoms in the undoped GaN QW [18].

Sheet carrier density further improves due to large spontaneous and piezoelectric polarization effect of Wurtzite Crystal structure of GaN based semiconductor materials [7].

When a p-GaN layer is sandwiched between the metal gate and the doped AlGaN layer, it forms a p-GaN Enhancement-mode HEMT. Higher thickness and high p-type doped p-GaN layer leads to a positive V_T for the normally-OFF operation [30].

4. Sensor applications

AlGaN/GaN HEMTs show extraordinary sensitivity to change in surface charges generated by materials being sensed *viz.* gas, liquids, chemical, bio-sensing *etc.* Classification of sensors is shown in Fig. 5.

We have attempted to summarize most of the published material on AlGaN/GaN heterostructure based sensor applications in the Table 2.

4.1. Radiation sensors

Ternary and quaternary alloys of III-V nitride family with energy bandgap within 1.8 eV to 6.3 eV range are most suitable for UV detectors, Waveguides, Visible LEDs, Surface Acoustic Waves, Bragg reflectors and LASER diodes [6]. After commercialization of blue-green LEDs and injection laser diodes, attention to GaN based optical devices has exponentially increased [6].

4.1.1. UV and X-rays

Gallium nitride (GaN) has come up as the most favorable materials for visible–blind UV Photo Detectors due to large direct bandgap (3.4 eV) at ambient temperature in wurtzitic symmetry, monocrystalline character, extraordinary saturation and electron drift velocity (310 cm/s), outstanding surface properties, great thermal and chemical stability, higher radiation toughness, large temperature impedance, compact size, meagre ingest and remarkable tolerance to harsh ambience [1].

J. C. Carrano reported that GaN photo detectors can achieve higher quantum efficacies with no internal gain [31]. These photo detectors display a steep, visible-blind cutoff at the verge of band and depict a flat responsivity beyond the bandgap energy.

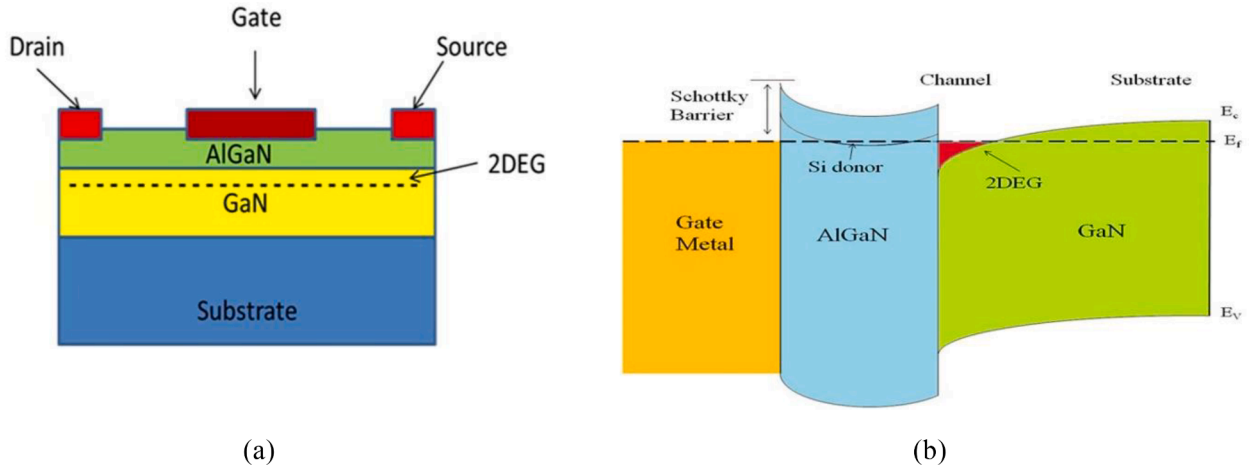

Fig. 4. (a) AlGaN/GaN HEMT, (b) Energy band diagram.

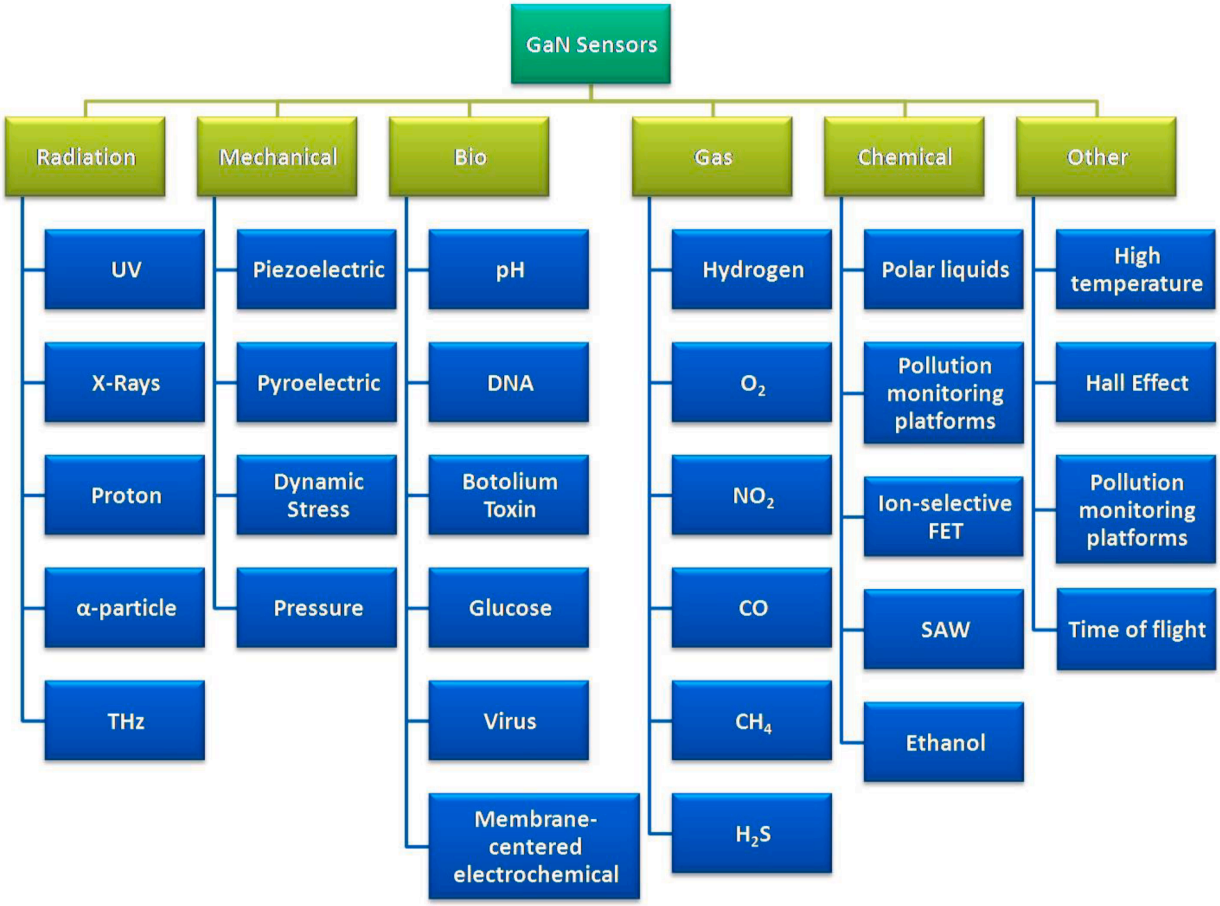

Fig. 5. Classification of GaN Sensors.

4.1.2. Proton and α-particle detector

The cosmic rays of earth's environment consist of mainly protons (about 90%) and secondary α- particles (about 9%), which affect the microelectronics structure. Vaiktus et al. were the first ones to introduce GaN-based device for α- particle detection [32]. A review of GaN based particle detectors has been published by Wang [33]. They have discussed different structures implemented for particle detection *viz.* DSC structure [32], PIN [34], double-Schottky contact structure [35,36], mesa structure [34], sandwich structure [37].

Hu *et al.* reported the I-V characteristics of proton-irradiated AlGaN/AlN/GaN MODFETs up to 1×10^{15} doses and also reported the effect of radiation on AlGaN/GaN heterostructures at *15, 40*, and *105* MeV proton energy up to 10^{13} doses [38]. Luo *et al.* reported the comparison of electrical characteristics of without passivation and with Sc_2O_3-passivation layer on AlGaN/GaN HEMT up to 5×10^9 doses proton irradiation. AlGaN/GaN HEMTs show reduction in threshold voltage, transconductance and current as the effect of irradiation with 40 MeV protons at amounts corresponding to years in Earth-centered satellite systems [39].

Fig. 6 shows the current characteristics of MgO passivated GaN cap HEMT. There are very slight changes in drain current I_{DS} and transconductance g_m for passivated and unpassivated HEMT, however the change in threshold voltage is noticeable.

H Y Kim studied the effect of radiation on GaN/AlGaN/GaN heterostructures exposed to 17 MeV protons. They have reported a 43% decrease in current and 29% decrease in transconductance at highest dose 2×10^{16} protons/cm^2 [40].

4.1.3. Terahertz frequency detector

Terahertz (THz) radiations have niche application area in the field of Biochemical systems for detection of say concealed weapon and explosives. These days, THz imaging allow for solving several challenges in security, food, pharmacy and life sciences. One of the most striking and socially-impactful branches of THz bio photonics is a label-free identification of malevolent neoplasms. THz radiation is non-ionizing in nature. Hence, THz-beams with low-power are undamaging for humans. Water molecules heavily absorb THz waves, thereby, restrict their infiltration into tissues depending upon the frequency of electromagnetic-wave. While THz-wave absorption by water restricts the THz diagnosis by probing only the external levels of biological fluids and tissues, the high sensitivity of THz radiation to water molecules also makes it interesting for the discrimination of healthy tissues with malignant ones by utilizing water as an endogenous indicator [41].

Nezih Pala [42] and A. El Fatimy [43] demonstrated a GaN/AlGaN heterostructure for the plasma detection of THz radiation at room and high temperatures. An important parameter for detection of THz is noise equivalent power (NEP). NEP is defined as "*signal power that gives a signal-to-noise ratio of one in a one hertz output bandwidth*" [42]. Dyakonova *et al.* have measured the photo response of AlGaN/GaN HEMT by varying THz radiation power [44]. They have shown that the GaN heterostructures can be utilized as a THz sensor in continuous regime and in pulsed system up to several kW/cm^2 radiation intensity.

H. Hou *et al.* reported GaN HEMT based sub-terahertz (THz) detector with nanoantennas [45]. With the help of simulations, they have shown that nanoantennas can efficiently improve the detection response by enhancing local electric field induced by sub-THz radiation. M. Bauer *et al.* presented an optimized GaN heterostructure with integrated bow-tie antenna for broadband THz detection (bow-tie TeraFET) [46]. They claimed that their TeraFET has double improvement in performance as compared to the formerly realized TeraFETs.

Table 2
Noteworthy Literature Published on Sensors based on AlGaN/GaN Heterostructure.

Type of Sensors	Year	First Author	Type of work and the tools used	Application	Details	Summary
Radiation Sensors	1999	M. Henini [6]	Review	FET and UV application	–	A thin AlGaN barrier, with high doping, increases the active input capacitance. GaN based device technology improved output power with six fold.
	1999	M. S. Shur [7]	Review	Piezoelectric, pyroelectric sensors and microwave detector	I-V characteristics Analysis	GaN HEMTs with SiC substrates tend to reduce the self-heating effects.
	1999	J. I. Pankove [19]	Review	Solar- screened UV detectors, X-ray detectors, LEDs, laser diodes, SAW devices, Cold cathodes, HBTs	Current gain vs. Temperature analysis	Direct bandgap of GaN increases the optical transition probability which is advantageous feature for UV detectors
	2001	S. J. Pearton [20]	Review	AlGaN/GaN rectifier, BJT, Heterojunction bipolar transistor, GaN MOSFET	Analysis based on breakdown voltage vs. Guard ring width, Resistance vs. breakdown voltage, and I-V Characteristics	In AlGaN rectifier, reverse breakdown voltage increases slowly with E_g at higher Al mole fractions.
	2002	H. Morkoc [28]	Review	MODFET and UV detector	I-V characteristics Analysis	GaN photo-diodes showed zero-bias responsivity of about 0.21 A/W at 356 nm and internal quantum efficiency of 82%.
	2003	X. Hu [38]	Experimental, MOCVD	Proton Irradiation Detection	I-V characteristics Analysis (I_{ds}- V_{gs} and G_m- V_{gs})	The device degradation is significantly low due to higher energy protons than to lower energy protons.
	2003	J. Vaitkus [32]	Experimental, MOCVD	Alpha particles Detection	I-V characteristics Analysis	This change of device current is related to alpha particle pulse height spectrum peculiarities.
	2006	A. El Fatimy [43]	Experimental, MOCVD	THz radiation response	NEP Measurement	At lower temperatures, the voltage response is resonant. Above 70 K, radiation response is non resonant.
	2008	H-Y. Kim [40]	Experimental	Proton Irradiation Detection	Current–voltage characteristics	Cathodoluminescence spectroscopy confirmed the damage in the GaN crystal layer with Proton irradiations.
	2009	A. Y. Polyakov [34]	Fabrication of GaN Schottky diode	Alpha particle detection	Reverse currents characteristics	Epitaxial lateral overgrowth ELOG sample showed charge collection efficiency near cent-percent for sensing alpha-particles
	2010	L. Min [36]	Fabrication of GaN Schottky diode	Alpha particle detectors	I-V characteristics Analysis	With bias voltage of -8 V, the device showed an ideal Gauss peak for sensing 241Am alpha particles
	2015	J. Wang [33]	Review	Gallium nitride for ionizing radiation detection	Summary of state-of-the-art development of GaN detectors for direct–indirect detection of ionizing emission	Radiation may change the induced strain inside GaN, lattice constant resistivity of GaN. Radiation degrades the device performance
	2015	N. Dyakonova [44]	Experimental, MOCVD	THz radiation response	Transfer characteristics Analysis	Voltage response of THz radiation becomes sub linear at high input signals.
	2016	S. Boppel [163]	Experimental, TeraFETs	THz Power Detectors and Intensity-Gradient Sensors	Voltage response	Response of the sensor is dependent on spatial derivative of the incident power.
	2016	M. Hou [164]	Experimental, fully-suspended AlGaN/GaN device with GaN cap Layer	Ultraviolet photodetector	transient photocurrent responses	Decay time can be reduced by three orders of magnitude by in-situ 2DEG heating.
	2016	H. Hou [45]	Experimental setup of GaN HEMT with nano-antenna	Sub-terahertz broadband detector	Responsivity	Use of nano-antennas tends to slightly increase the drain current transcendence.
	2017	K. Ahi [165]	Review	GaN devices for THz operation	Analysis of different GaN Based devices	Properties of GaN help to use GaN based device for generation and detection of THz
	2018	P. Igic [166]	Experimental, dual-drain HEMT	Magnetic field sensor	Electrical current distribution	In magnetic field, the Lorentz force and asymmetrical accumulation of electrons at the device's 2DEG results in the simulated current distribution.
	2018	C. Fares [167]	Experimental on AlGaN/GaN MISHEMTs	Alpha particle detectors	Transfer characteristics Analysis	At higher frequency radiation, performance of device degrades more prominently.
	2019	M. Bauer [46]	Experiment and Modeling	THz radiation Detector	Absolute NEP and broadband SNR measurements	
	2020	H. S. Alpert [162]	Experimental, AlGaN/GaN and InAlN/GaN	Hall-Effect sensor	Voltage scaled sensitivity and current scaled sensitivity	Voltage-scaled sensitivity decreased with increase in temperature, and Scattering effects results reduction in mobility.

(*continued on next page*)

Table 2 (*continued*)

Type of Sensors	Year	First Author	Type of work and the tools used	Application	Details	Summary
Mechanical Sensors	2010	G. Vanko [47]	Experimental, AlGaN/ GaN based Circular HEMT, 4H-SiC substrate	Dynamic stress detection	Carrier concentration w.r.t. change in external stress at different frequencies	Maximum sensitivity can be obtained by increasing the area of diode ring.
	2010	S. Vittoz [168]	Experimental, Analytical and Numerical modeling, Silicon Substrate	Cantilevers for Mechanical Sensing	Mechanically induced electrical field and polarization	External load directly affects the polarization and 2DEG density.
	2012	V. Kutis [61]	FEM piezoelectric simulations, ANSYS, Si substrate	Pressure Sensor	Maximum deflection and induced Charge vs. radius of electrodes	AlGaN/GaN C-HEMT with circular and ring designs
	2013	E.D. Le Boulbar [60]	Experimental, MOCVD, sapphire substrates	Pressure Sensor	I-V characteristics Analysis	Sensitivity of drain current is enhanced by applying gate voltage in weak inversion regime.
	2014	J. Dzuba [169]	FEM based simulation	Piezoelectric pressure sensor	I-V characteristics Analysis	High temperature can originate the mechanical stress variations
	2018	D. Gajula [52]	Experimental, MOCVD,	Circular membrane diaphragm based Pressure sensor	I-V characteristics Analysis	Pressure varies Source-drain resistance which affects current.
	2018	X. Tan [196]	Experimental, Gateless AlGaN/GaN HEMT	Wheatstone bridge structured Pressure sensor	I-V characteristics Analysis	Sensitivity of 1.25 μV/kPa at wide range of pressure.
	2020	L. Chen [48]	Experimental, InGaN/ GaN microwire	Strain Sensor	Piezotronic effects on *I-V* characteristics	Sensitivity is higher at low strain and low bias.
	2020	N-I Kim [59]	Experimental, GaN Heterostructure	Pressure sensor	Change in output potential at different pressure	Output potential increases linearly with pressure
	2020	X. Tan [62]	Experimental, AlGaN/ GaN HEMT in Wheatstone bridge circuit configuration	Pressure sensor	Resistance and Voltage with pressure	72 μV/kPa/V sensitivity achieved with bridge structure.
Bio Sensors	2006	T. Kokawa [82]	Experimental, MOVPE	pH sensor, Polar liquid sensor	I-V characteristics Analysis	A Sensitivity of 57.5 mV/ pH reached
	2008	B.S. Kang [170]	Review	Progress on glucose, kidney marker injury molecules, prostate cancer detection	I-V characteristics and Drain current vs. time Analysis	Protein can easily stick to GaN surface due to its ionic bond. This key factor is important for making a sensitive biosensor with a useful lifetime.
	2009	S. Alur [92]	Experimental, HEMT consists thin AlN layer	Biosensor (DNA Detection)	I-V characteristics Analysis	Charge density changes due to hybridization of charged ssDNA molecules; this variation causes change in the surface potential.
	2009	T. Schubert [66]	Experimental, MOCVD, c-plane sapphire substrates	Biosensor	Analyze interface capacitance and absolute Impedance of GaN sample at various bias potentials	Impedance spectra of the GaN electrode change when come in the exposure of the lipid vesicle suspension
	2010	Y-L. Wang [21]	Experimental, Molecular Beam Epitaxy (MBE) on Al_2O_3substrates	Bio Sensor for Botulinum toxin detection	Drain Current vs. time	The device could sense the Botulinum toxin after 9-month of putting away, however, detection sensitivity reduced.
	2011	F. Ren [22]	Review	Biosensors (DNA, pH, Glucose, Bio-toxin) Prostate cancer , kidney injury, Lactic acid detection	Analysis based on Drain current vs. Time	AlGaN/GaN HEMTs applications in field of biosensors are discussed which can help in early detection of diseases.
	2011	I. N. Cimalla [80]	Experimental, PIMBE and MOCVD, Al2O3 Substrate	pH, DNA sensors	I-V characteristics and Drain current vs. time Analysis	Passivation helps to improve performance in acid and alkaline solution, and LTCC encapsulation helps to improve stability and reduces noise.
	2011	M. S. Z. Abidin [13]	Experimental, MOCVD, c-plane sapphire substrates	pH sensors	I-V characteristics Analysis	Open-gated undoped AlGaN/GaN HEMT structure
	2012	Z. Guo [171]	Experimental, MOCVD, designed Gateless HEMT on c-plane sapphire substrates	pH sensor	I-V characteristic curve at different pH values	Deduced that shorter gate length devices touch saturation at lower bias voltage
	2012	S. Rabbaa [81]	Numerical modeling	Biological sensor for pH and dipole moment measurement	I-V characteristics Analysis	Triangular QW numeric model for an u-AlGaN/GaN MODFET
	2013	H. Trevino II [172]	Experimental, Floating gate configuration	Detection of MIG	Drain Current vs. time	Addition electrons get attracted in the channel due to negatively charged antibody upon immobilization and result in drain current enhancement.
	2013	C–C. Huang [173]	Experimental, MOCVD, sapphire substrates	Protein detector	Analysis based on Drain current vs. Time	Dissociation constant between protein peptide and the antibody plays important role in detection of protein.
	2015	N. Espinosa [18]	Experimental, MOCVD, SiC substrates	DNA Detection	I-V characteristics Analysis	The threshold voltage shifted to positive value therefore drain-source current decreases with DNA functionalization.
	2017	C–H Chu [72]		Protein detection in human serum	Drain Current response with time	Antibodies increase the drain current significantly.

(*continued on next page*)

Table 2 (*continued*)

Type of Sensors	Year	First Author	Type of work and the tools used	Application	Details	Summary
			Experimental, Electric-double-layer (EDL) AlGaN/GaN HEMT			
	2018	J Yang [73]	Experimental, AlGaN/GaN HEMT with disposable cover glass	Zika virus detection	Drain current analysis	Drain current increases with concentration of antigen
	2018	Ju-Young Pyo [83]	Experimental, MOCVD, Extended Gate Structure	pH sensor	I-V characteristics Analysis	Sensitivity of device is close to the Nernst limit
	2018	S. Yang [174]	Experimental, Disposable gate AlGaN/GaN HEMT	prostate-specific antigen (PSA)Bio sensor	Change in current with PSA Concentration	Concentration of PSA results increase in negative charge at gate area which cause change in current.
	2018	A. Varghese [70]	Analytical model and simulation	Detection of c-erbB-2 protein	Transfer characteristics Analysis	With the interaction of bio molecules gate potential get change that caused change in current.
	2019	A. G. Gudkov [175]	Review	Bio sensor	Review Study	Manufacturing cost is gradually decreasing.
	2019	A. Varghese [93]	Fabrication, AlGaN/GaN MOS HEMT	c-erbB-2, MIG, Glucose protein detection	Conductance based sensitivity and drain current analysis	The variation occurs in channel potential when exposed in serum or saliva to detect cancer caused biomolecules.
	2019	T-Y Tai [75]	Experimental, AlGaN/GaN HEMT	Protein detection in human serum	Current gain with different concentration with change in sensing area gap.	Sensitivity can be enhanced by introducing a small gap between the gate electrode and the sensing area.
	2020	N. Sharma [84]	Fabrication, AlGaN/GaN HEMT	Electrochemical sensor for biomedical applications	Current analysis at different pH value	Gate leakage current increases with pH value, Sensitivity is higher.
	2020	X. Liu [91]	Experimental, AlGaN/GaN HEMT	Detection of pH and Potassium Ions in Sweat	pH hysteresis measurement	Al_2O_3 film improves stability, and a wearable sensor has higher sensitivity.
	2019	S. N. Mishra [71]	Analytical model and simulation of MOS-HEMT	Bio sensor	Threshold voltage and Transfer characteristics Analysis	Change in threshold voltage with exposure of biomolecule in cavity is considered as sensitivity. Sensitivity is higher with thicker bio molecule.
	2020	K. Woo [74]	Experimental, AlGaN/GaN HEMT	stress hormone, cortisol detection	Transfer and output characteristics with light incidence	Green light pumping source in HEMT results enhancement of cortisol detection.
	2020	J. Liu [95]	Experimental, AlGaN/GaN HEMT	Glucose sensor	I-V characteristics Analysis	Higher sensitivity can be achieved with the use of APTES at sensing area.
	2020 DONE	J. Wang [176]	Experimental, AlGaN/GaN HEMT with magnetic beads (MBs)	Protein analysis	Change in current with concentration of protein	Device shows higher sensitivity as compared to convention HEMT
Chemical/ Gas Sensors	2004	R. Mehandru [23]	Experimental, MOCVD, Al_2O_3 substrate	Liquid Sensor	I-V characteristics Analysis	Device current reduces significantly with exposure of polar liquid.
	2008	X. H. Wang [108]	Experimental, MOCVD, sapphire substrates	Hydrogen Gas Sensor	I-V characteristics Analysis	Peak-sensitivity achieved in the diode mode of the sensor.
	2010	T. Lalinsky [143]	Experimental, MOCVD, sapphire and SiC substrates	Chemical Gas Sensors	Amplitude characteristics of SAW structures with decent quality factor as well as stop-band rejection ratio	Sensing principle based on SAW, and AlGaN/GaN HEMT.
	2011	I. Ryger [144]	Experimental, MOCVD, SiC substrate	Chemical Gas detectors operational in GHz range	The Frequency response of sensor to ethanol vapour analyzed.	SAW sensors show higher sensitivity with atmospheric pressure
	2011	P. Offermans [116]	Experimental, Silicon Substrate	Detection of NO and NO_x Gas	Drain current vs. time Analysis	Upon the exposure of Gases device current decreases about 400%. Response time is inversely proportional to humidity.
	2011	W. S. Jeat [177]	Fabrication, two terminal AlGaN/GaN Heterostructure	Liquid Sensor	Change in current in different pH liquid	Surface potential changes at GaN layer due to different dipole moment of liquid.
	2012	I. Ryger [178]	Experimental, MOCVD, heterostructure device with Pt-IrO_2 based gate absorption coatings, SiC substrate	Hydrogen Gas Sensor	I-V characteristics Analysis	Supplementing IrO_2 gate interfacial layer considerably improved the sensitivity of the Pt gate Schottky diode
	2012	H. Kim [106]	Experimental, MOCVD, sapphire substrates	Hydrogen Gas Sensor	I-V characteristics and Drain current vs. time Analysis	AlGaN/GaN based diode sensors incorporating platinum nano-networks
	2013	Z. Guo [109]	Experimental, MOCVD, c-plane sapphire substrates, Theoretical modeling	Hydrogen Gas Sensor	I-V characteristics Analysis	Sensitivity increases with concentration of H_2
	2014	K. Maiera [179]	Experimental, plasma-assisted MBE on Si substrates	Optochemical Sensors for Gases detection	Photo luminance intensity analysis.	Photoluminescence intensity decreases with exposure of gases. PL decreases about 40% at 150 °C.
	2015	I. Ryger [180]	Experimental, MOCVD	Hydrogen Gas Sensor	I-V characteristics Analysis	Sensitivity can be increased by using shorter acoustic wavelengths
	2016					

(*continued on next page*)

Table 2 (*continued*)

Type of Sensors	Year	First Author	Type of work and the tools used	Application	Details	Summary
		Y. Halfaya [117]	Experimental, metal organic vapor phase epitaxy (MOVPE)	NO, NO_2 and NH_3 gas sensor	I-V characteristics Analysis and response time with concentration	Sensitivity increases at higher temperature
	2016	K. H. Baik [111]	Experimental, Pt nano-network was placed on the gate area of HEMT	Hydrogen Gas Sensor	I-V characteristics Analysis	Pt nanoparticles helps to improve drain current response
	2016	X. L. Jia [139]	Experimental, AlInN/GaN and AlGaN/GaN HEMT	Phosphate detection	Change in Current with Phosphate concentration	AlInN/GaN HEMT shows higher sensitivity as compare to AlGaN/GaN.
	2016	M. Asadnia [140]	Experimental, AlGaN/GaN HEMT with PVC material gate area	Mercury sensor	Change in device voltage with concentration of mercury ions.	Sensor voltage decreases with increase in concentration of mercury ions.
	2016	C. Bishop [10]	Device Modeling and fabrication	NO, NO_2, and NH_3 Gas Detection	Transient response and Sensitivity Vs concentration of gas	At higher temperature > 300C NO_2 sensitivity increases rapidly due to diffusion of O_2.
	2016	M. Sciullo [181]	Simulation study	pH Sensor	Current slope Vs pH	Sensitivity of device increases with drain voltage. Drain current decreases with increase in pH value
	2017	S. Jung [113]	AlGaN/GaN HEMT incorporating poly (methyl methacrylate) (PMMA) membrane layer	Hydrogen sensor	I-V characteristics	Excellent sensitivity for *500* ppm hydrogen even in *100%* relative humidity
	2017	S. Jung [145]	Fabrication of AlGaN/GaN HEMT with silver Schottky diode	Ethanol Sensor	Current-Voltage (I-V) characteristic	Schottky barrier height increases with exposure of ethanol, which decrease the drain current. Maximum sensitivity observed at 250 °C
	2017	R. Sokolovskij [131]	Experimental, Pt-AlGaN/GaN HEMT	H_2S sensor	Transient response characteristics	Sensitivity increased with concentration of gas.
	2017	R. Sokolovskij [194]	Experimental	Hydrogen sensor	I-V characteristics	Significant increase in sensing sensitivity with larger W_g/L_g ratio devices
	2017	S. Jung [182]	Experimental, AlGaN/GaN HEMT with ZnO nanorods	Carbon Dioxide	I-V characteristics	Current response was more unique with higher temperature caused by reduced activation energy.
	2017	T. Ayari [141]	Experimental, AlGaN/GaN HEMT with h-BN layer	N_2 and NO_2 Gas Sensor	Change in current under the gas exposure	Sensitivity increases by 100% and response time reduced by 6 times.
	2018	K. H. Baik [195]	Experimental, PMMA Coated Pt-AlGaN/GaN Diode	Hydrogen sensor	I-V characteristics, current peak Vs H_2 concentration	PMMA encapsulation works only for H2 detection, it cannot work effectively for other gas sensors.
	2018	R. Anvari [183]	Theoretical Study of ISFET	Chemical Sensor	Surface potential and Nernstian-slope analysis	Sensitivity of device is higher for pH at higher concentration of salt
	2018	Y. Dong [184]	Experimental, AlInN/GaN open gate HEMT	pH sensor	Current variation with pH	Smaller thickness of AlInN achieved similar 2DEG as with AlGaN
	2018	N. Chaturvedi [185]	Experimental, AlGaN/GaN HEMT four designs	liquid sensor	Current characteristics for different polar liquids	Multiple gates arrangement in electrodes fashion shows the better sensitivity.
	2019	A Nigam [137]	Experimental, AlGaN/GaN HEMT	Cadmium ion detection	Current response w.r.t. Cd + concentration	The sensor shows higher sensitivity over other heavy metal ions.
	2019	J Zhang [132]	Experimental, Pt -AlGaN/GaN HEMT with H_2 pre treatment	H_2S gas detection	Gas response with H_2S concentration	With H_2pre treatment higher concentrated H_2S detection can achieve.
	2019	A Ranjan [118]	Experimental	NO_2 gas sensors	I-V characteristics, Sensitivity Vs Temperature	Sensitivity increases with temperature
	2019	G. H. Chung [115]	Experimental, AlGaN/GaN HEMT with Pt floating electrode.	Hydrogen Gas Sensor	I-V characteristics Analysis	Effective Schottky barrier height reduced due to interfacial dipole layer at Pt-GaN interface layer which is result of penetration of hydrogen atoms into Pt electrode, it tends to increase drain current. Sensing sensitivity increases with temperature.
	2019	J. Shahbaz [133]	Experimental, GaN/GaInN heterostructures	H_2S Sensor	Change in photoluminescence (PL) intensity with concentration of H2S	With the concentration of H2S intensity and wavelength is increases.
	2019	L. Zhao [142]	Experimental, differential extended gate (DEG)-AlGaN/GaN	Ionic pollutants detection	Output current with concentration of Fe+	Change in the current with exposure of Fe3 + was about 30 times larger than that by interfering actions
	2019	H.O. Chahdi [186]	Experimental, AlGaN/GaN HEMT	H_2 and O_2 detection	Current Vs Time	Sensor's sensitivity increases with temperature and concentration of gas.
	2019	J. Sun [119]	Experimental, AlGaN/GaN HEMT sensors with WO3 nano-film integrated with micro-heater	NO_2 gas sensors	Transient response to concentration of NO2	Sensitivity can be increase by using WO_3layer deposition.

(*continued on next page*)

Table 2 (*continued*)

Type of Sensors	Year	First Author	Type of work and the tools used	Application	Details	Summary
	2019	A. Varghese [187]	Experimental, Linear and Circular AlGaN/AlN/GaN MOS-HEMT	pH sensor	Cannel conduction variation with pH	Performance of Circular MOS HEMT is better for resolution, complexity and cost.
	2019	M. Mishra [130]	Experimental, nanostructure GaN and AlGaN/GaN HEMT	CO sensor	Recovery time, sensitivity and response	Nanostructure AlGaN/GaN HEMT shows 33% higher sensitivity.
	2019	H. Zhang [90]	Experimental, open Gated AlGaN/GaN HEMT	pH sensor	Current response at different pH value and sensing membrane	pH sensing membrane may degrade the sensitivity of device.
	2019	G. Parish [188]	Experimental, GaN caped AlGaN/GaN HEMT	pH sensor	Drain- Source voltage vs pH	GaN cap layer prevents from degradation and achieve the stability.
	2020	N. Sharma [84]	Experimental, Gated AlGaN/GaN HEMT	pH sensor	pH sensing and Salinity Sensing Response	Gate leakage current increases with pH values. Change in drain current was decreased with molar concentration of salt in solution.
	2020	H-H Park [189]	Experimental, AlGaN/GaN open gate HEMT with Pt nanoparticulate films	Hydrogen sensor	Current response of device	Sensitivity can be increased by increasing the deposition rates and grain size of the Pt nanoparticulate films.
	2020	H. Zhang [190]	Experimental, AlGaN/GaN HEMT with 3 types of packaging	Liquid sensor	I-V characteristics, Leakage mechanism analysis	Large voltage can be achieved with SiO_2/Si_3N_4/PI packaging.
	2020	S.S.B. Hashwan [191]	Review	Chemicals and Pesticides Detection	Changes in current, capacitance, resistance, impedance, wavelength, reflectivity, intensity.	Presence of different bio-chemicals affects the sensing parameters.
	2020	K. H. Baik [112]	Experimental, AlGaN/GaN heterostructure serially connected Pt diode and reference diode.	Hydrogen sensor	Responsivity	Serial connection of diode gives high stable output voltage.
	2020	Q. Cheng [88]	Experimental, Dual gate GaN HEMT Amplifier	pH sensor	Output voltage response with respect to pH values.	Dual gate HEMT shows 45 times higher sensitivity.
	2020	K. H. Baik [192]	Experimental, AlGaN/GaN based Pt nanonetwork Schottky diodes with a PMGI water-blocking layer	Hydrogen sensor	Forward and reverse current voltage characteristics	Highly sensitive and reliable operation of hydrogen sensors in both dry and humid ambient
	2020	C. V. Nguyen [122]	Experimental, Pd-AlGaN/GaN HEMT	NO_2 gas sensors	Transient characteristics	Dissociated NO_2 results negative charge oxygen ion at gate area which affects the 2DEG of device.
	2020	N. Chaturvedi [135]	Experimental, AlGaN/GaN HEMT with low temperature co-fired ceramic (LTCC) packaging	Polar Liquid sensor	Current and Surface potential with dipole moment and permittivity of different polar liquids	Device is sensitive to polar liquid concentration.
Temperature Sensors	2018	F. Cozette [193]	Experimental, AlGaN/GaN HEMT	Temperature Sensor for RF Applications	Change in sensor resistance with temperature	Drain resistance linearly increases with temperature.
	2019	A. Hassan [151]	Experimental, GaN based wireless data transmission	High temperature sensor	I-V Characteristics	

GaN in plasma HFETs. III-N based devices have been proposed as promising advanced plasmonic electronic devices for detection, mixing, and generation of THz radiation due to their exceptional characteristics. The fundamental plasma frequencyω_0 is given by Eq. (1) [43,44]

$$\omega_0 = \frac{\pi s}{2L} \tag{1}$$

where L is the length of the channel and *s* is the speed of propagation. In a FET, Eigen modes of the plasma oscillations are odd harmonics of the fundamental plasma frequency. For HFETs to be able to function in plasma mode, the *L* should be less than the critical length of the channel $L_{critical}(= s\mu m/r)$ and $\omega_0 \gg 1/\tau$ where μ is mobility in low electric field, *m* is the electron effective mass and τ being the momentum relaxation time.

For GaN, material dependent critical frequency ω_{cr} remains in the THz regime for a wide temperature range. ω_{cr} is 10 THz and 1.6THz at 300 K and 77 K respectively for GaN. These values are much more than corresponding values for Si (1.7 THz, 0.46 THz) and GaAs (3.5 THz, 0.093 THz).

4.2. Mechanical sensors

Unique PE properties of III-N materials are very helpful for stress and strain sensing applications. GaN also has few important advantages like high biocompatibility, mechanical and physical stability of epitaxial films. Hence, it has a prospect of being incorporated into MEMS and NEMS automatic sensors. High thermal stability helps to retain their PE properties in varied thermal choices. PE reaction of AlGaN/GaN devices incorporated in membrane devices is also stated in the literature [47-63].

4.2.1. Stress sensor

External force on AlGaN/GaN based sensors cause changes in the piezo-polarization in the nitride film. These changes tend to vary the sheet concentration narrowed at the AlGaN/GaN heterojunction that helps to acquire the gauge aspect of the device [47].

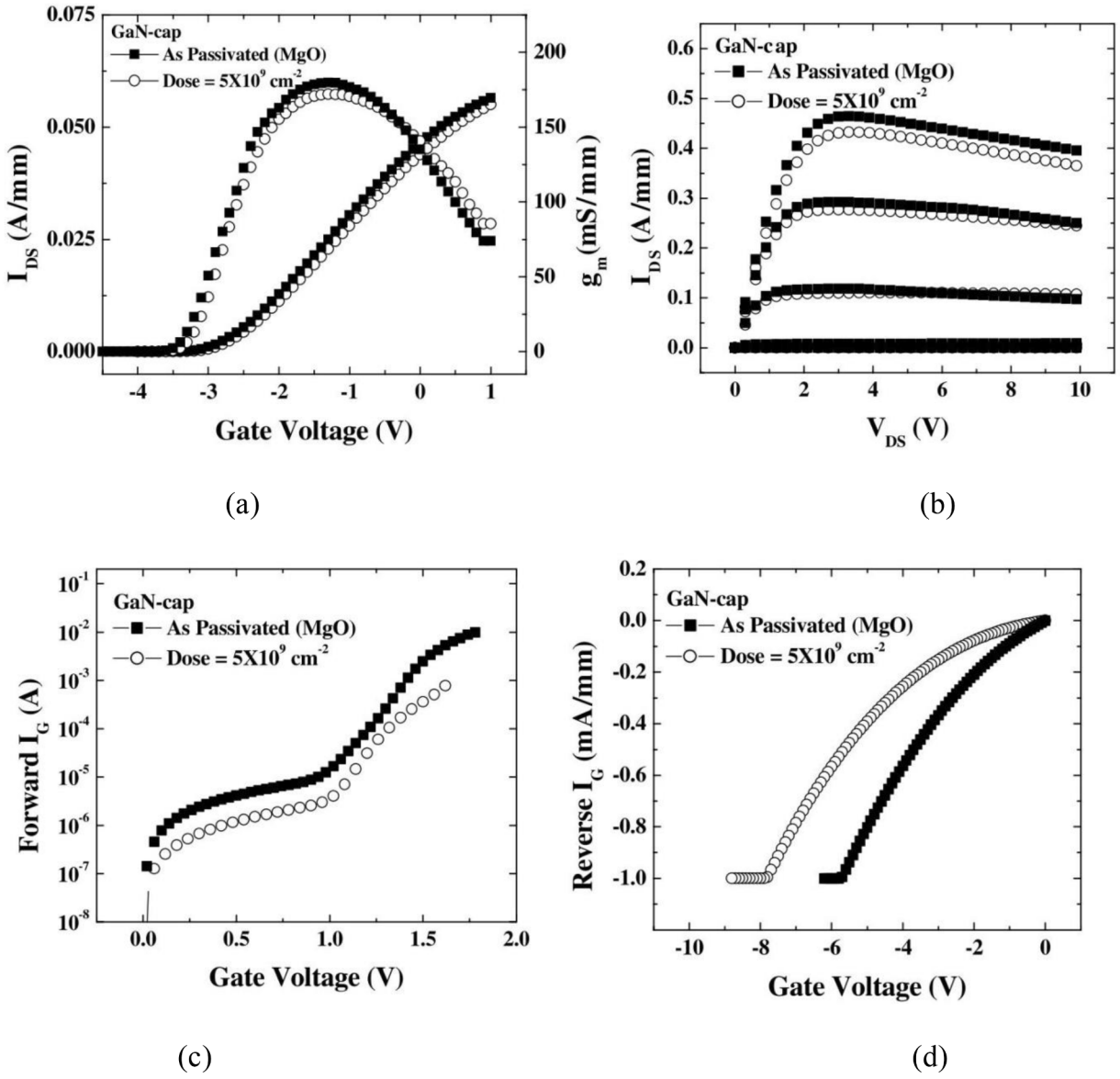

Fig. 6. (a) the I_{DS}–V_{DS} Characteristics, (b) the I_{DS}–V_{DS} Characteristics, (c) and forward Characteristics, and (d) reverse Characteristics of MgO passivated, GaN-cap HEMTs before and after proton irradiation. Reprinted from [39] B. Luo, F. Ren, K.K. Allums, B.P. Gila, A.H. Onstine, C.R. Abernathy, S.J. Pearton, R.Dwivedi, T.N. Fogarty, R.Wilkins, R.C. Fitch, J.K. Gillespie, T.J. Jenkins, R. Dettmer, J.Sewell, G.D. Via, A.Crespo, A.G. Baca, R.J. Shul, Proton irradiation of MgO- or Sc2O3 passivated AlGaN/GaN high electron mobility transistors, Solid-State Electronics, vol. 47, pp.1015–1020, Copyright (2003), with permission from Elsevier.

AlGaN/GaN circular-HEMT's piezo-polarization based stress sensor was introduced by G. Vanko *et al.* [47]. The basic hetero-arrangement was developed on the 4H-SiC substrate. It consisted of a 30 nm thin AlN nucleation layer topped up by a 2 μm Fe- doped GaN buffer layer and a 25 nm u-AlGaN active layer with 0.25 M fraction of Al. The proposed C-HEMTs were having five different structures with fixed drain-source gaping, flexible gate area and a gate-less structure. The observed circular-HEMTs on the bulk SiC cantilever were vigorously stressed with a fixed frequency.

The sensor structure exhibits respectably linear PE response under vigorous stress environments. Sensitivity was directly proportional to the gate area of the structure. The results indicated that the induced voltage response is independent of the external strain frequency. Induced charge increases linearly with external stress at different frequencies.

Chen *et al.* designed a piezotronic strain sensor based on InGaN/GaN multiple quantum-well heterojunction microwire (MQWH-MW) with ultrahigh sensitivity. The InGaN/GaN MQWH-MW with orientation along *a*-axis, was accomplished by conductivity-choosy EC etching of epitaxial film on substrate. Back-to-back Schottky junction was employed to fabricate the strain sensor. When 0.55% tensile strain was put under external bias of +0.4 V, the gauge factor of the device reached more than 2000. Authors theoretically analyzed energy band in the MQWH-MW based strain sensor to clarify their practical results [48]. The change in current characteristics with compression and stretching reported is as shown in Fig. 7.

4.2.2. *Pressure sensor*

Requirement for pressure monitoring is rising exponentially in multiple applications like automotive, petroleum, nuclear power, and aerospace production [49-52]. Specific sensors are needed to identify problems, like engine, brake and tyre in vehicle; oil-drilling pipe in gasoline; reactor container and steam producer in nuclear power plant; cabin and frame in aerospace engineering etc. to avoid malfunctioning, and, for lifetime observation [53]. The operating temperature range in the automotive (100–350 °C), petroleum (150–300 °C), aerospace

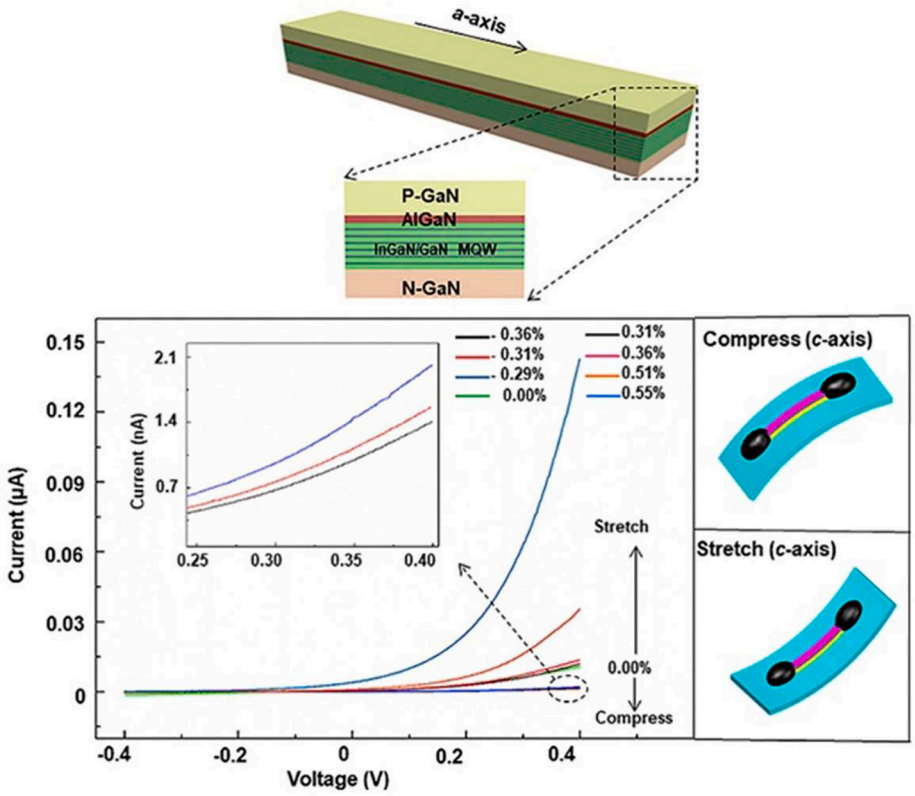

Fig. 7. Current characteristic curve under compressing and stretching. The structure representation of stretching and compression is placed at the right side of graph [48] "Reprinted from L. Chen, K. Zhang, J. Dong, B. Wang, L. He, Q. Wang, M. He, X. Wang, The piezotronic effect in InGaN/GaN quantum-well based microwire for ultrasensitive strain sensor, Nano Energy, vol. 72, p.104660, Copyright (2020), with permission from Elsevier.

(−60–900 °C), and nuclear plant (30–250 °C) industries is very high [51,54-56]. Another critical condition faced in these fields is presence of very high pressures of the order of 6. On- the- spot sensing of pressure in such severe environments require sturdiness and resilience along with a high sensitivity [57].

PE-type sensors have various advantages as compared to other types of sensors under extreme conditions. Due to their wider bandgap, they can produce significant output voltages with broad choice of pressure levels (~10^6 Pa). The PE pressure sensors are tough and enduring even in extreme environment. Lastly, small size and low-power devices can be made as the external power supply is not imperative in PE sensors [58].

Classic PE-type sensors very much depend on lead zirconate titanate (Pb [Zr_xTi_{1-x}] O_3, PZT) transducers. Nevertheless, the PZT is a not an optimized option because of its unbalanced output at temperatures more

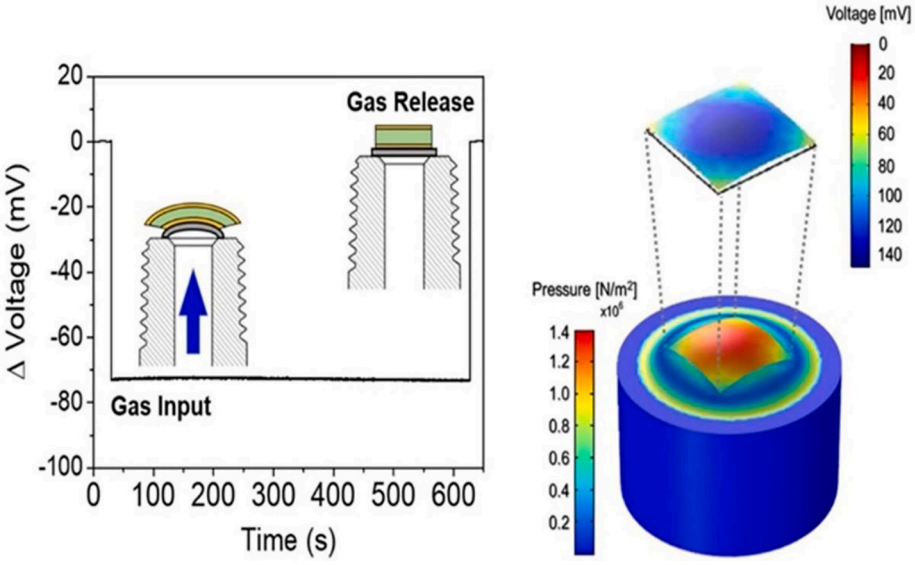

Fig. 8. Voltage response and schematic of GaN HEMT based gas pressure sensor. Reprinted from N-I Kim, *et al.*, "Piezoelectric Pressure Sensor Based on Flexible Gallium Nitride Thin Film for Harsh-Environment and High-Temperature Applications," Sensors and Actuators: A. Physical, Copyright (2020), with permission from Elsevier [59].

than 200 °C and probable ecological threat. Therefore, it is a challenge to produce a more efficient and safer environmental material than PZT for PE pressure sensors by integrating lead-free materials like Ceramics and polymeric composites. GaN is a lead-free material and has a noteworthy PE coefficient. It exhibits the highest prospect to replace the PZT as a result of its show in high temperature and pressure operating conditions [59].

Kim *et al.* used GaN thin film as a sensing substance. The device is prepared by a layer relocation process after the elimination of the Si body. The values of output potential for GaN relating to gas pressure levels 50, 100, 150, and 200 psi were found to be 42.3, 76.8, 98.7, and 122.1 mV respectively. Their results agreed well with the simulated data [59]. Furthermore, the measured voltages at elevated temperatures produced reliable outputs at temperatures up to 350 °C. In addition, they confirmed the stability of sensor outputs elevated temperatures with various pressure levels. Fig. 8 shows voltage response and schematic of gas pressure sensor introduced by Kim *et al.*

Variation in the PE polarization P_{pz} at the gate and the channel interface of sensor cause change in the 2DEG conductivity and form a possible piezoresistive contribution.

Boulbar *et al.* have investigated the sensitivity of AlGaN/GaN HEMT drum skin sensor (Fig. 9 (a)), under static pressure for strong, moderate and weak inversion working regimes as shown in Fig. 9(b). The sensitivity in the weak inversion region was approximately 150 times better than the strong inversion region of the HEMT [60]. The pressure variation response was found to follow a $\{1 - \exp(x)\}$ relation where $x = qVT/kT$. Such behavior is typical of HEMT operation in the weak inversion region.

V Kutiš *et al.* [61] had demonstrated PE MEMS pressure sensor based membrane AlGaN/GaN circular-HEMT structure, with two different designs - circular and ring. The electrode metallization plays significant role in enduring stress dissemination.

2D and 3D models have been introduced, in literature, to endorse naiver 2D FEM model, which was laden by outer pressure. Model was included with residual stress because of big mismatched lattice and the difference in thermal expansion coefficient's difference. The model has been used to study the effect of position and magnitude of the electrode and bring optimization in designs.

D. Gajula *et al.* [52] pioneered a diaphragm centred AlGaN/GaN MODFET embedded circular membrane pressure sensor for high temperature pressure sensing, with ultra-high sensitivity. A regular pressure difference of 20 kPa, when applied to the diaphragm, leads to increase in the R_{ds}.

Tan *et al.* [62] realized pressure sensor by using four gateless GaN HEMTs in Wheatstone bridge structure to enhance the sensitivity of sensor. The impedances of the four AlGaN/GaN HEMTs, rose with the applied pressure. Differential operation of the Wheatstone bridge circuit helps to achieve linear outputs with a non-linearity of *0.8%* and a sensitivity of 7 $\mu V/kPa$ at a wide pressure-range.

They demonstrated pressure sensing with a specifically designed Wheatstone bridge arrangement by considering the isotropic PE property of III-nitrides and the stress division in the round diaphragm. Two pairs of gateless HEMTs were placed at the tensile and compressive stress areas of the rounded diaphragm to exploit the pressure sensor's responsivity and stability. Consequently, the 2DEG resistors positioned diagonally, presented entirely contradictory P_{pz} effects, which transformed to a linear response of the sensor with a high sensitivity of 72 μV/kPa/V. Large output capability of 64.8 mV/V was obtained, signifying potentially low power consumption in the real-world use. As shown in Fig. 10, at the center of the diaphragm, stress surface is minimal and is maximum at the boundary. So, output can be taken out by putting sensor at the boundaries.

The piezoelectric polarization (P_{pz}) of the AlGaN/GaN heterostructure, along the growth direction, caused by lattice mismatch between GaN and AlGaN, can be expressed by the Eq. (2) as follows

$$P_{pz} = 2\left(e_{31} - e_{33}\frac{C_{13}}{C_{33}}\right)\left(\frac{a - a_0}{a_0}\right) \tag{2}$$

where e_{31}, e_{33} are the PE coefficients, C_{13}, C_{33} are the elastic constants, a_0 is the equilibrium lattice constant and $a$is the strained lattice parameter. Therefore, by putting either tensile or compressive stress to the AlGaN layer, P_{pz} changes in the opposite directions. The surface radial stress δ_r and tangential stress δ_t for a strained circular diaphragm under the fixed support edge condition can be computed by Eq. (3) and Eq. (4) respectively [62].

$$\delta_r = \frac{3P}{8t^2}\left(-r^2(1+v) + x^2(3+v)\right) \tag{3}$$

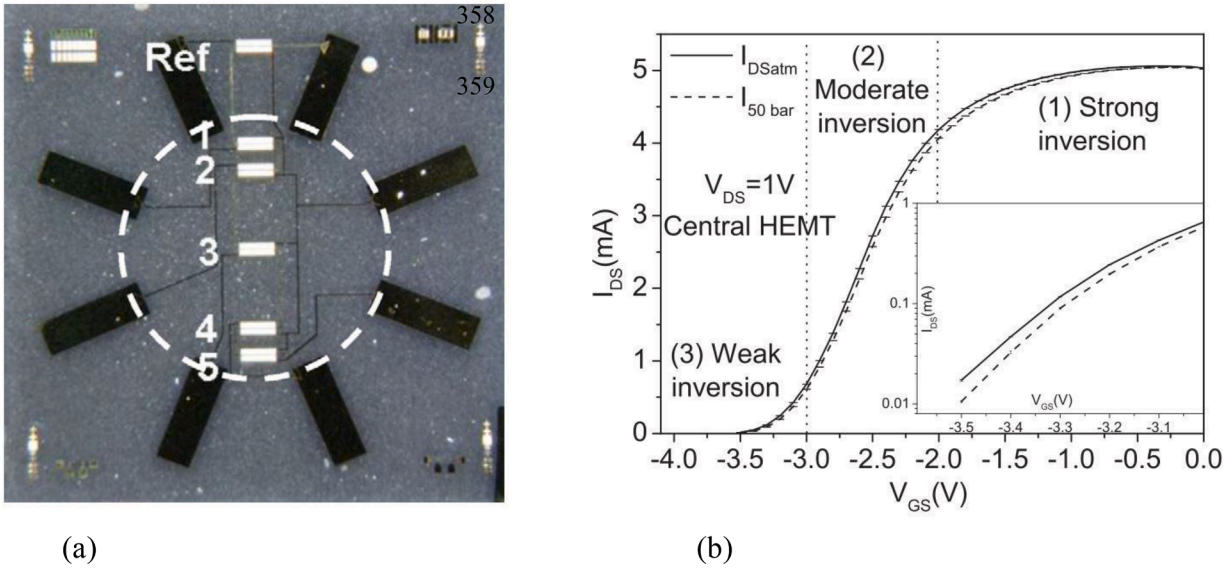

Fig. 9. (a) Drum skin sensor, (b) I_{DS}- V_{GS} current characteristics at atmospheric and 50 bar pressure. The weak inversion regime with I_{DS} plotted on a logarithmic scale is shown in inset [60]. Reprinted from E.D.L. Boulbar, M. J. Edwards, S. Vittoz, G. Vanko, K. Brinkfeldt, L. Rufer, P. Johander, T. Lalinsky, C. R. Bowen, D. W. E. Alisopp, Effect of bias conditions on pressure sensors based on AlGaN/GaN high electron Mobility Transistor, Sensors and Actuators A, vol. 194, pp. 247–251, Copyright (2013), with permission from Elsevier.

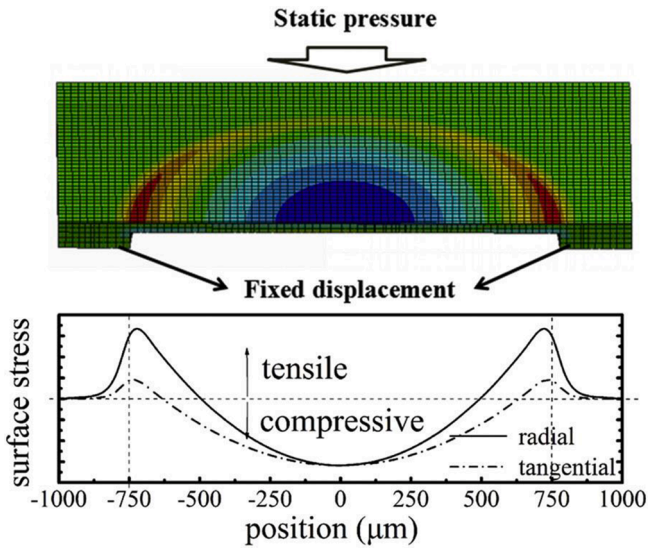

Fig. 10. Surface stress distribution of a strained circular diaphragm, Radial and tangential stresses measurement at centre (Minimum value) and at edges (Maximum value). Reprinted from X. Tan et. al, High performance AlGaN/GaN pressure sensor with a Wheatstone bridge circuit, Microelectronic Engineering, Vol. 219, High performance AlGaN/GaN pressure sensor with a Wheatstone bridge circuit, 111143, Copyright (2020), with permission from Elsevier [62].

$$\delta_t = \frac{3P}{8t^2}\left(-r^2(1+v)+x^2(1+3v)\right) \tag{4}$$

Here, P is the applied pressure, v is the Poisson's ratio, t and r are the thickness and effective radius of the circular membrane, x is the relative distance to the centre or the diaphragm.

4.3. Bio sensors

Biosensors were introduced by Clark in 1962 [64]. Ever since, they have been extensively employed in a variety of applications such as cancer identification, toxicity recognition, food analysis, health prospects, etc. Biosensors are analytical devices that convert biological pointers into electrical signal, usually consisting of at least two basic components combined together. One is a biological receptor that converts response from the biochemical domain, into a chemical or physical output signal; and second one is a physical–chemical transducer that transduces the output signals of the bio-recognition system, to the electrical signals [65].

Combination of biological systems and electronic transducers has better sensitivity to translate explicit tasks of biomolecules into electrical signals. Semiconductor sensors have the capacity to engineer their energy bandgap by selectively doping the layers in heterostructures, and realize simultaneous multimodal opto-electrical sensing [66]. Biochemical micro-sensors, such as photo, thermal, resistance, and semiconductor biosensors etc., are widely researched because of their compactness and high sensitivity. Amid such sensors, FET-based biosensors own the essential qualities of quick response, low-cost, ease of use and real-time diagnosis. In a typical FET system, the sensing ingredients are functionalized on the sensing feed. These feeds are coupled to the source and the drain electrodes, to arrest the targets by means of extraordinary specificity and binding affinity. A modulated bias potential is applied to the gate. An electrical measurement system records and processes the channel conductance, varied by the detection of the targets. Diverse materials such as Si, GaN, graphene oxide, and carbon nanotube (CNT), have been utilized for the FET based biosensors. Because of their chemical stability, absence of the need to use reference electrodes, and the prospect of their scaling down in size, AlGaN/GaN HEMTs have also gained significant consideration.

Charge screening or Debye screening at the interface of semiconductor device and the aqueous solution has been a foremost challenge in the realistic implementation of FET biosensors. Debye protection is a screening phenomenon based on the impact of the Debye radius where the sensing scope of the sensor is less than 1 nm in the physiological solution. In reality, size of most of the biomolecules is above 1 nm. Thus, clear of the Debye radius [67].

From the Guoy-Chapman electrical double layer (EDL) model, relationship of Debye length and ionic strength of the aqueous medium is given by Eq. (5) below [68]

$$\frac{1}{K} = \left(\frac{\varepsilon_r \varepsilon_0 k_b T}{2N_A z e^2 I}\right)^{\frac{1}{2}} \tag{5}$$

Debye length is predicted to be ~0.7 nm in solutions with high ionic strength like whole blood. Normally, the size of immobilized receptors, at the gate region of FET, is around 10 nm. The ligand binding site has upward orientation in the z direction. Hence, the voltage changes induced by receptor-ligand binding get cordoned off and do not vary the drain current. This observable fact at the device-solution junction causes a main challenge for clinical applications of FET based biosensors [68].

Grahame equation exhibits the relation between the surface potential and the surface charge density on a metal or non-metal planar surface [69]:

$$\sigma = \sqrt{(8n\varepsilon_r\varepsilon_0 kT)}\sinh\left(\frac{ze\psi_0}{2kT}\right) \tag{6}$$

where σ,n, ψ_0, ε_r and ε_0 are respectively the surface charge density, the electrolyte concentration in bulk solution, the surface potential, the relative permittivity and the permittivity in vacuum. One may infer from Eq. (6), that a larger surface potential can generate a higher charge density. In HEMTs, when large gate voltage is applied, higher current gain is obtained. In Grahame equation, the charge density is not relevant to the gap between the gate electrode and the channel.

In literature, a variety of biosensors built on HEMTs technology are described. With proper variation in the gate area of HEMTs, they have applications in pH sensing, detection of DNA, Prostate specific antigen (PSA), Glucose, Protein, Botulinum toxin, Lactic acid and breast cancer biomarker [70,71].

Chu *et al.* demonstrated a FET-based novel biosensor for point-of-care, home healthcare, and mobile diagnostics. Their device was able to defeat the complexity of severe charge-screening effect caused by high ionic strength in solution. They sensed proteins in physiological environment. Antibody -immobilized GaN HEMTs were directly utilized to sense proteins, including NT-proBNP, CRP, CEA and HIV-1 RT in human serum. The samples did not require dilution or washing procedure to lessen the ionic potency. The sensor showed high sensitivity and the finding took mere 300 s time [72].

An efficient strategy is to make use of the EDL to identify biomolecules further than the Debye length. A functionalized gate electrode, separated from the transistor channel by a short gap, is used to apply high electric field across the test solution. In the process, EDL is formed on the gate electrode and channel interfaces with the solution. Thus, the voltage sketch in the structure with the separated gate electrode is changed from the traditional FET sensor design [72]. The receptors are arrested on the gate electrode. When they bind with the target in the solution, a charge re-distribution in the local region leads to prompts equivalent charge re-organization at the transistor dielectric-solution interface. This changes the potential difference across the transistor dielectric and hence the drain current. Thus, biomolecule detection takes place unconstrained by the well-built EDL in physiological saline concentrations [68].

The Zika virus (ZIKV) is a flavivirus similar to West Nile virus, dengue, or yellow fever. Aedes mosquito is its primary transmitor. Zika causes improper brain development in foetuses. ZIKV detection was demonstrated by Yang *et al.* using cover glasses functionalized with

antibody, and attached to the gate electrode of an AlGaN/GaN HEMT [73]. A 0.5 V pulsed bias was applied to an electrode on the antibody-functionalized cover glass area, and the resultant variation in drain current of the HEMT were used to establish the existence of ZIKV antigen concentration of 0.1 to 100 ng/ml. The ZIKV concentration dependent dynamic and the static drain current changes were modelled with an elastic relaxation model and the Langmuir extension model, respectively. Exceptional matching was found with relaxation time constants of antibody and antigen molecules in the range of 11 ls and 0.66–24.4 ls, respectively. Since the HEMT was not bared to the bio-solution, it could be used repetitively. The functionalized glass was the non- reusable component in the detection system. Therefore, this approach has potential in hand-held, low cost sensor packages for point-of-care (POC) applications [73]. Device designed by Yang *et al.* with detachable glass cover is shown in Fig. 11.

Gu *et al.* presented a new quick analytical stage for electronic enzyme-linked immunosorbent assay (e-ELISA) based on AlGaN/GaN HEMT with Magnetic beads (MBs). MBs-based e-ELISA decouples customized region from sensing surface to simplify the evaluation. Merging the benefits of MBs and e-ELISA, sensing competence further than the Debye-screening limit and reusable capacity was obtained. This scheme offers a fast response toward Prostate specific antigen (PSA) with a low concentration of detection of 1 fg/mL. Within the limitation of the emergency care application, it showed higher sensitivity (3.73 μA/dec) in the linear range (1 fg/ mL to 1 pg/mL) as compared to conventional AlGaN/GaN HEMT biosensors [67].

Woo *et al.* studied the HEMT as an immunity-sensor to measure concentration of a stress hormone, cortisol. The sensitivity was enhanced in the HEMT sensor through laser light illumination of 532 nm wavelength, as shown in Fig. 12. The optical pumping supported the biosensor in differentiating meticulous alteration, which could cause an increment of limit of detection (LOD) to 1.0 pM cortisol level. It is claimed to be the lowest level of detection with HEMT-based cortisol biosensors. Amplified output current, was higher than the dark current by 3.39% with $V_g = -3$ V [74].

Tai *et al.* developed a protein immunoassay using aptamer functionalized AlGaN/GaN HEMT [75]. They reported a tunable and amplified sensitivity of solution-gated EDL HEMT-based biosensors as shown in Fig. 13. When a higher gate voltage was applied, sensitivity was enhanced by crafting a smaller gap between the gate electrode and the solution. Sensitivity is calculated by quantifying NT-proBNP, a medical biomarker of heart collapse, in buffer and in unprocessed human sera. The authors claimed to have achieved a sensitivity of 80.54 mV/decade protein concentration. This equipment verified prospects in developing surface affinity sensors for medical diagnostics.

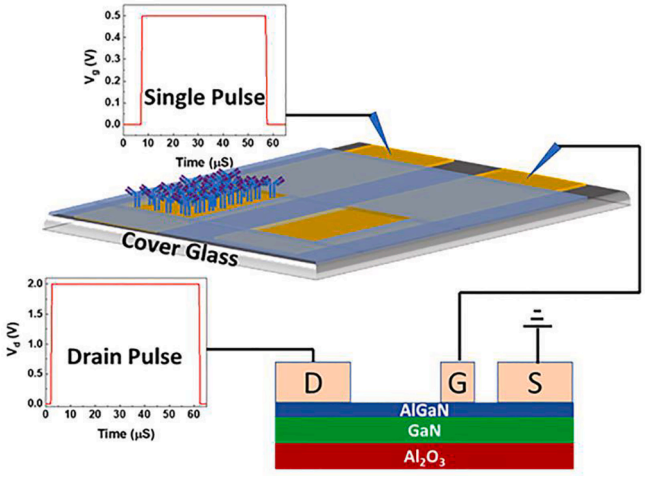

Fig. 11. Structure and setup of Zika virus sensor with glass cover where the antigen can place, and afterword glass cover can be changed. Reprinted from J. Yang, *et al.*, "Zika virus detection using antibody-immobilized disposable cover glass and AlGaN/GaN high electron mobility transistors," Appl. Phys. Lett. 113, 032,101 (2018), with the permission of AIP Publishing [73]

4.3.1. Membrane- centered electrochemical sensors

For membrane centered biosensors, GaN is a better alternative as it is a chemically stable compound. GaN electrodes can be activated in biological buffers with no noticeable drift or retardation. T. Schubert *et al.* have demonstrated the strength of wet chemically oxidized GaN by using electrochemical (EC) resistance spectroscopy measurements for many frequencies and voltage biases [66].

Si-doped GaN layers on *c*-plane bulk sapphire, grown by MOCVD were utilized to examine the electrical properties of lipid membranes held on GaN conductors. The dynamics of the membrane creation can be observed by plotting the variation in impedance and capacitance of membrane with respect to time.

4.3.2. pH sensors

The pH measurement is essential in a lot of applications like medicine, food science, biology, environmental science, chemistry and oceanography. The variation in the pH values of a biomolecule is often taken as a diagnostic tool while finding the severity of ailment. EC liquid sensors are useful in various biomedical processes requiring pure deionised (DI) and unsalted water [76]. These sensors become very helpful to distinguish between the fluids with unlike polarities by detecting the pH levels, specially the recycled water. A noticeable pH measurement EC sensor is the ion-sensitive field-effect transistor (ISFET)-based sensor [77,78]. In contrast with the conventional FETs, the gate electrode is absent in ISFETs. The gate area in an ISFET is susceptible to the charging effects. A reference electrode biases the gate area above the threshold voltage to let the drain current flow. HEMTs, however, do not require a gate voltage to turn on. Therefore, the fact that the reference electrode is not an essential prerequisite becomes a substantial advantage of HEMTs over the ISFETs. The pH of blood of a well human body varies in the range of 7.35 to 7.45. Any deviation from this scale can be taken as an indicator of ailment with severe effects [79].

GaN based pH sensors show high sensitivity to hydronium ions [80]. Gallium Nitride has a great pH sensitivity of *57.3 mV/pH* [66]. The sensitivity of these sensors is related to the action between ions in the electrolyte on the open region of devices and positive surface charges induced by polarization. This action causes change in the surface charges of the devices. Undoped-AlGaN/GaN has advantages like reduced gate-leakage current, lesser $V_{pinch\text{-}off}$ and lower noise over doped structures due to donor absence in the AlGaN layer. That is why non-modulation doped GaN heterostructures are researched for electronic sensor utilities [13,81].

The ungated HEMTs structure shown in Fig. 14 with Sc_2O_3 in the gated region showed current linearity for pH *3–10*. The pH HEM sensors exhibit stability with a resolution of <0.1pH for the whole pH range and the remarkable sensitivity to fairly small changes in liquid concentration. I-V characteristics depict that with less value of pH, the drain current of HEMTs significantly increases [22].

Abidin *et al.* [13] and Kokowa *et al.* [82] also demonstrated open-gated heterostructures with unpassivated u-AlGaN/GaN. Fig. 15 shows that the variation in pH level cause variation in threshold voltage and drain current. Increase in pH level shifts the threshold voltage to positive side.

Ju-Young Pyo in ref. [83], introduced a HEMT with an extended-gate (EG) with MIS structure for application in pH sensing. Fig. 16 shows the transducer and EG HEMT with low gate leakage MIS structure which can be stabilized, unlike the MS structure, consisting of Schottky junctions. They have reported a linear response of fabricated sensor to different values of pH solutions. Fabricated sensor showed sensitivity close to the Nernst limit, and a linearity of 98.93%.

N. Sharma *et al.* studied the characteristics of pH and salinity sensor fabricated using the gated AlGaN/GaN HEMT structures in phosphate

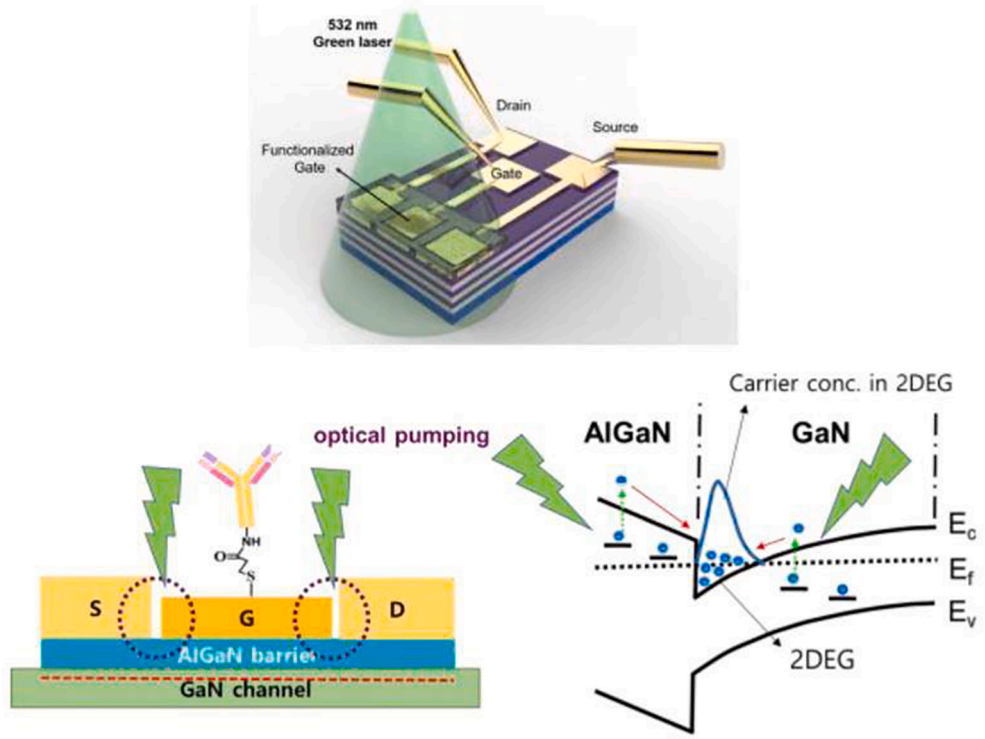

Fig. 12. Schematic diagram and set up of laser illumination and optical pumping to AlGaN/GaN HEMT biosensor and energy band diagram. Reprinted from K. Woo, *et al.*, "Enhancement of cortisol measurement sensitivity by laser illumination for AlGaN/GaN transistor biosensor," Biosensors and Bioelectronics (2020) with permission from Elsevier [74].

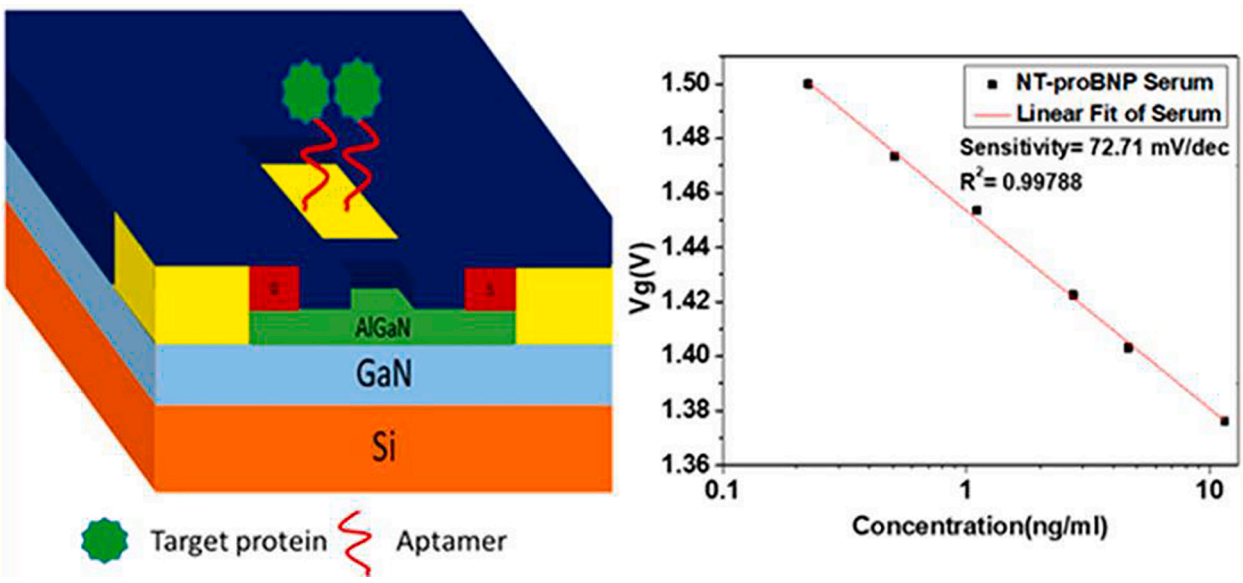

Fig. 13. Schematic diagram and sensitivity of Aptamer functionalized AlGaN/GaN HEMT biosensor. Reprinted (adapted) with permission from Tse-Yu Tai, et al., Design and Demonstration of Tunable Amplified Sensitivity of AlGaN/GaN High Electron Mobility Transistor (HEMT)-Based Biosensors in Human Serum, Analytical Chemistry 2019 91 (9), 5953–5960 [75], Copyright (2019) American Chemical Society.

buffer saline (PBS) and aqueous salt solutions [84]. The HEMT devices in DI water showed drain I –V features, close to the output characteristics of the classic HEMT structures in the air. They observed noteworthy alteration in the I-V characteristics curves signifying the variation in the pH values of PBS solutions. These GaN HEMT structures were susceptible toward the aqueous salt solution and exhibited fast response to the pH changes. A sensitivity of 6.48 mA/mm-molar and a response time of 250–350 ms at $V_{ds} = +1$ V was attained [84].

The possible mechanism of adsorption of positive and negative charges that change the potential at AlGaN/Au and Au/electrolyte surface related to H + concentration is explained by the site binding model introduced by Yates *et al.* and Munch *et al.* [85,86].

In this model, hydroxyl groups at the surface act as amphoters. They could be dependent on the H^+ concentration and the equilibrium constants for the related reactions, in the following method:

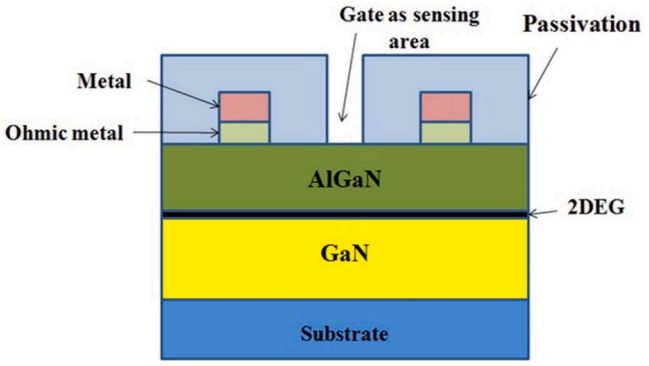

Fig. 14. Ungated AlGaN/GaN HEMT.

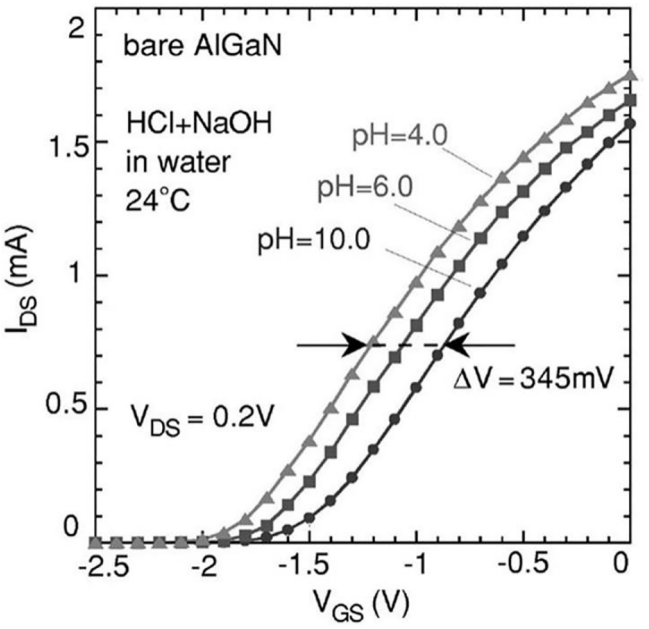

Fig. 15. Transfer characteristics evaluated by Kokawa *et al.* for device exposed in different pH value. "Reprinted with permission from T. Kokawa, T. Sato, H. Hasegawa and T. Hashizume, Liquid-phase sensors using open-gate Al Ga N/ Ga N high electron mobility transistor structure. Journal of Vacuum Science & Technology B: Microelectronics and Nanometer Structures Processing, Measurement, and Phenomena, vol.24, no.4, pp.1972–1976 (2006). Copyright (2006), American Vacuum Society [82].

$$MOH \leftrightarrow MO^{-} + H^{+} \tag{7}$$

$$MOH + H^{+} \leftrightarrow MOH_2^{+} \tag{8}$$

In MOH, M is either Si or metal. Because of increased protonized hydroxyls MOH^{+}_2 formations, 2DEG concentration increases to balance the induced positive charge in the surface. *Vice-versa*, negative charges at the insulator surfaces decrease the H^{+} concentration of the solution. The high sensitivity to hydronium ions of GaN-based pH sensors was reported in [87]. The sensitivity S of the sensors can be regarded as the modification of the surface potential $\psi_0$with dependence on the concentration of hydronium ions $(\Delta C_{H_3O^+})$ in the electrolyte as

$$S = \frac{\Delta\psi_0}{\Delta C_{H_3O^+}} \tag{9}$$

The pH sensitivity S_{pH} can be explained by Eq. (10) as:

$$S_{pH} = \frac{\Delta I_{ds}}{\Delta pH} \tag{10}$$

where ΔI_{ds} is change in drain-to- source current, and ΔpH is the change in pH level.

Q. Cheng *et al.* presented a pH sensor based on a planar dual-gate AlGaN/GaN HEMT cascode amplifier that enhanced the pH sensitivity for about 45 times from 45 mV/pH to 2.06 V/pH with linearity of 1.27%. Their sensor was capable of regulating the sensor's sensitivity by altering the gate voltage and the resistance values for diverse pH values [88].

D. Xue *et al.* demonstrated how to adjust the V_T of the AlGaN/GaN HEMT based pH sensor by the method of the photo-electrochemical (PEC) oxidation on the GaN cap layer surface. Post- PEC oxidation process, the V_T of the device shifted from −3.46 V to −1.15 V. The V_g corresponding to the maximum transconductance of the device shifted from −2.6 V to −0.1 V. The drain current variation per pH of the AlGaN/GaN HEMT based pH sensor without reference electrode increased from 0.7 μA to14 μA with V_d = 0.5 V. They postulated that the sensitivity of this reference electrode sensor can be considerably improved by varying the V_T to make $V_G|g_{mMAX}$ approach the corresponding gate voltage when droplet is put on the sensing window plane. This may be advantageous in the scaling down and integration of the future AlGaN/GaN HEMT pH sensors [89].

Zhang *et al.* analyzed, theoretically and experimentally, the effect of the gate geometry on the pH sensor sensitivity. The series resistance (R_S) of the packaged sensor was established as an important feature limiting the current sensitivity. They found that an optimal W/L ratio, can be reached when W/L = ρ (2DEG)/R_S condition is met. The current sensitivity of the AlGaN/GaN sensor could reach a value of 157 μA/pH [90].

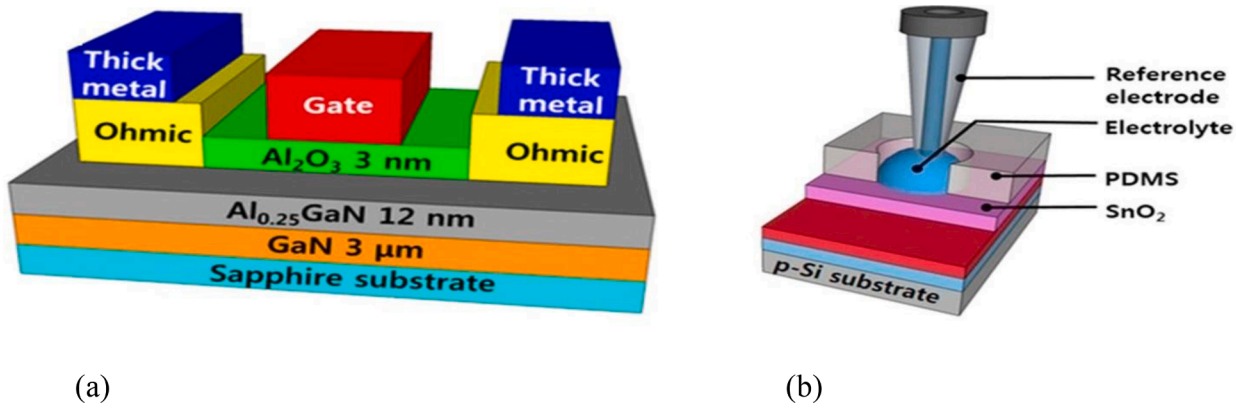

Fig. 16. (a) Schematic of the transducer and (b) extended gate HEMT pH sensor introduced by J-Y Pyo [83]. Reprinted with permission from J. Y. Pyo, *et al.* AlGaN/GaN high-electron-mobility transistor pH sensor with extended gate platform. AIP Advances, 8(8), p.085106 (2018) with licensed under a Creative Commons Attribution (CC BY) license (http://creativecommons.org/licenses/by/4.0/).

Liu *et al.* designed a solid-state biosensor sweat detection platform. The results showed that the Al_2O_3 films and the potassium ion-selective films get modified on different GaN surfaces, as depicted in Fig. 13. The HEMTs can be used repetitively and can stably detect pH and potassium ions in sweat. Their experimental data showed that for pH 3–7, sensitivity was 45.72 μA/pH; for pH 7.4–9, sensitivity was 51.073 μA/pH; K^+ sensitivity was4.94 μA/lgαK^+). They claimed that the stability could be maintained for 28 days. Their experiment was the first verification of AlGaN/GaN HEMTs as steady, quick-response, low-hysteresis, low-cost biosensors with impending application projection in wearable sensors [91].

4.3.2.1. Sensing mechanism. ALD-Al_2O_3 film gets ionized in aqueous solution, forming a binding site on the surface of GaN for pH detection. When an acid or alkali solution is added, two reactions

$$-OH + H^+ = -OH_2^+ \tag{11}$$

And

$$-OH_2^+ + OH^- = -OH + H_2O \tag{12}$$

occur on the surface, and the surface potential can be explain as follows [25,26]:

$$\psi = 2.3\frac{\beta^{'}}{\beta^{'}+1}\left(pH_{Pt,c} - pH\right) \tag{13}$$

Here, $\beta^{'}$ is a constant of acid equilibrium associated with the added electrolyte. The K-ISM modification on the GaN surface is an efficient technique of pushing in K^+ in the PVC layer, as shown in Fig. 17. The K^+ form a barrier that blocks other ions from reaching the sensor surface by chemically reacting with specific ions. Only K^+can go through and transfer their charge to the gate of the HEMT. The source-drain current is explained by the following equation [14]:

$$I_{ds} = \frac{\in_{AlGaN}\mu_{2EG}W}{Ld}\left[\left(V_g - V_t\right)V_{ds} - \frac{V_{ds}^2}{2}\right] \tag{14}$$

where $\in_{AlGaN}$ is the permittivity of AlGaN, μ_{2EG} means the electron mobility of the 2DEG, W and L are the width and length of the channel, d represents the distance between the 2DEG channel and the surface; V_{ds} is the source and drain voltage [91].

4.3.3. DNA sensors

One of the most important applications of biosensors is the DNA analysis [22]. Detection of specific DNA sequences is critical for bacteria detection, medical analysis and other biotechnology and genomics fields. The large numbers of cases of bacterial contamination demand the development of biosensors for detecting bacteria. Optical, changes in mass, EC detection are few of the technologies that have been developed for this. However, these methods are expensive, time consuming, tedious, destructive and use a labelling agent. Biosensors based on semiconductor based field effect transistors are better options to overcome these disadvantages [92].

Spontaneous and piezoelectric polarization make AlGaN/GaN based HEMTs sensitive to variation in surface potential, leading to its suitability for converting a biological signal into an electrical signal [92].

For DNA recognition, arrest of complementary single stranded DNA (ssDNA) on the gate area is essential [18]. Fig. 18 shows the functionization of AlGaN/GaN HEMT for detection of target-ssDNA. Because the DNA molecules are charged, the hybridization of two ssDNA molecules with matching complementary sequence will result in the charge density change on the surface where this hybridization has occurred. This variation in the carrier density results in a modification of the surface potential on the surface [92]. Fig. 19 depicts the threshold voltage shift towards the positive value after DNA hybridization. On using target-DNA, double stranded DNA hybridization takes place. Additional charge varies channel conductivity and onset voltage in FETs [18].

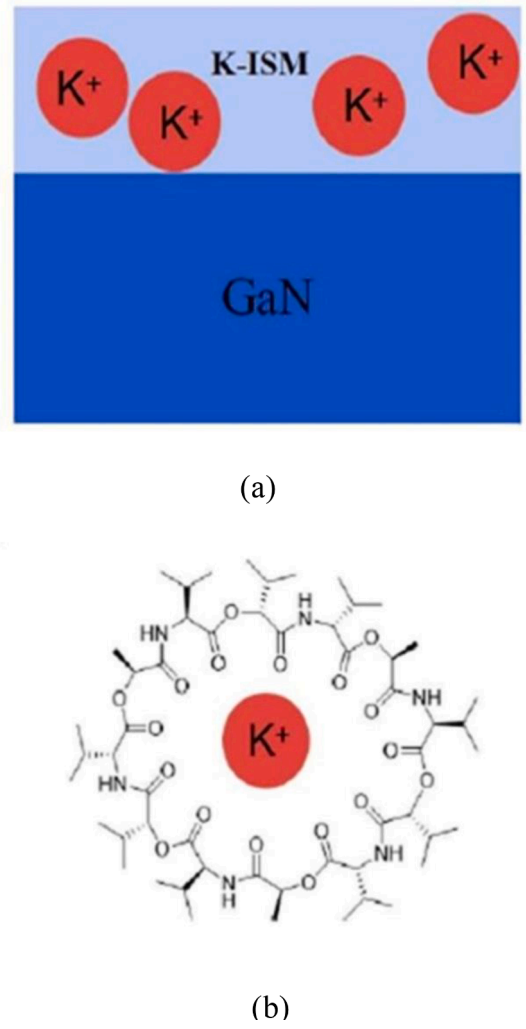

Fig. 17. (a) Modification of GaN surface due to Potassium ions, b) Transportation of potassium ion over GaN by entering in molecule. Reprinted (adapted) with permission from X. Liu *et al.* Wearable Multi-parameter Platform Based on AlGaN/GaN High electron mobility transistors for Real-time Monitoring of pH and Potassium Ions in Sweat, Electro analysis 2020, 32, 422 [91]. Copyright (2020) John Wiley and Sons.

S. Alur *et al.* fabricated GaN heterostructures with TI/AL/Ni/Au ohmic contact and Ni/Au Schottky contacts for the purpose of biosensing. The DNA immobilization on the Au gate was carried out using thiol based chemistry which showed the possibility of DNA detection [92]. N. Espinosa *et al.* successfully detected various target-DNA strengths using AlGaN/GaN HEMTs. With two different density of DNA HEMT gate has bio-functionalized before application of target-DNA [18]. They have concluded that the threshold voltage reduced to − 0.6 V from − 0.5 V when functionalized with probe-DNA.

4.3.4. Botulinum toxin detection

The antibody-immobilized bio detectors have been put in use to sense type-A Botulinum toxin with a reproducible limit of detection below 1 mg/ml. The drain current variation in HEMTs was attributed to bonding of botulinum toxin to the botulinum antibody. The botulinum sensors are eco-friendly, show good rejuvenation, and therefore are best for durable stability training [21]. Schematic of Botulinum Toxin detector is illustrated in Fig. 20. Functionalization of botulinum antibody on thioglycolic acid takes place at Au-coated gate area. Wang *et al.* demonstrated that the sensor could detect the toxin and reactivated right after the test with buffer solution even after 9-month storage. Their

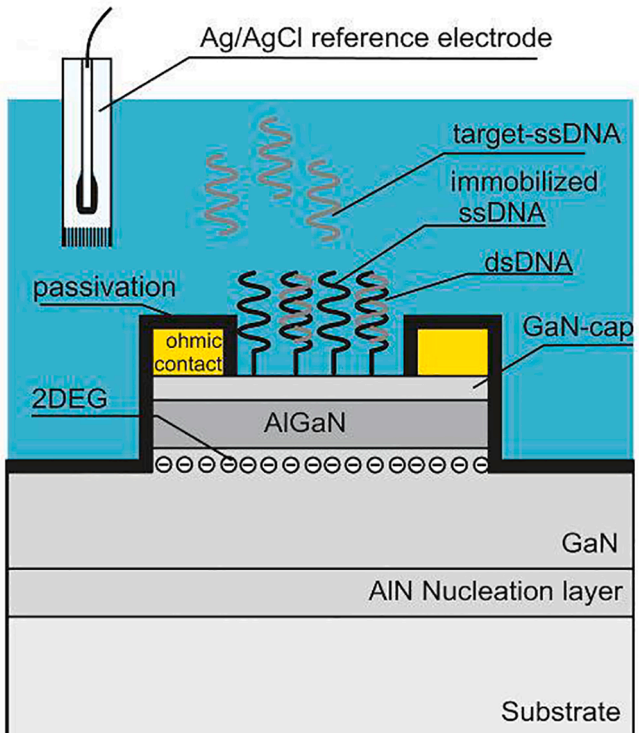

Fig. 18. Functionalization of AlGaN/GaN HEMT for electrical detection of a target-ssDNA [18]. Reprinted from Publication N. Espinosa, S. U. Schwarz, V. Cimalla, O. Ambacher, Detection of different target-DNA concentrations with highly sensitive AlGaN/GaN high electron, Sensors and Actuators B, vol. 210, pp. 633–639, Copyright (2015), with permission from Elsevier.

results are shown in the Fig. 21.

4.3.5. Glucose sensor

The glucose oxides enzyme (GO_x) is used in biodetectors for detection of sugar level in patients. The concentration of glucose varies with the number of electrons that enter the enzyme. The pH value of the solution affects the activity of GO_x. Accurate glucose level can be achieved with a combined pH and glucose detector. A GaN heterostructure with modification of the electrons on the ZnO nano-rods has been demonstrated for measurement of glucose sensing [22]. The schematic is shown in Fig. 22. The response of these HEMTs is same as that of an EC detector, due to amplification effect [22]. Drain current of HEMT drastically increases when ZnO nano rods comes into contact with enzymes which provide higher sensitivity of device.

Varghese *et al.* presented a high resolution AlGaN/AlN/GaN MOS-HEMT for multiple bio detection and sensitivity-analysis. High sensitivity of 0.054 mA/μgml^{-1}, was attained by modification in the device design. Likewise, equivalent gate bias/interface charge was realized for other bio-markers such as PSA (Prostate Specific Antigen), KIM-1 (Kidney injury Molecule), MIG (Monokine Induced by Interferon Gamma) and GO_x. Effective sensitivities of 0.91 mA/μgml^{-1}, 0.254 mA/μgml^{-1}, 0.48 mA/$ngml^{-1}$ and 2.06 mA/$mmoll^{-1}$respectively were attained. The authors fabricated MOS-HEMT device with Al_2O_3 as the gate dielectric prior to the real packaging. The device demonstrated high sensitivity of 1.83 mA/pH [93].

Liu *et al.* fabricated a high sensitivity glucose sensor using GaN based HEMTs. The 3-aminopropyltriethoxysilane (APTES) was aligned to the GaN surface by forming the covalent linkage between them. The negatively charged gold nanoparticles (AuNPs) could be effectively self-assembled on the positively charged APTES surface. The morphology of the immobilized AuNPs was observed by the field emission scanning electron microscope (FE-SEM). The chemical groups after APTES/AuNPs functionalization were confirmed by X-ray photoelectron spectroscopy (XPS). GO_x was immobilized on the APTES/AuNPs functionalized gate surface through electrostatic attraction. Its complete function process is depicted in Fig. 23. The glucose sensor exhibited wide detection ranges from 0.001 to 9 mM with higher sensitivity of above 1×10^6 μA mM^{-1} cm^{-2} A fast response time of less than 8 s and a detection limit of 1 nM was observed. The authors verified that, the performance can be increased by 15% after AuNPs attachment as compared to the HEMT sensor without AuNPs. The Michaelis-Menten constant KM^{app}, indicating high affinity of GO_x to glucose, was computed as 0.06 mM [94].

J. Liu *et al.* also fabricated a highly sensitive glucose sensor based on HEMTs. As depicted in Fig. 24, the hydroxyl groups on the GaN surface were result of the decomposition of UV irradiated hydrogen peroxide solution (H_2O_2) [95]. The self-assembled monolayers (SAMs) of APTES formed on the hydroxylation plane were used for GO_x arrest. The

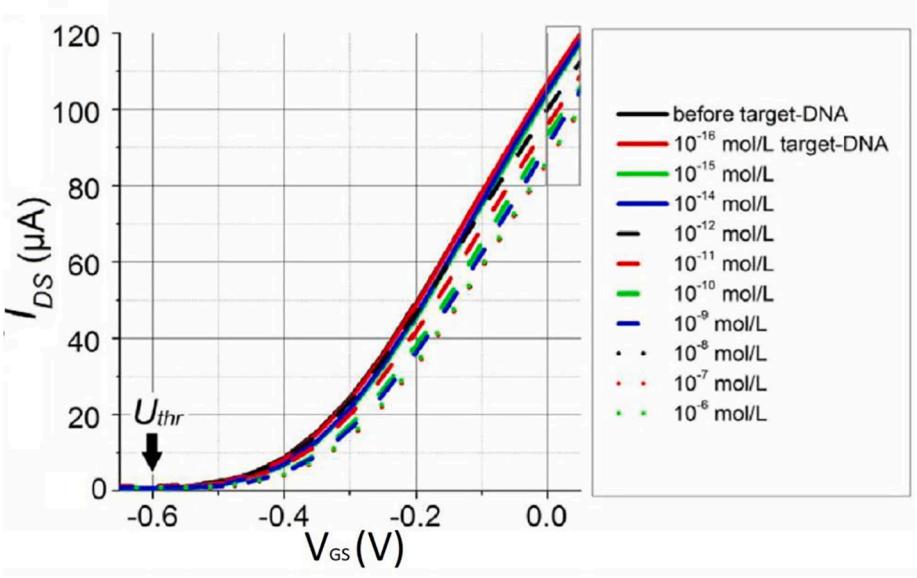

Fig. 19. Transfer characteristics and change threshold voltage before and afterDNA hybridization[18]Reprinted from Publication N. Espinosa, S. U. Schwarz, V. Cimalla, O. Ambacher, Detection of different target-DNA concentrations with highly sensitive AlGaN/GaN high electron, Sensors and Actuators B, vol. 210, pp. 633–639, Copyright (2015), with permission from Elsevier.

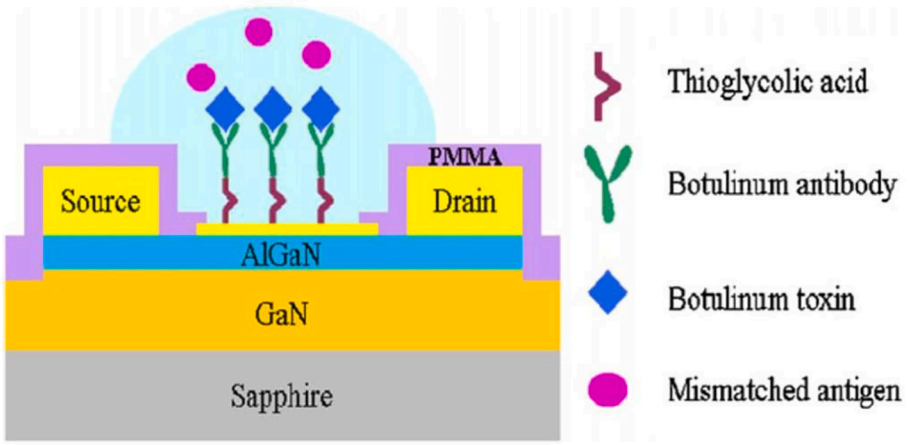

Fig. 20. Schematic of AlGaN/GaN HEMT sensor with functionalization of botulinum antibody on thioglycolic acid at Au-coated gate area. Reprinted from Publication [21] Y. Wang, B.H. Chu, C.Y. Chang, C.F. Lo, S.J. Pearton, A. Dabiran, P.P. Chow, F. Ren, Long-term stability study of botulinum toxin detection with AlGaN/GaN high electron mobility transistor based sensors, Sensors and Actuators B, vol. 146, pp. 349–352, (2010), Copyright (2010), with permission from Elsevier.

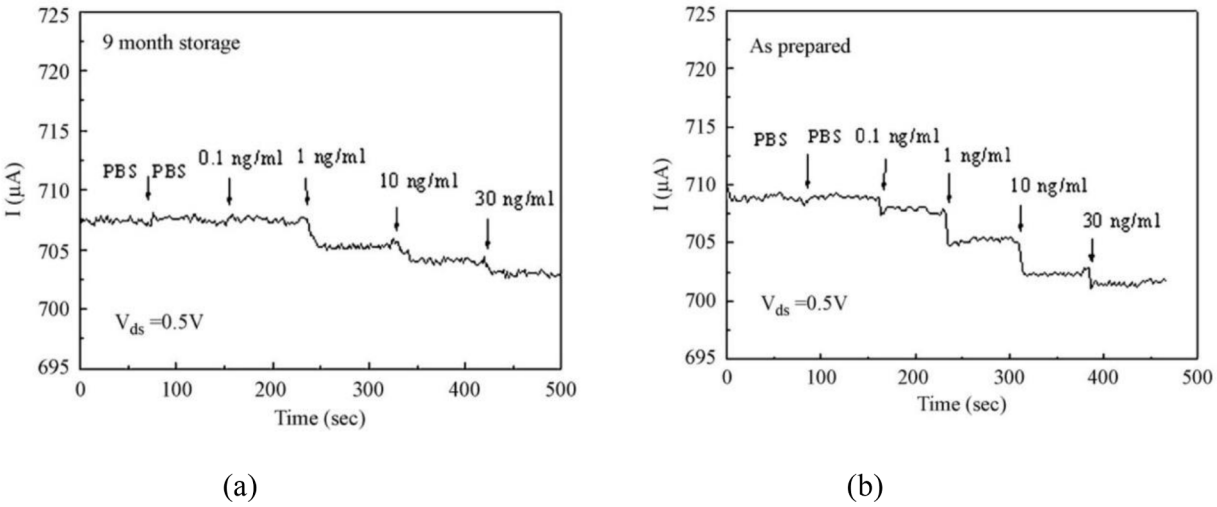

Fig. 21. Real time detection of botulinum toxin with (a) a fresh sensor and (b) the recycled 9-month-stored sensor. [21] Reprinted from Publication Y. Wang, B.H. Chu, C.Y. Chang, C.F. Lo, S.J. Pearton, A. Dabiran, P.P. Chow, F. Ren, Long-term stability study of botulinum toxin detection with AlGaN/GaN high electron mobility transistor based sensors, Sensors and Actuators B, vol. 146, pp. 349–352, (2010), Copyright (2010), with permission from Elsevier.

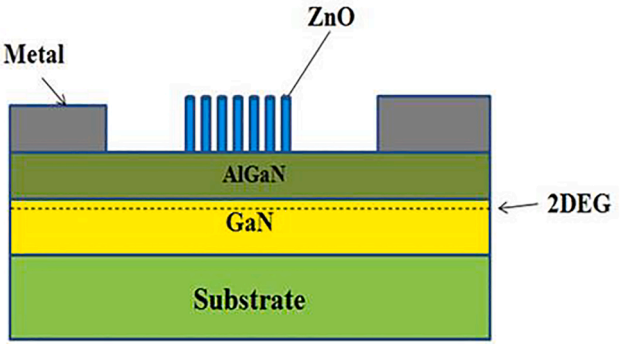

Fig. 22. Schematic of ZnO Nanorod functionalized HEMT.

functional process is graphical depicted in Fig. 25. The APTES/GO_x biosensor demonstrated excellent current response to glucose over a linear range from 10 to 100 μM with a sensitivity of 3.15 × 10^4μA mM^{-1} cm^{-2} and a detection limit of 10 nM.

4.4. Gas sensor

Modification in the electrical conductivity of the gas sensors occurs on gas contact with the semiconductor surface of the device, making it compatible for wireless monitoring. The GaN-based material systems' mechanical and chemical robustness enables reliable gas detection at high temperature operations.

FETs, Schottky diodes and MOS structures with catalytic Pd and Pt electrodes gas sensors have been extensively investigated. Pt and Pd catalytic activity of GaN in the presence of several ecologically significant gases, such as CO, NO_x, hydrogen or hydrocarbons is an interesting property for the gas-detection electronics. AlGaN/GaN heterostructure armed with such a catalytic gate contact can be used in high frequency applications and is fit to be fantastic detector for gases in its proximity [96].

The Internet of Things (IoT) is a *network of physical objects that utilizes sensors and application programming interfaces (APIs) to collect and exchange data over the internet* [97]. IoT network requires ultra-low power, low cost, long lifetime, integrable into electronic circuits, and mini-sized gas sensors for remote air quality monitoring and enhanced automated system. EC gas sensors fulfill the criteria required by IoT platforms and

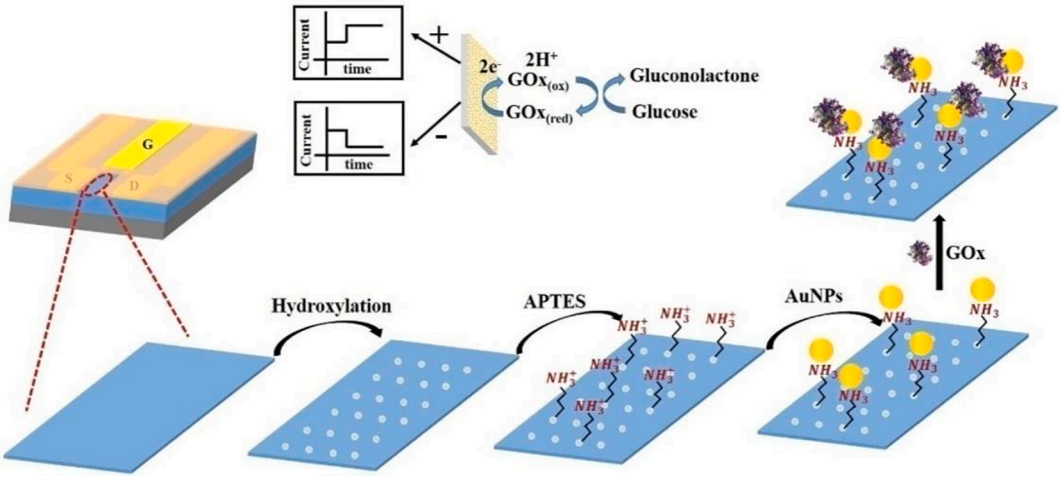

Fig. 23. Graphical representation of functionalization process of APTES, AuNPs and glucose detection with AlGaN/GaN HEMT. Reprinted from J. Liu, H. Zhang H, X. Xiaochuan, A. Ahmad, D Xue, H Huang H, N Xu, Q Xi, W Guo, H Liang, "High sensitivity detection of glucose with negatively charged gold nanoparticles functionalized the gate of AlGaN/GaN High Electron Mobility Transistor," Sensors and Actuators: A. Physical (2020), Copyright (2020), with permission from Elsevier [94].

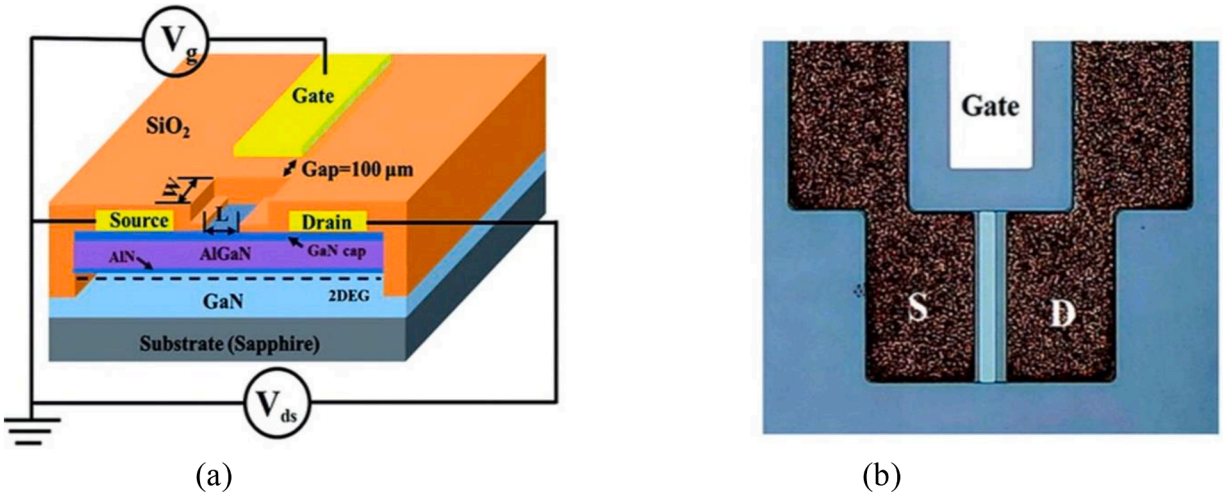

Fig. 24. (a) Schematic structure of AlGaN/GaN HEMT for glucose detection. (b) micrograph of the fabricated HEMT sensor. Reprinted from [95] J. Liu, H. Zhang, D. Xue, A. U. Ahmad, X. Xia, Y. Liu, H. Huang, W. Guo and H. Liang, "An effective hydroxylation route for a highly sensitive glucose sensor using APTES/GOx functionalized AlGaN/GaN high electron mobility transistor," RSC Adv., **10**, 11393, (2020). Copyrights (2020), with permission fromThe Royal Society of Chemistry.

thus can be suitable components for specific IoT applications like smart city, smart home, smart parking system etc. [98,99]. Kumar *et al.* incorporated toxic gas sensors into a multi-purpose field surveillance robot which uses multiple IoT cloud servers [100]. High performance gas sensors are utilized in IoT-based vehicle emission monitoring systems [101]. Furthermore, wireless sensor networks (WSNs) have been engaged for toxic gas area recognition in large-scale petrochemical industries [102]. But, the gas sensing performances heavily vary with scaling of sensor and its components. Therefore, research on miniaturized gas sensors may expedite the deployment of toxic gas sensors in the IoT platforms [103].

4.4.1. *Hydrogen sensor*

Ambient temperature hydrogen gas-leak sensing is essential for applications in hydrogen-driven vehicles, proton exchange thin film, hydrogen oxide energy cells for spaceships *etc.*, as high concentration of Hydrogen gas is explosively combustible. Characteristically, HEMTs with a higher drain current exhibit better sensitivity for the gas detection in oxygen-restricted or humid atmospheres.

In the traditional sensors, the variation in the conductivity or resistivity of sensing material is used for gas detection. However, variation in conductivity can be amplified through SD or FET operation by incorporating Pd or Pt metal on the gate electrode of the HEMTs. When hydrogen molecules come into contact with large area of platinum nanonetworks surface of HEMTs, they get dissociated into hydrogen ions, effectively creating high positive charge. At room temperature, H_2 is adsorbed on Pt and Pd and separated as follows:

$$H_{2(ads)} \rightarrow 2H^+ + e^- \tag{15}$$

The separated hydrogen sources a change in the channel conductance, making the sensors exceptionally sensitive. This improves 2DEG channel and drain current. Employing the surface roughening of active area shows high sensitivity toward hydrogen detection because of adsorption sites. These sensors also have a wide vibrant variety of the sensing concentration. Besides, a reference semiconductor device with covered surface may be designed along side with sensor to remove the ambient temperature deviation and supply voltage instability [104].

Schottky diodes on GaN heterolattices, adept to operate at extreme

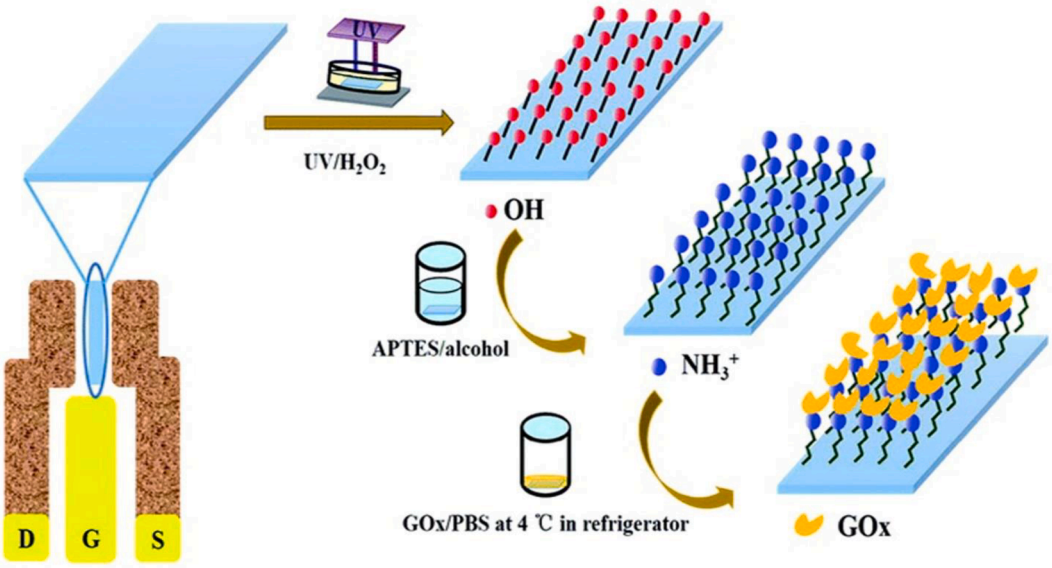

Fig. 25. Functionalization process on the AlGaN/GaN HEMT sensor. Reprinted from J. Liu, H. Zhang, D. Xue, A. U. Ahmad, X. Xia, Y. Liu, H. Huang, W. Guo and H. Liang, "An effective hydroxylation route for a highly sensitive glucose sensor using APTES/GOx functionalized AlGaN/GaN high electron mobility transistor," RSC Adv., **10**, 11393, (2020). Copyrights (2020), with permission from The Royal Society of Chemistry [95].

thermal conditions (~800 °C) were demonstrated by Song *et al.* with Pt catalytic metal [105]. According to Kim *et al.,* improvement in the sensitivity could be achieved as reported in Fig. 26 with Pt nano-networks having vast surface-to-volume proportion as shown in Fig. 27(a), and (b) [106,107].

In Non-polar or semi-polar GaN crystal planes, each crystal plane has a specific surface atomic plan, which leads to varying hydrogen-reactivity. Wang *et al.* found that the GaN Schottky diodes with c-plane N-polar (*0 0 0 1*) structure had greater sensitivity for hydrogen sensing as compared to the conventional Ga polar (*0 0 0 1*) structures. This finding is supported by earlier density functional theory summarizing much more affinity of hydrogen to nitrogen [108]. Further, sandwiching an AlN interlayer in AlGaN/AlN/GaN HEMT structure results in higher mobility and more charge concentration than the conventional AlGaN/GaN HEMTs [108,109].

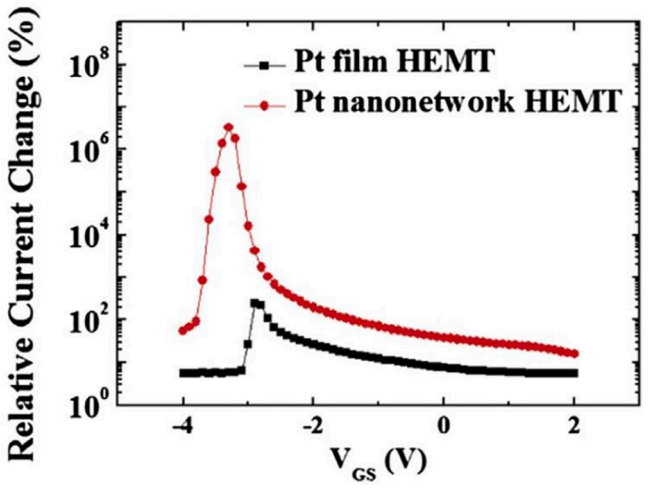

Fig. 26. Relative current change, S of Pt nanonetwork and Pt film gated HEMTs measured at VDS of 6 V under air and 500 ppm H2 in air ambient at 25C [107]. Reprinted from Publication H. Kim and S. Jang, AlGaN/GaN HEMT based hydrogen sensor with platinum nano-network gate electrode, Current Applied Physics, vol.13,no.8, pp.1746–1750 (2013), Copyright (2013), with permission from Elsevier.

Song *et.al* proved experimentally that the best sensing response was obtained at V_g equal to threshold voltage and the sensing response improved with temperature rise [105]. It was shown that the sensing response and logarithm of hydrogen concentration for certain values, are linearly related. For 10 times change in hydrogen concentration, the sensor showed response variation of 25.8% at 130 °C.

Ryger *et al.* grew an undoped SAW GaN/AlGaN/GaN heterostructure to evaluate sensory characteristic [110]. The sensor exhibited very good stability for observing hydrogen leakage at ambient temperature. GaN's PE coefficient makes it suitable for on wafer integration with SAW sensors for multi-sensing array digital signal processing.

K. H. Baik *et al.* [111] applied Pt nanonetworks on active gate area of HEMT to improve the conventional GaN based hydrogen sensor devices as shown in Fig. 27(b). With changes in the conventional Pt GaN HEMT, Baik reported maximum change in current percentage $3.3x10^6$ % at V_{GS} of -3.3 *V*. Later, they demonstrated an AlGaN/GaN-based hydrogen gas sensor set with a modest heat compensation assembly to make the hydrogen sensing ability independent of the ambient temperature. The hydrogen molecules decomposed only on the Pt diode of the device assembly when it was exposed to H_2 ambient. Thus, the ambient temperature effect on the output signal was compensated. The sensor demonstrated a stable output voltage change of 0.635 V for the temperature variation from 25 °C to 200 °C at the 5 V constant input bias. The serially connected diode pair, displayed delicate voltage response to 500–5000 ppm hydrogen exposure at 25 °C [112].

S. Jung *et al.* fabricated HEMT with polymethyl methacrylate (PMMA) membrane layer for investigation of hydrogen in dry and wet environment [113]. They found highest sensitivity of 2.6×10^5% for *500* ppm hydrogen.

Choi *et al.* fabricated a Pd-functionalized H_2 sensor on an AlGaN/GaN-on-Si heterostructure platform [114]. The sensor response was augmented by low standby current level due to the AlGaN layer under the Pd catalyst area, partially recessed by plasma etching. Operating condition dependent sensor stability and power consumption were cautiously explored with two separate bias modes *viz.* constant voltage and constant current. The authors inferred that the constant current bias operation resulted in stable operation with lesser standby power expenditure. The fabricated AlGaN/GaN-on-Si H_2 sensor displayed a response of 120% with a response time of less than 0.4 s at 200 °C and a standby power spending of 0.54 W/cm^2. The schematic and the details

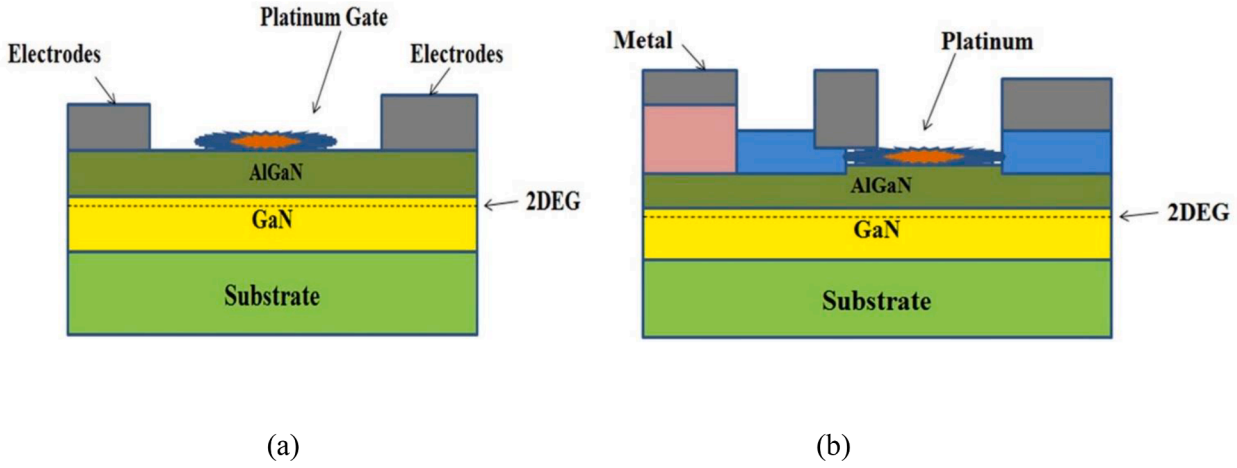

Fig. 27. Schematic diagram of (a) Pt film with nano-networks AlGaN/GaN diode, (b) Pt nanonetwork gated AlGaN/GaN HEMT for Hydrogen Sensor.

of the device fabricated by Choi *et al.* are shown in Fig. 28 (a) and (b). We observe from Fig. 28 (c), that the effect of hydrogen gas on the Schottky barrier height affects the current response.

G. H. Chung demonstrated a hydrogen sensor with SiN_x passivation layered HEMT in extreme environment like high temperature and energetic irradiation [115].

4.4.2. O_2 sensor

Oximetery- the current technology for O_2 measurement, is suitable for medical use. However, it does not completely gauge the respiratory adequacy. A patient suffering from poor gas exchange in the lungs i.e. hypoventilation, if given 100% oxygen shall have superb blood oxygen levels but may still be ailing due to excessive CO_2. The O_2 measurement is also not a full evaluation of circulatory adequacy.

Presently available ZrO_2 or the semiconductor metal oxide (TiO_2, Nb_2O_5, $SrTiO_3$, CeO_2) based O_2 sensors can function at extreme temperatures from 400 to 700 °C [22]. Development of a small, low cost O_2 sensor with operation at low temperature and with high sensitivity for biomedical applications is need of the hour [104]. The conductivity mechanism of most metal oxides based semiconductors is attributed to electron hopping from intrinsic defects in the oxide layer. Intrinsic defects are associated with the oxygen vacancies created during oxide growth. Characteristically, the conductivity is directly proportion to the concentration of oxygen vacancies in the oxide coating. The conductivity of the InZnO (IZO) is found to depend on the oxygen partial pressure during oxidation. IZO is a potential contender for O_2 detection. Fig. 29 (a) shows the schematic of O_2 detector. Fig. 29 (b) and (c) depict the device response when tested at 120 °C in pure nitrogen and pure oxygen alternately at V_{ds} = 3 V. The current I_{ds} is reduced when the device is exposed to oxygen. However, the current increased when the device is exposed to nitrogen. Since the IZO film can supply a lot of oxygen vacancies, it can sense oxygen and thus can generate a potential on the gate region of the AlGaN/GaN HEMT. IZO based oxygen detector with high sensitivity can operate at a comparatively lower temperature than many oxide-based oxygen sensors [104].

4.4.3. NO_2 sensor

Nitrogen dioxide (NO_2) is a harmful air pollutant gas which is associated with daily-need combustion sources. In long-term, it can lead to development of asthma and hamper lung growth of users and thus warrants development of sensors for detecting even low concentration of NO_2. AlGaN/GaN HEMT is one good option. Relative humidity helps in sensing of NO_2 when exposed to AlGaN. Positive surface charge is formed by water molecules on AlGaN, thus increasing the conductivity of channel upon gas contact. This positive charge is counterbalanced by NO_2, causing reduction in the charge carrier density (CCD). Consequently, current through 2DEG channel decreases. This concept is put to use in continuous ultra-low-power air pollution checking, at an ambient

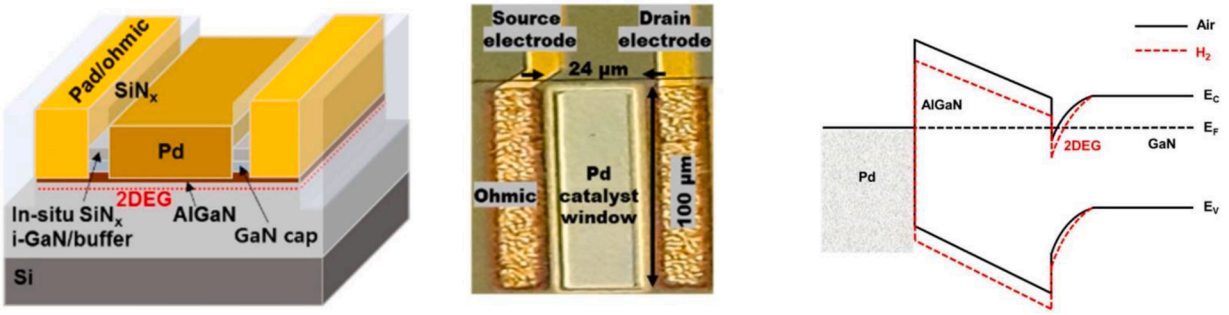

Fig. 28. (a) Hydrogen sensor based on Pd- AlGaN/GaN schematic, (b) Fabricated sensor's microscopic view and (c) Energy band structure with hydrogen absorption. Reprinted from J.-H. Choi, *et al.*, "Investigation of Stability and Power Consumption of an AlGaN/GaN Heterostructure Hydrogen Gas Sensor Using Different Bias Conditions," *Sensors*, *19*, 5549, (2019) under the conditions of the Creative Commons Attribution (CC BY) license (http://creativecommons.org/licenses/by/4.0/) [114].

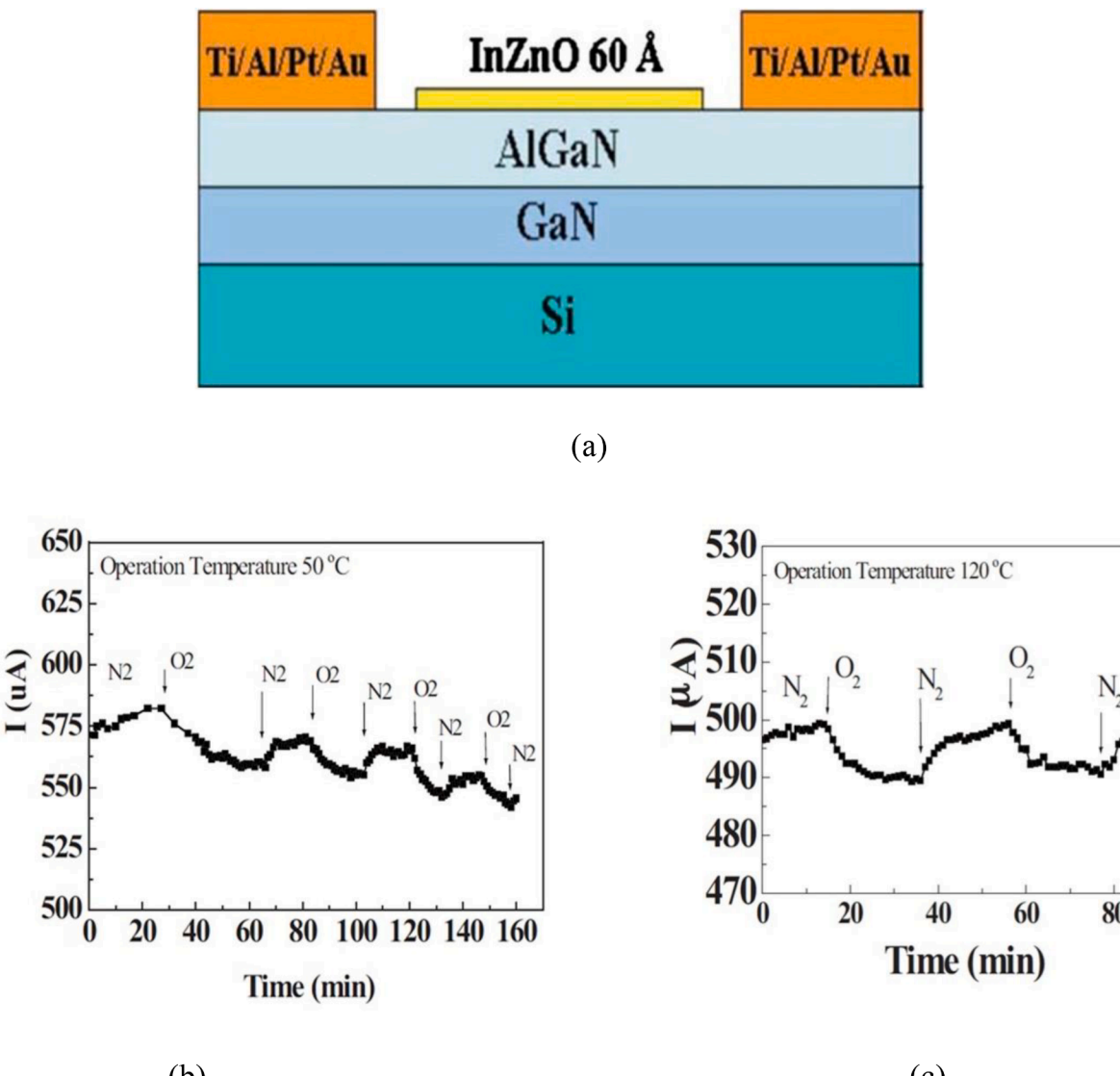

Fig. 29. (a) Schematic of O_2 sensor HEMT, current response of N_2 and O_2 (b) at 50 °C, (c) 120 °C. Reprinted with permission from Y-L. Wang, *et al.*, "Oxygen gas sensing at low temperature using indium zinc oxide-gated AlGaN/GaN high electron mobility transistors," Journal of Vacuum Science & Technology B 28, 376 (2010) Copyright [2010], American Vacuum Society [104].

temperature and at varied humidity range of 10% [116].

Fig. 30 shows the schematic of interdigitated two-terminal AlGaN/GaN sensor for NO_x where chemically stable GaN is prepared to permit ultra-low power, low ppb level sensing sans warmers.

Y. Halfaya reported AlGaN/GaN HEMT with Pt catalyst for NO, NO_2 and NH_3 gas sensing in harsh environment of diesel exhaust system [117]. They have demonstrated that their devices can trace miniscule variations in the gas concentrations, even for contact duration as low as 1 s. Fig. 31 shows fabrication details and the schematic of one of the device with two different sized gate areas. They have reported higher sensitivity at 600 °C than that at 300 °C and lower responsivity at higher temperature as shown in Fig. 32.

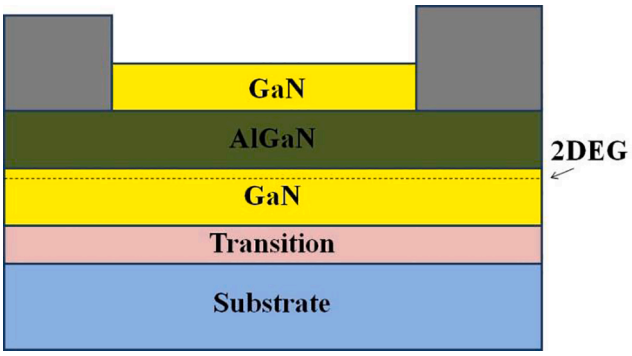

Fig. 30. Interdigitated two-terminal AlGaN/GaN sensor for NO_x.

Ranjan *et al.* demonstrated low concentration sensing of NO_2 at temperature range of 30 °C–300 °C and relative humidity from 0% to 90% by GaN HEMT-based gas detectors having interdigitated electrodes and a platinum (Pt) functionalization layer [118]. The sensors revealed by them displayed a change in current of 0.5 mA with sensitivity of 1.2% for 10 ppm of NO_2. They have investigated influence of humidity on NO_2 sensitivity at room temperature and found that the sensitivity is directly proportionate to relative humidity.

Sun *et al.* used a tungsten trioxide (WO_3) nano-film modified gate of a GaN HEMT based sensor for NO_2 sensing. The sensor had a hanging round film arrangement and incorporated a micro-heater. For a 1 ppm NO_2 gas, a sensitivity of 1.1% and a response time of 88 s were obtained. The dependence on relative humidity and temperature on the response

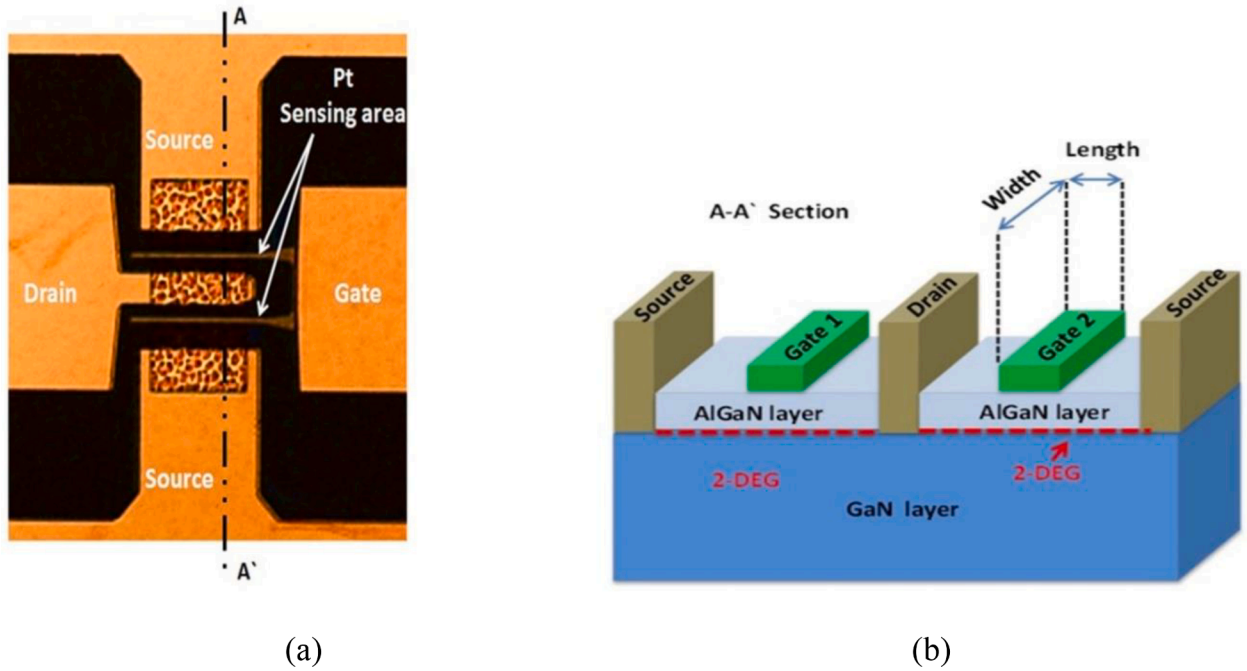

Fig. 31. (a) Fabricated device (b) Schematic of HEMT with different sensing area dimensions. Reprinted from Y. Halfaya *et al.*, Investigation of the performance of HEMT-based NO, NO_2 and NH_3 exhaust gas sensors for automotive antipollution systems. Sensors, 16(3), p. 273 (2016) [117], under the Creative Commons Attribution License.

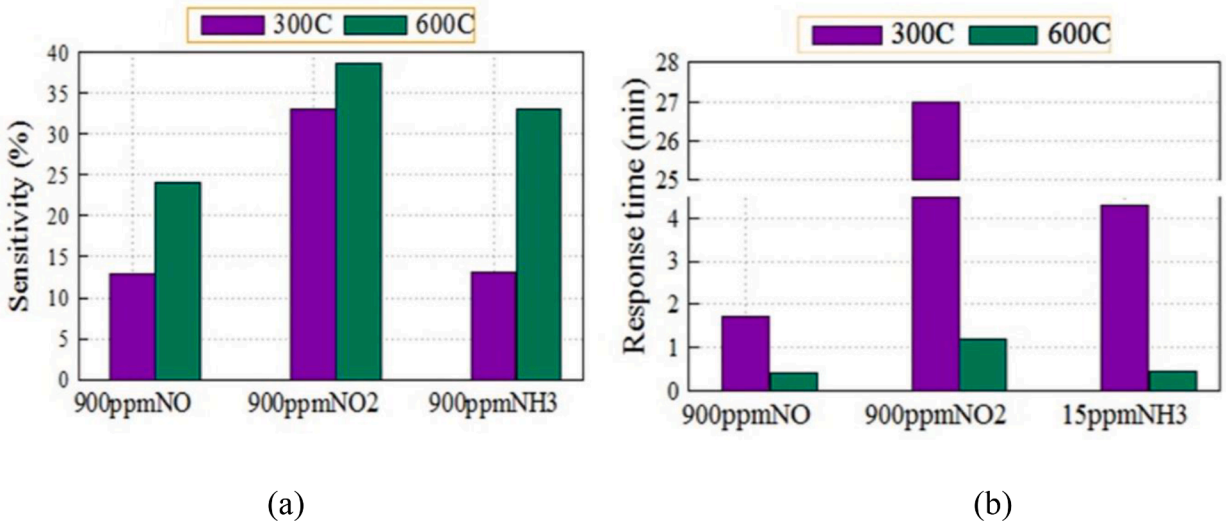

Fig. 32. (a) Sensitivity and (b) Responsivity reported by Halfaya *et al.* at different temperatures for NO, NO_2 and NH_3. Reprinted from Y. Halfaya *et al.*, Investigation of the performance of HEMT-based NO, NO_2 and NH_3 exhaust gas sensors for automotive antipollution systems. Sensors, 16(3), p.273 (2016), under the Creative Commons Attribution License.

characteristics of the gas detector were taken into consideration. The device was found suitable for constant environment measuring under elevated temperatures [119].

The authors later micro fabricated and characterized a similar structure for ppm-level acetone gas sensing. High operating temperature of 300 °C augmented the sensitivity to 25.7% and drain current changed to 0.31 mA for 1000-ppm acetone in dry air. [120]

When the sensors are bared to NO_2 gas, chemisorption reaction on the WO_3 surface cause gas ions to rapidly diffuse at the surface. NO_2 gas gets adsorbed on the surface of WO_3 layer and reacts with adsorbed O^- ions as per the reaction shown below [121]

$$NO_2(gas) + e^- NO_2^-(ads) \tag{16}$$

$$NO_2^-(ads) + O^-(ads) + 2e^- NO(gas) + 2O^{2-}(ads) \tag{17}$$

The surface states are transformed by the polar NO_2 molecules, which influence the 2DEG concentration, causing deviation of the drain current of the HEMT device. The modified surface potential may be expressed by the Helmholtz model as follows [81]:

$$\Delta V = \frac{N_S p(cos\theta)}{\varepsilon\varepsilon_0} \tag{18}$$

where N_S is the dipole density per unit area, p is the dipole moment, θ is the angle between the dipole and the normal surface, ε is the relative permittivity of the material, and ε_0 is the free space permittivity. The

value of $\frac{p}{\varepsilon}$ of the polar molecules mainly governs the surface potential.

Nguyen *et al.* investigated the performance of AlGaN/GaN HEMT based NO_2 gas sensors with 10 nm AlGaN barrier. Their sensors, as shown in Fig. 33, were planned to operate in μA range to give good sensing performance with reduced power expenditure. The Pd and Pt catalyst layer were used to functionalize the gate region of the HEMT sensor for NO_2 sensing. Pd-functionalized sensors depict superior sensing properties as compared to the Pt-functionalized sensors. The sensors when exposed to 100 ppm of NO_2 at 300 °C, measured relative sensitivity of 53% with the response and recovery times of 136 s and 196 s respectively. In addition, there was a considerable change in the drain current in different concentrations of 10 to 100 ppm NO_2 for 30 s exposure duration. The authors inferred that the Pd-AlGaN/GaN HEM sensors with a thin barrier were able to detect NO_2 gas and they could be used in the harsh environment in real-time condition [122].

4.4.4. Carbon monoxide (CO) sensor

Silent Killer– is another name for Carbon monoxide (CO). It is a poisonous and deadly gas generated by fuel burning. It has no colour, no taste and no smell. Hence, it is barely discernible by humans. It can be fatal within no time at concentrations above 6000 ppm. On contact, CO gas restrains the attachment of oxygen with carboxyhaemoglobin (COHb) of the red blood cells (RBC) due to its higher affinity (~200 times) towards COHb in contrast to the oxygen. It lessens the valuable oxygen transfer and causes oxygen deficiency in the person leading to fatal histo-toxic hypoxia. Hence, the development of a low-cost, reliable and stable CO detector sensing between 70 and 100 ppm concentrations within 2–5 min of exposure can be a life saving tool for many.

Characteristics properties of GaN allow its potential application in the field of developing toxic-gas detectors operable under harsh circumstances over the traditional metal oxide based gas sensors [123-125]. In addition, the biocompatibility of these materials makes them environment friendly. GaN based CO sensors operating at temperatures above 300 °C, with performance enhancing Pt catalysts, have been reported in references [126–129]. Fig. 34 represent the change in the barrier height ϕ_{SCO}, the interfacial polarization, the SCR width W_{CO} when CO gets absorbed in Pt. The working requirements at high-temperature and prerequisite of expensive Pt catalyst remain difficult hindrances in the progress of GaN based CO sensors. Hence, a catalyst-free low temperature operating CO sensor is desired for advancement in the future of GaN based technology. Mishra *et al.* fabricated catalyst-free CO sensors operating at lower temperature developed by nano-structured AlGaN/GaN heterostructures using their remarkable surface and interfacial properties. Catalyst-free sensing operation is represented in Fig. 35. The measurements revealed a sensitivity of 33% at 100 °C with response and recovery times of 94 s and 44 s respectively. Their in-depth investigation divulged that nanostructured surfaces with lower barrier height, charge buildup and higher amount of surface native oxide increase CO adsorption and give effective and optimal sensing. Alternatively, hydroxyl species (OH^-) associated with water vapours act as electron donor and thus cause an unfavorable outcome of CO detection [130]. Hence, the CO detection can be improved in dry environment with least quantity of the adsorbed hydroxyl species. The change in resistance ΔR associated with CO sensing is measured and considered in computing of sensitivity of the designed sensor.

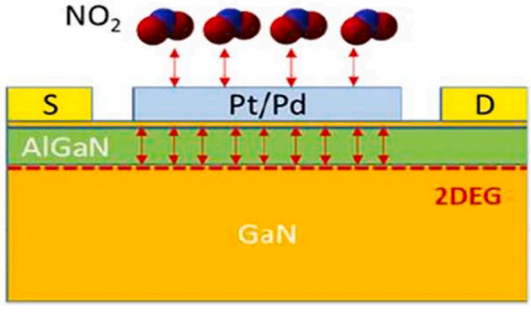

Fig. 33. Schematic of NO_2 gas sensing mechanism in AlGaN/GaN HEMT. Reprint permission from C. V. Nguyen and H. Kim, "High Performance NO_2 Gas Sensor Based on Pd-AlGaN/GaN High Electron Mobility Transistors with Thin AlGaN Barrier," Journal Of Semiconductor Technology And Science, Vol.20, No.2, (2020), under the terms of the Creative Commons Attribution Non-Commercial License (http://creativecommons.org/licenses/by-nc/3.0/) [122].

4.4.4.1. Sensing mechanism. The performance of gas sensors is ruled by the chemical states of chemisorbed oxide. Formation of amorphous oxide (Ga-O) films happens when the GaN layer is exposed to atmospheric oxygen.

$$\frac{1}{2}mO_2 + (vacantsite) + e^- \xrightarrow{k} O_m^- \tag{19}$$

The chemisorbed oxygen present in O^-, O^{2-} and O^{2-} bonding state are the essential components at the back of CO sensing system. When GaN surface with O^{2-} species contacts the CO molecule, the CO adsorption causes transfer of electron to chemisorbed oxygen which releases the e^- occupied from the GaN layer. The released electron becomes a part of conduction band resulting in a reduction in resistance across the surface as shown in following equation [130]:

$$O^{2-} + CO \rightarrow CO_2 + e^- \tag{20}$$

4.4.5. H_2S gas sensors

Harsh industrial environment requires high temperature compatible H_2S sensor. Sokolovskij *et al.* designed and fabricated a H_2S gas sensors based on Pt- AlGaN HEMT [131]. They have tested their device in concentration of H_2S from *80* ppm to *0.5* ppm and reported high sensitivity order of 10^3% at ppm level of H_2S gas concentration.

Devices fabricated by Zhang *et al.* demonstrated sensing signal saturation at 30 ppm H_2S exposure. They reported the response of gas sensor with and without H_2 pre-treatment at 250 °C, as shown in Fig. 36. The H_2 treated H_2S gas sensor sensed an elevated H_2S concentration of 90 ppm without complete saturation at 250 °C [132].

Shahbaz *et al.* investigated GaN/GaInN QWs as optical transducers for the H_2S sensing. The QW photoluminescence (PL) is sensitive to changes in the sensor surface potential. A rise in the quantum confined Stark effect in the QW is caused by near-surface band bending as a result of the adsorption of H_2S on the Au cover layer. This rise leads to a red shift in its luminescence. This phenomenon is expected to distinguish presence of small amounts of H_2S in a person's breath for early disease diagnosis. The authors detected a concentration of 0.01 ppm of H_2S in nitrogen [133].

4.4.5.1. Sensing mechanism. The likely reaction mechanism of H_2S adsorption in air ambient is as follows [132]:

$$H_2S_{(ad)} + SH_{(ad)} + H_{(ad)} \tag{21}$$

$$SH_{(ad)} \rightarrow S_{(ad)} + H_{(ad)} \tag{22}$$

$$S_{(ad)} + O_{2(ad)} \rightarrow SO_{2(gas)} \tag{23}$$

The S-H bonds are broken sequentially as illustrated by eq. (21) and eq. (22). The residual sulphur reacts with O_2 near the Pt surface and forms SO_2. The hydrogen ions rapidly diffuse through the Pt to the M−S interface. Interfacial oxide layer present on the GaN surface provides bonding sites for the diffused H resulting in a dipole layer at the junction. The layer reduces metal work function ϕ_m and lowers the barrierϕ_b, leading to the changed ΔV_t and increase in drain current in H_2S ambient. To assess the performance of the Pt-HEMT based H_2S sensor, the sensing response is taken as:

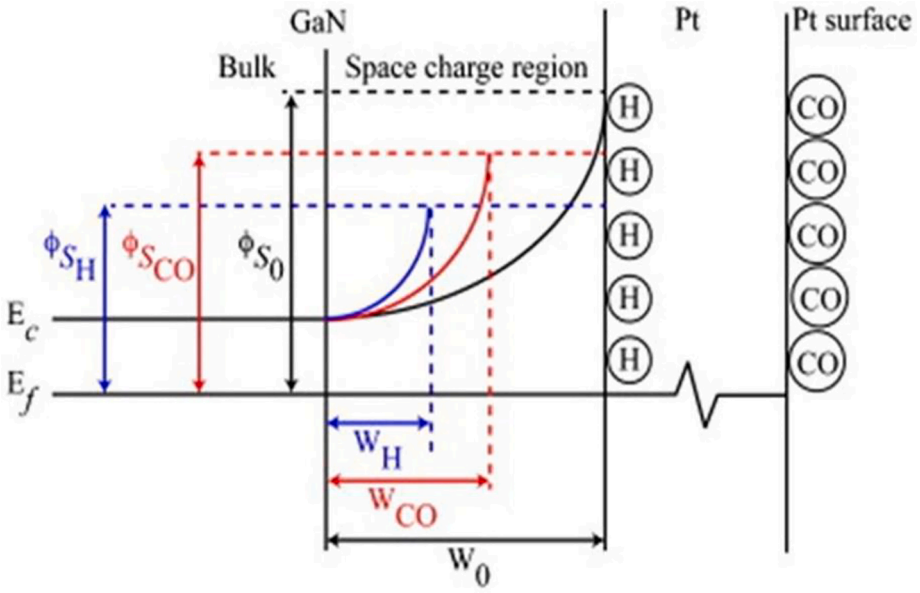

Fig. 34. The Change in interfacial polarization, the barrier height, ϕ_{SCO}, and the SCR width, W_{CO}, When CO adsorbs on the surface of Pt [127].“Reprinted from Publication B.K. Duan, P.W. Bohn, Response of nanostructured Pt/GaN Schottky barriers to carbon monoxide, Sensors Actuators A,vol. 194, p. 220, (2013)., Copyright (2013), with permission from Elsevier.

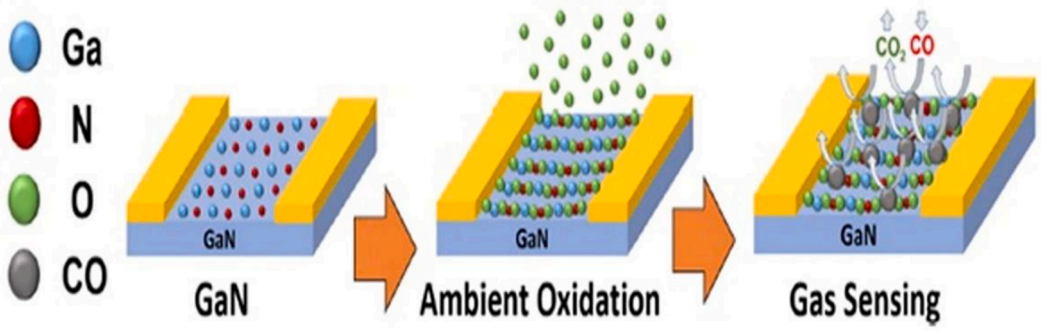

Fig. 35. Schematic diagram representing sensing mechanism at GaN surface [130]. Reprinted from Publication M. Mishra, N. K. Bhalla, A. Dashd, G. Gupta, Nanostructured GaN and AlGaN/GaN heterostructure for catalyst-free low temperature CO sensing, Applied Surface Science ,vol.481, pp.379–384, (2019), Copyright (2019), with permission from Elsevier.

$$S(\%) = \frac{\Delta I_{DS}}{I_{DS,air}} \times 100\% \tag{24}$$

where $\Delta I_{DS} = I_{DS,H_2S} - I_{DS,air}$ is the drain current variation between H_2S and air ambient.

4.5. Chemical sensors

4.5.1. Polar liquids

When a solid surface is exposed to a polar liquid, an adsorption layer is built at the solid/liquid interface. The interaction of the liquid molecules with the solid causes a drop in the surface potential. To determine this change, the Helmholtz condenser model is used by assuming that the dipoles of the liquid molecules are oriented in two separated layers like a condenser [13,134].

Putting a polar liquid on the HEMT's surface, changes the surface charge density of the transistor, which reduces the surface potential. This drop changes the original gate and threshold potentials, affecting the interface charge concentration and finally I_d. This means that the change in the transistor surface charge due to its interaction with the liquid is compensated by the charge of the conducting channel. Mehandru *et al.* deduced that the forward current reduces when gate area is brought in contact with solvents like H_2O or acids like HCl [23].

N. Chaturvedi *et al.* designed an interdigital electrode based AlGaN/GaN HEMT sensor for polar liquid sensing (as shown in Fig. 37). The sensor showed characteristic I_d of 21.2 mA at 3.3 V. It also showed an alteration of 1.78%, 2.18% and 6.3% in I_d for mercury chloride, copper chloride and sodium chloride respectively with respect to the I_d of uncontaminated water. The device arrangement detected different polar liquids and readout an amendment of 0.15, 0.20 and 0.34 mA in I_d for acetone, water and methanol respectively. A sensitivity of 5.98 mA/mm/Debye at a V_d = 3.3 V was observed. Alteration in the dipole moment of the liquid causes a variation in surface potential at the gate detecting area [135].

4.5.2. Ion-selective FET sensors

Heavy metals have been put to use in since old times, though the health hazards created by them are known to humans. The heavy metals get ingested in us by water pollution and our sustained exposure to goods that contain them. Some metals like Iron (Fe), Cobalt (Co), Manganese (Mn), Zinc (Zn), etc. form the micronutrients essential for human well being. But, many other heavy metals such as Mercury (Hg), Lead (Pb), Nickel (Ni), Arsenic (As), Cadmium (Cd), Tin (Sn), Chromium (Cr), etc. are not only toxic in nature but also are carcinogenic and can

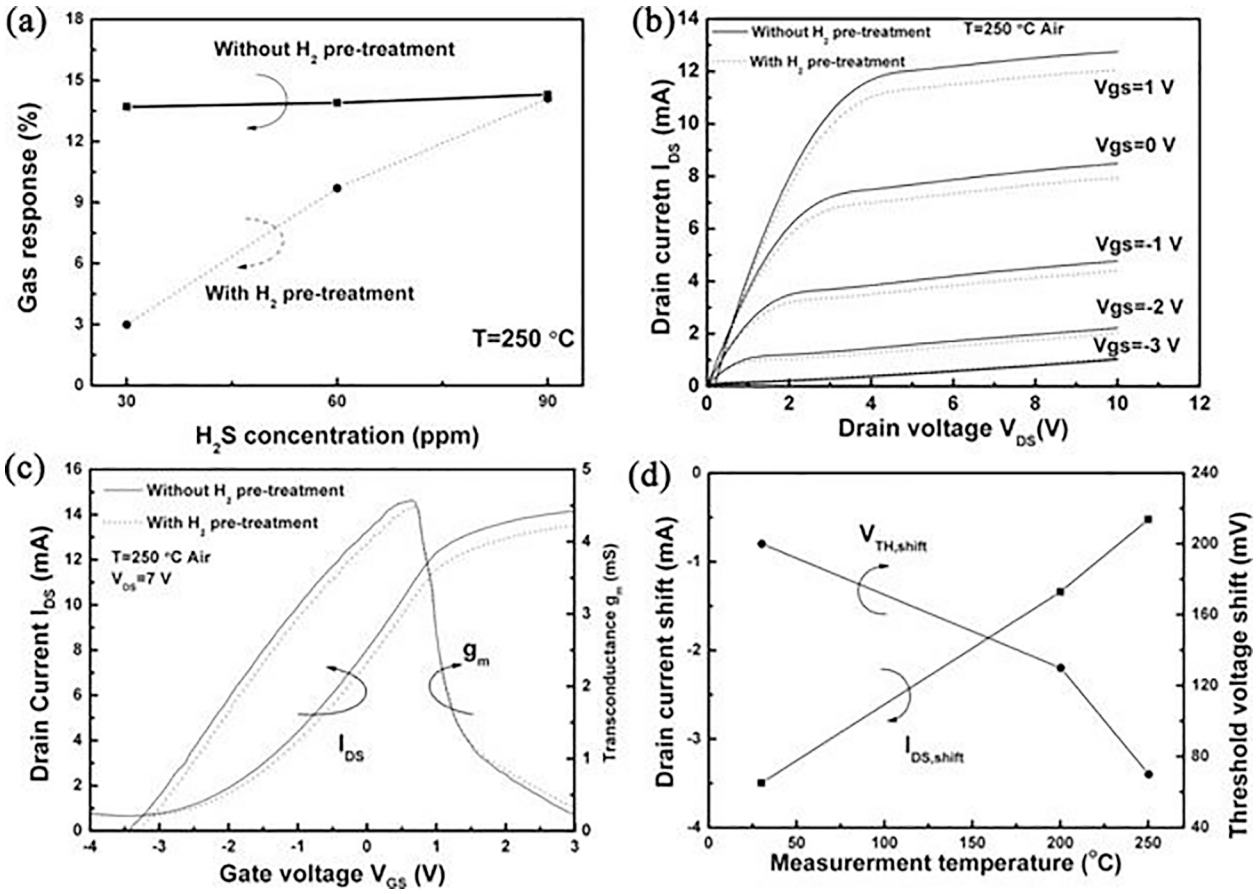

Fig. 36. (a) Gas responses for sensors, (b) Output curves for sensors, (c) Transfer and g_m curves for sensors with and without H_2 pre-treatment, (d) influence on I_{DS} shift and threshold voltage shift With H_2 pre-treatment the measurement temperature. [132] Reprinted from Publication J. Zhang, R. Sokolovskij, G. Chen, Y. Zhu, Y. Qi, X Lin, W Li, G. Q. Zhang, Y-L. Jiang, H. Yu, Impact of high temperature H_2 pre- treatment on Pt-AlGaN/GaN HEMT sensor for H_2S detection, *Sensors and amp; Actuators: B.Chemical, vol.280*, pp.138–143,(2018), Copyright (2018), with permission from Elsevier.

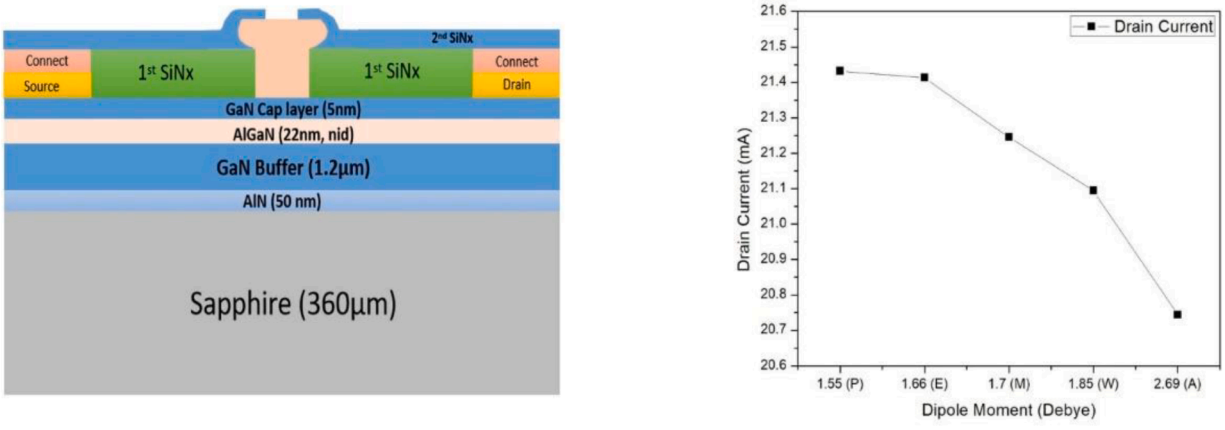

(a) (b)

Fig. 37. Inter digital electrode based GaN HEMT. Reprinted from N. Chaturvedi, *et al.*, "AlGaN/GaN HEMT based sensor and system for polar liquid detection," Sensors and Actuators A 302, 111799, (2020), Copyright (2020), with permission from Elsevier [135].

cause neuro-degenerative diseases. These metals can affect liver and kidney functions too. Our liver cannot metabolize or decompose heavy metals. The heavy metals thus get accumulated in various organs like brain, liver and kidney resulting in severe health problems.

Pb is the most common heavy metal that exists in our routine life through polluted air, drinking water, eatables, fertilizer, dyes etc. As humans consume lead-contaminated foods, it hoards in bones as levels larger than the natural metabolizing rate of 300 µg per day. Thus, checking Pb concentration in water bodies is vital for minimizing the health threats.

Chen *et al.* presented Lead ion selective membrane (Pb-ISM) coated AlGaN/GaN HEMT for ion-selective FET sensors with sensitivity of − 36

mV/log [Pb^{2+}]. The ideal sensitivity in a typical Nernst equation for lead ion is − 29.58 mV/log [Pb^{2+}]. Fig. 38 shows schematic of HEMT the transient response without and with the ion selective membrane (ISM). The hugely enhanced sensitivity immensely reduced the detection limit of 10^{-10} M compared to typical ion-selective electrode (ISE) limit of 10^{-7} M. The elevated sensitivity was acquired by generating a strong field between the gate electrode and the channel. They combined the ISM with a high sensitivity EDL gated FET to overcome the shortcomings of the traditional technique and improve the device usefulness [136].

Following semi-empirical model integrates the sensor response dependence on the electric field strength $E_{Pb-ISHEMT}$:

$$E_{Pb-ISHEMT} = c + 0.02958\eta \log[Pb^{2+}] \quad (25)$$

where η is V_g dependent parameter with value greater than 1 in linear or high field region; and equal to 1 in saturation region.

Cadmium is another toxic metal that is carcinogenic and occurs from mining and rubber industries, electroplated parts, batteries, and engraving processes. Cd accumulation can lead to fatigue, bone damage, kidney failure, loss of weight, respiratory fibrosis, hypertension etc. Nigam *et al.* demonstrated a GaN HEMT-based cadmium ion (Cd^{2+}) detector by means of mercapto propionic acid (MPA) and glutathione (GSH) functionalization. The sensing response of the sensor was analyzed by sensing Cd^{2+} ions at different concentrations. Their sensor exhibited a sensitivity of 0.241 μA/ppb, a quick response time of around 3 s, and a lesser sensing limit of 0.255 ppb. The detected lower detection limit was noticeably lower than the WHO suggested limit for Cd^{2+} ions in potable water. The results indicated that the sensitivity of 2DEG toward the variation of charges at the gate region make the device highly sensitive with rapid detection of Cd^{2+} ions [137].

The limit of detection (*LoD*) and sensitivity are the important parameters to evaluate the performance of a sensor. The *LoD* is detected by 3-sigma method given by [138]:

$$LoD = \frac{3\sigma}{m} \quad (26)$$

Here, σ is the Standard Deviation of the least concentration and m is the slope of the calibration curve.

AlInN/GaN sensor by X. L. Jia *et al.,* exhibited an ultrasensitive response and touched a sensing limit below 0.02 mg/L level for detecting phosphate anion [139]. Asadnia *et al.* presented the first polymer approach to detect metal ions using GaN HEMT-based sensor by functionalising the gate region with a polyvinyl chloride (PVC) based ion selective membrane. Sensors based on this technology are convenient, sturdy and extremely sensitive to the target analyte *viz.* $Hg_2þ$. This detector demonstrated a rapid, stable response when it was open to the solutions of varying $Hg_2þ$ concentrations, as depicted in Fig. 39 (a). Fig. 39 (b) shows accumulation of Hg ions at gate area. At a pH of 2.8 in a 10^{-2} M KNO_3 ion buffer, a detection limit below 10^{-8} M and a linear response in the range of 10^{-8} M to 10^{-4} M were achieved [140]

4.5.2.1. Pollution monitoring platforms. With suitable relocation procedure, AlGaN/GaN sensors can be incorporated into wearables. The handy and transportable air pollutant measuring systems may constantly collect data related to air pollutant types and their concentration levels. Such systems require low-cost, miniaturized, fast

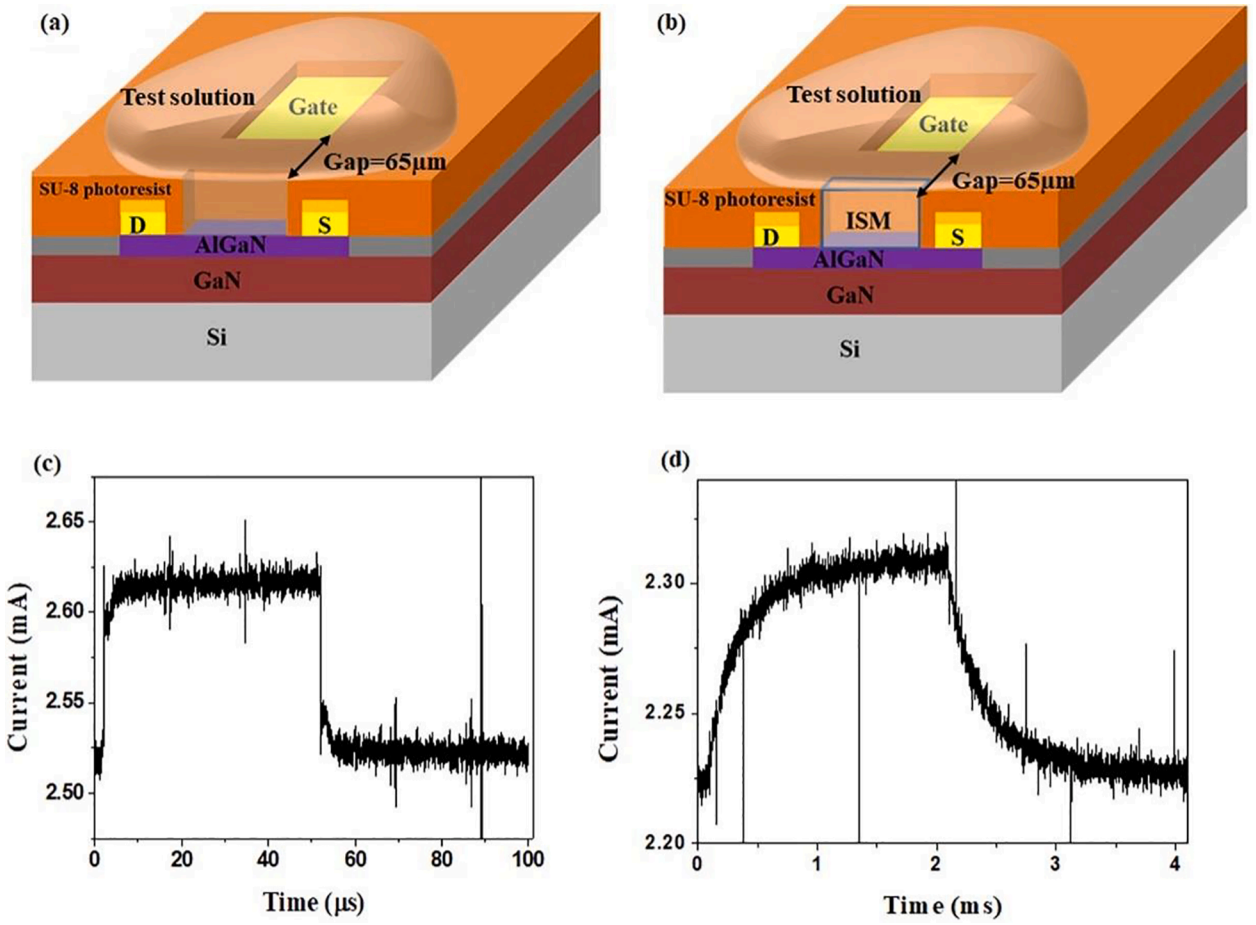

Fig. 38. Schematic of High field gated AlGaN/GaN HEMT sensor (a) without ISM (b) with ISM (c) Transient response without ISM, (d) with ISM. Reprint from Y. Chen, et.al, "High-field modulated ion-selective field-effect-transistor (FET) sensors with sensitivity higher than the ideal Nernst sensitivity," Sci Rep 8, 8300 (2018) under a Creative Commons Attribution 4.0 International License. [136].

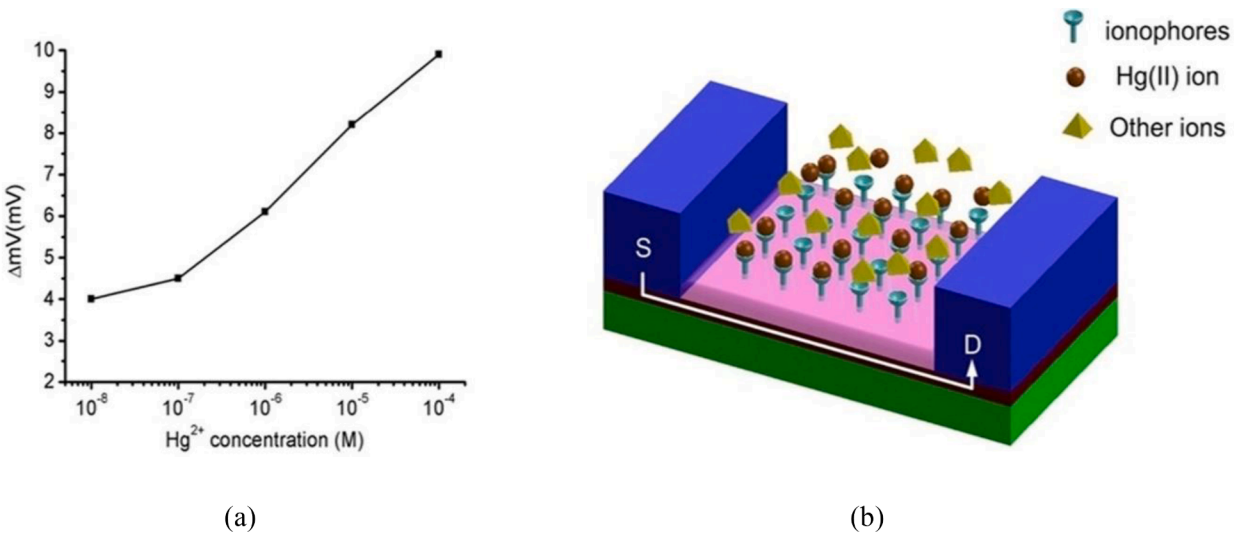

Fig. 39. (a) Mercury sensor response with respect to concentration, (b) Schematic of device with mercury ions. Reprinted from M. Asadnia, *et al.*, "Mercury (II) selective sensors based on AlGaN/GaN transistors," Analytica Chimica Acta, Volume 943, Pages 1–7, (2016). Copyright (2016), with permission from Elsevier [140].

responding and greatly sensitive gas sensors that can be functional on flexible and low-weight substrates. T. Ayari *et al.* fabricated 2-inch wafer scale AlGaN/GaN gas sensors on 2D nano-layered h-BN devoid of any cracks and then transferred sensors to an acrylic surface on metallic foil. The sensitivity to NO_2 gas was doubled using this technique. A 6 times faster response time was achieved by modifying the relevant device properties. This new approach for GaN-based sensor design is promising for new-gen optoelectronic wearables [141].

AlGaN/GaN HEMT devices do not require a reference electrode because of their high gain and always-on channel. This makes them easier to scale down. Zhao *et al.* developed a differential extended gate (DEG) AlGaN/GaN HEMT sensor for the real-time sensing of ionic pollutants. They corroborated the DEG design by effective sensing of Fe^{3+} in a solution. 2-Mercaptosuccinic acid was used to form a self-assembled monolayer on the EG of the measuring unit to selectively bind Fe^{3+}. DEG-AlGaN/GaN HEMT sensors can efficiently diminish the influence of noise factors; hence can achieve sensing limits as low as 10 fM. The sensor also showed a broad-ranging detection of 10 fM to 100 μM for Fe^{3+} with enhanced linearity of $R^2 = 0.9955$[142].

4.5.3. Other chemical sensors

Strong PE effect of GaN HEMTs can be used to realize highly sensitive PE microbalances. Furthermore, because of weak temperature dependence of the PE constants at temperatures upto *800 °C*, temperature independent SAW based chemical sensors operating at GHz frequencies can be fabricated and embedded in wireless remote sensing electronics. The velocity-change and the phase-change of the acoustic wave traveling laterally with the embedded chemical captivating sheet sandwiched between the input and output electro-mechanical inter digital transducers – IDTs is used for sensing by the SAW detectors [144]. The direct interaction of SAW with free 2DEG in AlGaN/GaN channel prevents further insertion losses. It is common to put an array of SAW detectors, with different coatings, for identifying explicit chemicals or bioreagents for improved selectivity [144].

Ethanol is one of most widely used chemical in food and biomedical industries. Excess of ethanol can spoil the carbohydrate food prematurely. Employment of ethanol gas sensors is requisite in electronic products like refrigerator and mobile devices to cut down the cons of ethanol. S. Jung introduced a Schottky diode based on GaN HEMT using silver as sensing material [145]. Ethanol tends to reduce the potential energy barrier at reasonably high temperature of 250 °C resulting in reduction of diode current.

4.6. Time of flight sensor

The time-of-flight (ToF) principle is used to determine the distance between a sensor and an object and build 3-D images by detecting the time or the phase difference between emission of a signal and its return to the sensor, after being reflected by an object. A number of applications such as light ranging and detection (LiDAR), machine vision and biomedical engineering employ ToF principle. Nonetheless, the bulky system requirement and sluggish switching has stalled the extensive use of ToF methodology so far. To alleviate these issues, Park *et al.* demonstrated hetero-integration of GaN- HEMTs and GaAs-based vertical cavity surface emitting lasers (VCSELs) by the use of a cold-welding process. The superior rise and fall time of the GaN HEMTs enables fast –switching devices. The hetero-integrated HEMTS with VDSELs operate in compatible voltage and current levels for a ToF operation. ToF sensors show higher switching performance as compared to the conventional Si-based arrangements, miniaturizing dimension and exhibiting stable ranging and high-resolution depth-imaging with reduced parasitic connection. This hetero-integrated system of dissimilar materials suggests a new pathway towards enabling high-resolution 3D imaging via higher degree of scalability and compatibility [146].

4.6.1. Sensing mechanism

Direct ToF ranging is calculated using following equation

$$d_{so} = 0.5c \times \tau_{ToF} \tag{27}$$

whered_{so} is the distance between a sensor and the object, c is the speed of light, and τ_{ToF} is the time difference between transmitted and received signals. The τ_{ToF} may be calculated by the phase difference between the transmitter and receiver signals as

$$\varphi = 2\pi f \tau_{ToF} \tag{28}$$

where f is the modulation frequency, and φ is the phase difference between illumination and reflection. The intensity of received signal at four different points is used to calculate the phase difference, as follows:

$$\varphi = arctan\left(\frac{A_1 - A_3}{A_2 - A_4}\right) \tag{29}$$

where A_1, A_2, A_3nd A_4 are the measurements at four different phases i.e. 0°, 90°, 180° and 270° respectively. Owing to its high accuracy in the range of millimeters, the phase-shift-based ToF model is generally used to build 3D image.

4.7. High temperature Hall-effect sensors

There have been substantial efforts to develop GaN devices operating at temperatures above 600 ◦C [147], 800 °C [148], 900 °C [149] and 1000 °C [150].

Recently, Hassan *et al.* proposed a fully-integrated data transmission system based on GaN transistors. This system targeted aerospace applications involving pressure and temperature sensors where the ambient temperature goes beyond 350 °C. A new demodulator architecture based on digital circuits was proposed to retrieve the data. The performance of the whole system was validated by simulation over the wide operating temperature range of 25 to 350 °C [151].

Hall-effect sensors are widely used in the power electronics, and in the automotive industry for direction-finding and location detection. Hall-effect sensors that can operate in harsh environments such as deep underground and aerospace are in demand. Aerospace applications comprise current checking in power modules, hybrid rocket motors and spacecraft motor control units.

Conventionally, Hall-effect sensors are fabricated using Si due to its ease of cheap manufacturing, and compatibility with ICs. However, Si-based modules behave erratically at temperatures beyond 200 °C. On the other hand, electronic components made of wide bandgap materials such as GaN and AlN can operate at extreme temperatures (up to 1000 °C in vacuum) without need of additional cooling equipment [152]. Thus, III- nitrides are prime candidates for space electronics.

GaN-based Hall-effect sensors have shown room temperature sensitivity and reliable operation up to 400 °C [153-155] for short durations of time. The thermal stability of Hall-effect sensors based on materials like NiFe [156,157], InGaSb [158] and GaAs [159-161] has been presented in literature. These studies focused on sensitivity performance at low temperatures not exceeding 300 °C.

Alpert *et al.* measured the magnetic sensitivity of Hall-effect sensors made of InAlN/GaN and AlGaN/GaN heterostructures between 25 °C and 576 °C [162]. The two devices demonstrated decreasing voltage-scaled magnetic sensitivity at elevated temperatures, declining from 53 mV/V/T to 8.3 mV/V/T for the InAlN/GaN sample and from 89 mV/V/T to 8.5 mV/V/T for the AlGaN/GaN sample. Electron mobility decreases due to scattering effects at elevated temperatures. Because of the insignificant temperature dependence of the 2DEG, current-scaled sensitivity stayed stable over the temperature range. An AlGaN/GaN sample held at 576 °C for 12 h illustrated near full recovery at 25 °C, signifying that the potential of GaN-based Hall-effect sensor for high temperature applications. The schematic and the principle of operation are depicted in Fig. 40.

4.7.1. Principle of operation

Determining the sensitivity of a Hall-effect sensor requires measuring the Hall voltageV_H, defined as

$$V_H = \frac{IBr_nG_H}{qn_s} \tag{30}$$

where I is the applied current, B is the external magnetic field. The two proportionality constants: r_n (~1.1) and G_H are material-based and geometry-dependent respectively. The sensitivity of a Hall-effect device with respect to supply current S_I is given as

$$S_I = \frac{V_H}{IB} \tag{31}$$

Reducing the 2DEG leads to an increase in the sheet resistance; a constant supply voltage causes poorer supply current, thereby, enhancing the current-scaled sensitivity of the device.

The sensitivityS_V, proportional to electron mobility (μH), is related to the supply voltage as

$$S_V = \frac{V_H}{V_sB} = \frac{r_nG_H}{Rqn_s} = \frac{\mu_H r_nG_H}{(L/W)_{eff}} \tag{32}$$

where V_s is the supply voltage, R is the device resistance, and $(L/W)_{eff}$ is the effective number of squares.

5. Summary and future outlook

III-N wide bandgap semiconductors are established as most suitable constituents for high power and high frequency electronics, optoelectronics and sensors. The most popular III-N material being the Gallium Nitride, which is able to operate at much higher voltage, higher frequency and elevated temperatures, as compared to the conventional Si.

A comprehensive review of recent developments in fabrication and range of sensor applications of AlGaN/GaN based sensors has been

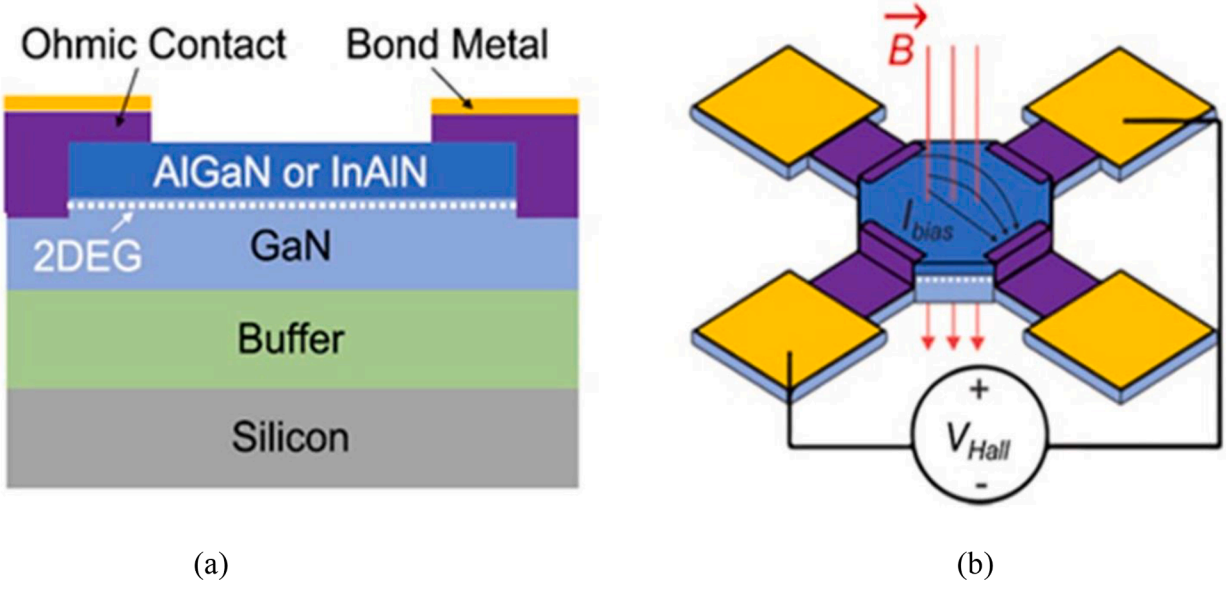

Fig. 40. (a) Schematic of Hall Effect sensor, (b) Principle of working. Reprinted from H. S. Alpert, C. A. Chapin, K. M. Dowling, S. R. Benbroo, H. Köck, U. Ausserlechner and D. G. Senesky, "Sensitivity of 2DEG-based Hall-effect sensors at high temperatures," Rev. Sci. Instrum. 91, 025,003 (2020), with the permission of AIP Publishing. [162].

carried out in this paper. We observe that new generation AlGaN/GaN based effective sensors are used for a number of sensing applications like gas sensing, liquid, biochemical, pressure, ultra violet rays, optical, stress and strain sensing *etc.* Predominantly, the responses of sensors are determined by variation in 2DEG formed at AlGaN/GaN interface. Surface alteration with sensing receptors can help in removing drawbacks like lack of selectivity of HEMTs to different analytes.

As demand escalates for components that can operate at high temperature, high frequency, high chemical resistance, high power capacity and high electron saturation velocity, GaN-heterostructure based sensors are expected to have much wider outreach. However, threshold voltage instability issues, material problems, lack of Ohmic contact know-how do still exist. In the last few years, the scientific discoveries have produced GaN fabrication and technological innovations for new identifying architecture opportunities. These may progress the fundamental considerations of the bio-chemical sensing tools and produce light weight and compact wearable detectors, ambient temperature sensors with innovative architectures. These innovations will definitely have a long term bearing on significant areas of concern such as defense, space-exploration, agriculture, healthcare, productivity, and environment.

Funding

This research did not receive any specific grant from funding agencies in the public, commercial, or not-for-profit sectors

Declaration of Competing Interest

The authors declare that they have no known competing financial interests or personal relationships that could have appeared to influence the work reported in this paper.

References

[1] Z. Alaie, S. Mohammad Nejad, M.H. Yousefi, Recent advances in ultraviolet photodetectors, Mater. Sci. Semicond. Process. 29 (2015) 16–55, https://doi.org/10.1016/j.mssp.2014.02.054.

[2] M.A. Mastro, A. Kuramata, J. Calkins, J. Kim, F. Ren, S.J. Pearton, Perspective—Opportunities and Future Directions for Ga_2O_3, ECS J. Solid State Sci. Technol. 6 (5) (2017) P356–P359, https://doi.org/10.1149/2.0031707jss.

[3] G. Meneghesso, M. Meneghini, E. Zanoni, Breakdown mechanisms in AlGaN/GaN HEMTs: An overview, Jpn. J. Appl. Phys. 53 (10) (2014) 100211, https://doi.org/10.7567/JJAP.53.100211.

[4] B. Monemar, G. Pozina, Group III-nitride based hetero and quantum structures, Prog. Quantum Electron. 24 (6) (2000) 239–290, https://doi.org/10.1016/S0079-6727(00)00009-4.

[5] H. Morkoç, Challenges and Opportunities in GaN and ZnO Devices and Materials, Proc. IEEE 98 (7) (2010) 1113–1117, https://doi.org/10.1063/1.4853535.

[6] M. Henini, III-V nitrides for electronic and UV applications, Nitride Electronics, III-Vs Review 12 (5) (1999) 28–32, https://doi.org/10.1109/5.90133.

[7] M.S. Shur, R. Gaska, A. Bykhovski, GaN-based electronic devices, Solid-State Electron. 43 (8) (1999) 1451–1458, https://doi.org/10.1016/S0038-1101(99)00088-X.

[8] S. Jang, P. Son, J. Kim, S.-N. Lee, K.H. Baik, Hydrogen sensitive Schottky diode using semipolar (1122) AlGaN/GaN heterostructures, Sens. Actuators, B 222 (2016) 43–47, https://doi.org/10.1016/j.snb.2015.08.056.

[9] S. Das, S. Majumdar, R. Kumar, S. Ghosh, D. Biswas, Thermodynamic analysis of acetone sensing in Pd/AlGaN/GaN heterostructure Schottky diodes at low temperatures, Scr. Mater. 113 (2016) 39–42, https://doi.org/10.1016/j.scriptamat.2015.10.015.

[10] C. Bishop, Y. Halfaya, A. Soltani, S. Sundaram, X. Li, J. Streque, Y. El Gmili, P. L. Voss, J.P. Salvestrini, A. Ougazzaden, Experimental Study and Device Design of NO, NO 2 , and NH 3 Gas Detection for a Wide Dynamic and Large Temperature Range Using Pt/AlGaN/GaN HEMT, IEEE Sensors J. 16 (18) (2016) 6828–6838, https://doi.org/10.1109/JSEN.2016.2593050.

[11] P. Offermans, A.S. Ali, G.B.Verheyden, K. Geens , S. Lenci , M.V. Hove , S. Decoutere , R.V. Schaijk, Suspended AlGaN/GaN membrane devices with recessed open gate areas for ultra-low-power air quality monitoring, IEEE International Electron Devices Meeting (IEDM), pp. 33.6.1–33.6.4, (2015), https://doi.org/10.1109/IEDM.2015.7409823.

[12] Y. Xi, L.u. Liu, F. Ren, S.J. Pearton, J. Kim, A. Dabiran, P.P. Chow, Methane detection using Pt-gated AlGaN/GaN high electron mobility transistor based Schottky diodes, J. Vacuum Sci. Technol. B, Nanotechnol. Microelectronics: Materials, Processing, Measurement, Phenomena 31 (3) (2013) 032203, https://doi.org/10.1116/1.4803743.

[13] M.S.Z. Abidin, A.M. Hashim, M.E. Sharifabad, S.F. Rahman, T. Sadoh, Open-gated pH sensor fabricated on an undoped-AlGaN/GaN HEMT structure, Sensors 11 (3) (2011) 77–3067, https://doi.org/10.3390/s110303067.

[14] C.-T. Lee, Y.-S. Chiu, Gate-Recessed AlGaN/GaN ISFET Urea Biosensor Fabricated by Photoelectrochemical Method, IEEE Sensors J. 16 (6) (2016) 1518–1523, https://doi.org/10.1109/JSEN.2015.2506986.

[15] B.H. Chu, B.S. Kang, S.C. Hung, K.H. Chen, F. Ren, A. Sciullo, B.P. Gila, S. J. Pearton, Aluminum Gallium Nitride (GaN)/GaN High Electron Mobility Transistor-Based Sensors for Glucose Detection in Exhaled Breath Condensate, J Diabetes Sci Technol 4 (1) (2010) 171–179, https://doi.org/10.1177/193229681000400122.

[16] B.H. Chu, H.W. Lin, S. Gwo, Y.L. Wang, S.J. Pearton, J.W. Johnson, P. Rajagopal, J.C. Roberts, E.L. Piner, K.J. Linthicuni, F. Ren, Chloride ion detection by InN gated AlGaN/GaN high electron mobility transistors, J. Vacuum Sci. Technol. B, Nanotechnol. Microelectronics: Materials, Processing, Measurement, Phenomena. 28 (1) (2010) L5–L8, https://doi.org/10.1116/1.3271253.

[17] J. Cheng, J. Li, B. Miao, J. Wang, Z. Wu, D. Wu, R. Pei, Ultrasensitive detection of Hg 2+ using oligonucleotide-functionalized AlGaN/GaN high electron mobility transistor, Appl. Phys. Lett. 105 (8) (2014) 083121, https://doi.org/10.1063/1.4894277.

[18] N. Espinosa, S.U. Schwarz, V. Cimalla, O. Ambacher, Detection of different target-DNA concentrations with highly sensitive AlGaN/GaN high electron, Sens. Actuators, B 210 (2015) 633–639, https://doi.org/10.1016/j.snb.2015.01.019.

[19] J.I. Pankove, GaN: from fundamentals to applications, Mater. Sci. Eng., B 61-62 (1999) 305–309, https://doi.org/10.1016/S0921-5107(98)00523-6.

[20] S.J. Pearton, F. Ren, A.P. Zhang, G. Dang, X.A. Cao, K.P. Lee, H. Cho, B.P. Gila, J. W. Johnson, C. Monier, C.R. Abernathy, J. Han, A.G. Baca, J.-I. Chyi, C.-M. Lee, T.-E. Nee, C.-C. Chuo, S.N.G. Chu, GaN electronics for high power, high temperature applications, Mater. Sci. Eng., B 82 (1-3) (2001) 227–231, https://doi.org/10.1016/S0921-5107(00)00767-4.

[21] Y.-L. Wang, B.H. Chu, C.Y. Chang, C.F. Lo, S.J. Pearton, A. Dabiran, P.P. Chow, F. Ren, Long-term stability study of botulinum toxin detection with AlGaN/GaN high electron mobility transistor based sensors, Sens. Actuators, B 146 (1) (2010) 349–352, https://doi.org/10.1016/j.snb.2010.02.026.

[22] F. Ren, S.J. Pearton, B.S. Kang, B.H. Chu, Biosensors for Health Applications, in P. A. Serra, ed., Biosensors for Health, Environment and Biosecurity, InTech, Chapter 2, pp. 15–68, (2011), https://doi.org/10.5772/17103.

[23] R. Mehandru, B. Luo, B.S. Kang, J. Kim, F. Ren, S.J. Pearton, C.-C. Pan, G.-T. Chen, J.-I. Chyi, AlGaN/GaN HEMT based liquid sensors, Solid-State Electron. 48 (2) (2004) 351–353, https://doi.org/10.1016/S0038-1101(03)00318-6.

[24] R.P. Strittmatter, R.A. Beach, J. Brooke, E.J. Preisler, G.S. Picus, T.C. McGill, GaN Schottky diodes for piezoelectric strain sensing, J. Appl. Phys. 93 (9) (2003) 5675–5681, https://doi.org/10.1063/1.1558960.

[25] R.P. Strittmatter, R.A. Beach, G.S. Picus, T.C. McGill, Piezoelectrically enhanced capacitive strain sensors using GaN metal-insulator-semiconductor diodes, J. Appl. Phys. 94 (9) (2003) 5958–5963, https://doi.org/10.1063/1.1611267.

[26] M.K. Chattopadhyay, S. Tokekar, Temperature and polarization dependent polynomial based non-linear analytical model for gate capacitance of AlmGa1−mN/GaN MODFET, Solid-State Electron. 50 (2) (2006) 220–227, https://doi.org/10.1016/j.sse.2005.10.016.

[27] J.I. Pankove, Luminescence in GaN, J. Lumin. 7 (1973) 114–126, https://doi.org/10.1016/0022-2313(73)90062-8.

[28] H. Morkoç, A.D. Carlo, R. Cingolani, GaN-based modulation doped FETs and UV detectors, Solid-State Electron. 46 (2) (2002) 157–202, https://doi.org/10.1016/S0038-1101(01)00271-4.

[29] C. Prall, C. Kaspari, F. Brunner, K. Haberland, M. Weyers, D. Rueter, In-situ photoluminescence measurements during MOVPE growth of GaN and InGaN MQW structures, J. Cryst. Growth 415 (2015) 1–6, https://doi.org/10.1016/j.jcrysgro.2014.12.023.

[30] F. Zeng, J. An, G. Zhou, W. Li, H. Wang, T. Duan, L. Jiang, H. Yu, A Comprehensive Review of Recent Progress on GaN High Electron Mobility Transistors: Devices, Fabrication and Reliability. Electronics 7 (12) (2018) 377, https://doi.org/10.3390/electronics7120377.

[31] J.C. Carrano, D.J.H. Lambert, C.J. Eiting, C.J. Collins, T. Li, S. Wang, B. Yang, A. L. Beck, R.D. Dupuis, J.C. Campbell, GaN avalanche photodiodes, Appl. Phys. Lett. 76 (7) (2000) 924–926.

[32] J. Vaitkus, W. Cunningham, E. Gaubas, M. Rahman, S. Sakai, K.M. Smith, T. Wang, Semi-insulating GaN and its evaluation for α particle detection, Nuclear Instruments and Methods in Physics Research Section A: Accelerators, Spectrometers, Detectors and Associated Equipment 509 (1-3) (2003) 60–64, https://doi.org/10.1016/S0168-9002(03)01550-X.

[33] J. Wang, P. Mulligan, L. Brillson, L.R. Cao, Review of using gallium nitride for ionizing radiation detection, Appl. Phys. Rev. 2 (3) (2015) 031102, https://doi.org/10.1063/1.4929913.

[34] A.Y. Polyakov, N.B. Smirnov, A.V. Govorkov, A.V. Markov, E.A. Kozhukhova, I. M. Gazizov, N.G. Kolin, D.I. Merkurisov, V.M. Boiko, A.V. Korulin, V.M. Zalyetin, S.J. Pearton, I.-H. Lee, A.M. Dabiran, P.P. Chow, Alpha particle detection with GaN Schottky diodes, J. Appl. Phys. 106 (10) (2009) 103708, https://doi.org/10.1063/1.3261806.

[35] D. Alquier, F. Cayrel, O. Menard, A.-E. Bazin, A. Yvon, E. Collard, Recent Progresses in GaN Power Rectifier, Jpn. J. Appl. Phys. 51 (1) (2012) 01AG08, https://doi.org/10.1143/JJAP.51.01AG08.

[36] L. Min, Z. Guo-Guang, F. Kai, Y. Guo-Hao, Gallium nitride room temperature α particle detectors, Chin. Phys. Lett. 27 (5) (2010), 052901, https://doi.org/10.1088/0256-307X/27/5/052901.

[37] I.-H. Lee, A.Y. Polyakov, N.B. Smirnov, A.V. Govorkov, E.A. Kozhukhova, V. M. Zaletin, I.M. Gazizov, N.G. Kolin, S.J. Pearton, Electrical properties and radiation detector performance of free-standing bulk n-GaN, J. Vacuum Scie. Technol. B, Nanotechnol. Microelectronics: Materials, Processing, Measurement, Phenomena 30 (2) (2012) 021205, https://doi.org/10.1116/1.3690644.
[38] Xinwen Hu, A.P. Karmarkar, Bongim Jun, D.M. Fleetwood, R.D. Schrimpf, R. D. Geil, R.A. Weller, B.D. White, M. Bataiev, L.J. Brillson, U.K. Mishra, Proton-irradiation effects on AlGaN/AlN/GaN high electron mobility transistors, IEEE Trans. Nucl. Sci. 50 (6) (2003) 1791–1796, https://doi.org/10.1109/TNS.2003.820792.
[39] B. Luo, F. Ren, K.K. Allums, B.P. Gila, A.H. Onstine, C.R. Abernathy, S.J. Pearton, R. Dwivedi, T.N. Fogarty, R. Wilkins, R.C. Fitch, J.K. Gillespie, T.J. Jenkins, R. Dettmer, J. Sewell, G.D. Via, A. Crespo, A.G. Baca, R.J. Shul, Proton irradiation of MgO- or Sc2O3 passivated AlGaN/GaN high electron mobility transistors, Solid-State Electron. 47 (6) (2003) 1015–1020, https://doi.org/10.1016/S0038-1101(02)00468-9.
[40] H.Y. Kim, J. Kim, S.P. Yun, K.R. Kim, T.J. Anderson, F. Ren, S.J. Pearton, AlGaN/GaN high electron mobility transistors irradiated with 17 MeV protons, J. Electrochem. Soc. 155 (7) (2008) H513–H515, https://doi.org/10.1149/1.2917256.
[41] K.I. Zaytsev, I.N. Dolganova, N.V. Chernomyrdin, G.M. Katyba, A.A. Gavdush, O. P. Cherkasova, G.A. Komandin, M.A. Shchedrina, A.N. Khodan, D.S. Ponomarev, I.V. Reshetov, V.E. Karasik, M. Skorobogatiy, V.N. Kurlov, V.V. Tuchin, The progress and perspectives of terahertz technology for diagnosis of neoplasms: a review, J. Opt. 22 (1) (2020) 013001, https://doi.org/10.1088/2040-8986/ab4dc3.
[42] N. Pala, D. Veksler, A. Muravjov, W. Stillman, R. Gaska, M.S. Shur, Resonant detection and modulation of terahertz radiation by 2DEG plasmons in GaN grating-gate structures, Sensors 2007 IEEE (2007) 570–572, https://doi.org/10.1109/ICSENS.2007.4388462.
[43] A. El, S.B. Fatimy, F. Tombet, W. Teppe, D.B. Knap, S. Veksler, M.S. Rumyantsev, N. Shur, R. Pala, Q. Gaska, X. Fareed, D. Hu, G. Seliuta, C. Valusis, D.T. Gaquiere, A. Cappy, Terahertz detection by GaN/AlGaN transistors, Electron. Lett. 42 (23) (2006) 1342–1344, https://doi.org/10.1049/el:20062452.
[44] N Dyakonova, D.B. But, D. Coquillat1, W. Knap, C. Drexler, P. Olbrich, J. Karch, M. Schafberger, S.D. Ganichev, G. Ducournau, C. Gaquiere, M.A. Poisson, S. Delage, G. Cywinski, C. Skierbiszewski,AlGaN/GaN HEMT's photo response to high intensity THz radiation, Opto-Electronics Review, 23 (3) (2015) 195–199, https://doi.org/10.1515/oere-2015-0026.
[45] H. Hou, Z. Liu, J. Teng, T. Palacios, S.-J. Chua, A sub-terahertz broadband detector based on a GaN high-electron-mobility transistor with nanoantennas, Appl. Phys. Express 10 (1) (2017) 014101, https://doi.org/10.7567/APEX.10.014101.
[46] M. Bauer, A. Ramer, S.A. Chevtchenko, K.Y. Osipov, D. Cibiraite, S. Pralgauskaite, K. Ikamas, A. Lisauskas, W. Heinrich, V. Krozer, H.G. Roskos, A High-Sensitivity AlGaN/GaN HEMT Terahertz Detector With Integrated Broadband Bow-Tie Antenna, IEEE Trans. THz Sci. Technol. 9 (4) (2019) 430–444, https://doi.org/10.1109/TTHZ.2019.2917782.
[47] G. Vanko, M. Držík, M. Vallo, T. Lalinský, V. Kutiš, S. Stančík, I. Rýger, A. Benčurová, AlGaN/GaN C-HEMT structures for dynamic stress detection, Sens. Actuators, A 172 (1) (2011) 98–102, https://doi.org/10.1016/j.sna.2011.02.049.
[48] L. Chen, K. Zhang, J. Dong, B. Wang, L. He, Q. Wang, M. He, X. Wang, The piezotronic effect in InGaN/GaN quantum-well based microwire for ultrasensitive strain sensor, Nano Energy 72 (2020) 104660, https://doi.org/10.1016/j.nanoen.2020.104660.
[49] I. Evseev, D. Zaitsev, V. Agafonov, Study of transfer characteristics of a molecular electronic sensor for borehole surveys at high temperatures and pressures, Sensors 19 (11) (2019) 2545, https://doi.org/10.3390/s19112545.
[50] H. Ngo, P. Mackowiack, N. Grabbert, T. Weiland, X. Hu, M. Schneider-Ramelow, O. Ehrmann, K. Lang, The roadmap for development of piezoresistive micro mechanical sensors for harsh environment applications, 2017 Eleventh International Conference on Sensing Technology (ICST), pp. 1-6, (2017), https://doi.org/10.1109/ICSensT.2017.8304457.
[51] W.J. Fleming, New Automotive Sensors—A Review, IEEE Sensors J. 8 (11) (2008) 1900–1921, https://doi.org/10.1109/JSEN.2008.2006452.
[52] D. Gajula, I. Jahangir, G. Koley, High temperature AlGaN/GaN membrane based pressure sensors, Micromachines 9 (5) (2018) 207, https://doi.org/10.3390/mi9050207.
[53] P. Mohankumar, J. Ajayan, R. Yasodharan, P. Devendran, R. Sambasivam, A review of micromachined sensors for automotive applications, Measurement 140 (2019) 305–322, https://doi.org/10.1016/j.measurement.2019.03.064.
[54] B. Hunt, A. Tooke, High temperature electronics for harsh environments, in: 18th European Microelectronics & Packaging Conference , IEEE, 2011, pp. 1–5.
[55] X. Jiang, K. Kim, S. Zhang, J. Johnson, G. Salazar, High-temperature piezoelectric sensing, Sensors, 14 (2014) 144–169, https://doi.org/10.3390/s140100144.
[56] H.M. Hashemian, J. Jiang, Nuclear plant temperature instrumentation, Nucl. Eng. Des. 239 (12) (2009) 3132–3141, https://doi.org/10.1016/j.nucengdes.2009.08.030.
[57] T. George, K.A. Son, R.A. Powers, L.Y.D. Castillo, R. Okojie, Harsh environment microtechnologies for NASA and terrestrial applications, IEEE Sensors (2005), https://doi.org/10.1109/ICSENS.2005.1597934.
[58] Q. Zheng, B. Shi, Z. Li, Z.L. Wang, Recent Progress on Piezoelectric and Triboelectric Energy Harvesters in Biomedical Systems, Adv. Sci. 4 (7) (2017) 1700029, https://doi.org/10.1002/advs.201700029.
[59] N.-I. Kim, Y.-L. Chang, J. Chen, T. Barbee, W. Wang, J.-Y. Kim, M.-K. Kwon, S. Shervin, M. Moradnia, S. Pouladi, D. Khatiwada, V. Selvamanickam, J.-H. Ryou, Piezoelectric pressure sensor based on flexible gallium nitride thin film for harsh-environment and high-temperature applications, Sens. Actuators, A 305 (2020) 111940, https://doi.org/10.1016/j.sna.2020.111940.
[60] E.D. Le Boulbar, M.J. Edwards, S. Vittoz, G. Vanko, K. Brinkfeldt, L. Rufer, P. Johander, T. Lalinský, C.R. Bowen, D.W.E. Allsopp, Effect of bias conditions on pressure sensors based on AlGaN/GaN High Electron Mobility Transistor, Sens. Actuators, A 194 (2013) 247–251, https://doi.org/10.1016/j.sna.2013.02.017.
[61] V. Kutiš, J. Dzuba, J. Paulech, J. Murín, T. Lalinský, MEMS Piezoelectric Pressure Sensor-modelling and Simulation, Procedia Eng. 48 (2012) 338–345, https://doi.org/10.1016/j.proeng.2012.09.523.
[62] X. Tan, Y. Lv, X. Zhou, X. Song, Y. Wang, G. Gu, H. Guo, S. Liang, Z. Feng, S. Cai, High performance AlGaN/GaN pressure sensor with a Wheatstone bridge circuit, Microelectron. Eng. 219 (2020) 111143, https://doi.org/10.1016/j.mee.2019.111143.
[63] S. Timoshenko, S. Woinowsky-Krieger, Theory of Plates and Shells, Second edition, McGraw Hill, New York, 1959, https://doi.org/10.1038/148606a0.
[64] L.C. Clark, C. Lyons, Electrode Systems for Continuous Monitoring in Cardiovascular Surgery, Ann. N. Y. Acad. Sci., 102 (1962) 29–45, https://doi.org/10.1111/j.1749-6632.1962.tb13623.x.
[65] C.-A. Vu, W.-Y. Chen, Field-Effect Transistor Biosensors for Biomedical Applications: Recent Advances and Future Prospects, Sensors 19 (2019) 4214, https://doi.org/10.3390/s19194214.
[66] T. Schubert, G. Steinhoff, H.-G.-V. Ribbeck, M. Stutzmannn, M. Eickhoff, M. Tanaka, Gallium nitride electrodes for membrane-based electrochemical biosensors, Eur. Phys. J. E 30 (2) (2009) 233–238, https://doi.org/10.1140/epje/i2009-10511-x.
[67] Z. Gu, J. Wang, X. Liu, L. Zhao, H. Peng, J. Li, An Electronic Enzyme-linked Immunosorbent Assays Platform for Protein Analysis based on Magnetic beads and AlGaN/GaN highelectron mobility transistors, Analyst 145 (7) (2020) 2725–2730, https://doi.org/10.1039/C9AN01809C.
[68] I. Sarangadharan, A.K. Pulikkathodi, C.-H. Chu, Y.-W. Chen, A. Regmi, P.-C. Chen, C.-P. Hsu, Y.-L. Wang, Review—High Field Modulated FET Biosensors for Biomedical Applications, ECS J. Solid State Sci. Technol. 7 (7) (2018) Q3032–Q3042, https://doi.org/10.1149/2.0061807jss.
[69] H. Ohshima, Theory of Colloid and Interfacial Electric Phenomena, Elsevier, 2006, pp. 1–38.
[70] A. Varghese, C. Periasamy, L. Bhargava, Analytical Modeling and Simulation-Based Investigation of AlGaN/AlN/GaN Bio-HEMT Sensor for C-erbB-2 Detection, IEEE Sensors J. 18 (23) (2018) 9595–9603, https://doi.org/10.1109/JSEN.2018.2871718.
[71] S.N. Mishra, K. Jena, A Dielectric-Modulated Normally-Off AlGaN/GaN MOSHEMT for Bio-Sensing Application: Analytical Modeling Study and Sensitivity Analysis, J. Korean Phys. Soc. 74 (4) (2019) 349–357, https://doi.org/10.3938/jkps.74.349.
[72] C.H. Chu, I. Sarangadharan, A. Regmi, Y.W. Chen, C.P. Hsu, W.H. Chang, G. Y. Lee, J.I. Chyi, C.C. Chen, S.C. Shiesh, G.B. Lee, Y.L. Wang, Beyond the Debye length in high ionic strength solution: direct protein detection with field-effect transistors (FETs) in human serum, Sci. Rep. 7 (1) (2017) 5256, https://doi.org/10.1038/s41598-017-05426-6.
[73] J. Yang, P. Carey IV, F. Ren, M.A. Mastro, K. Beers, S.J. Pearton, I.I. Kravchenko, Zika virus detection using antibody-immobilized disposable cover glass and AlGaN/GaN high electron mobility transistors, Appl. Phys. Lett. 113 (3) (2018) 032101, https://doi.org/10.1063/1.5029902.
[74] K. Woo, W. Kang, K. Lee, P. Lee, Y. Kim, T.-S. Yoon, C.-Y. Cho, K.-H. Park, M.-W. Ha, H.H. Lee, Enhancement of cortisol measurement sensitivity by laser illumination for AlGaN/GaN transistor biosensor, Biosensors and Bioelectronics 159 (2020) 112186, https://doi.org/10.1016/j.bios.2020.112186.
[75] T.-Y. Tai, A. Sinha, I. Sarangadharan, A.K. Pulikkathodi, S.-L. Wang, G.-Y. Lee, J.-I. Chyi, S.-C. Shiesh, G.-B. Lee, Y.-L. Wang, Design and Demonstration of Tunable Amplified Sensitivity of AlGaN/GaN High Electron Mobility Transistor (HEMT)-Based Biosensors in Human Serum, Anal. Chem. 91 (9) (2019) 5953–5960.
[76] E. Caló, V.V. Khutoryanskiy, Biomedical applications of hydrogels: A review of patents and commercial products, Eur. Polym. J. 65 (2015) 252–267, https://doi.org/10.1016/j.eurpolymj.2014.11.024.
[77] L. Bousse, N.F. De Rooij, P. Bergveld, Operation of chemically sensitive field-effect sensors as a function of the insulator-electrolyte interface, IEEE Trans. Electron Devices 30 (10) (1983) 1263–1270, https://doi.org/10.1109/T-ED.1983.21284.
[78] J.L. Chiang, Y.C. Chen, J.C. Chou, Simulation and experimental study of the pH-sensing property for AlN thin films, Jpn. J. Appl. Phys. 40 (10) (2001) 5900–5904, https://doi.org/10.1143/JJAP. 40.5900.
[79] R.M. Sawant, J.P. Hurley, S. Salmaso, A. Kale, E. Tolcheva, T.S. Levchenko, V. P. Torchilin, SMART' drug delivery systems: Double targeted pH-responsive pharmaceutical nanocarriers, Bioconjugate Chem. 17 (4) (2006) 943–949, https://doi.org/10.1021/bc060080h.
[80] I.N. Cimalla, AlGaN/GaN sensors for direct monitoring of fluids and bio reactions, Online edition, Universitätsverlag Ilmenau, 2011.
[81] S. Rabbaa, J. Stiens, J. Phys, Validation of a triangular quantum well model for GaN-based HEMTs used in pH and dipole moment sensing, J. Phys. D Appl. Phys. 45 (2012) 1–9, https://doi.org/10.1088/0022-3727/45/47/475101.
[82] T. Kokawa, T. Sato, H. Hasegawa, T. Hashizume, Liquid-phase sensors using open-gate Al Ga N/ Ga N high electron mobility transistor structure, J. Vacuum Sci. Technol. B: Microelectronics Nanometer Structures Processing, Measurement, Phenomena 24 (4) (2006) 1972–1976, https://doi.org/10.1116/1.2214701.
[83] J.-Y. Pyo, J.-H. Jeon, Y. Koh, C.-Y. Cho, H.-H. Park, K.-H. Park, S.W. Lee, W.-J. Cho, AlGaN/GaN high-electron-mobility transistor pH sensor with extended

gate platform, AIP Adv. 8 (8) (2018) 085106, https://doi.org/10.1063/1.5041847.
[84] N. Sharma, S. Mishra, K. Singh, N. Chaturvedi, A. Chauhan, C. Periasamy, D. K. Kharbanda, P. Parjapat, P.K. Khanna, N. Chaturvedi, High-Resolution AlGaN/GaN HEMT-Based Electrochemical Sensor for Biomedical Applications, IEEE Trans. Electron Devices 67 (1) (2020) 289–295, https://doi.org/10.1109/TED.2019.2949821.
[85] D.E. Yates, S. Levine, T.W. Healy, Site-binding model of the electrical double layer at the oxide/water interface, J. Chem. Soc., Faraday Trans. 1 70 (0) (1974) 1807, https://doi.org/10.1039/f19747001807.
[86] W. Mönch, Elementary calculation of the branch-point energy in the continuum of interface-induced gap states, Appl. Surf. Sci. 117-118 (1997) 380–387, https://doi.org/10.1016/S0169-4332(97)80111-0.
[87] G. Steinhoff, M. Hermann, W.J. Schaff, L.F. Eastman, M. Stutzmann, M. Eickhoff, *p*H response of GaN surfaces and its application for *p*H-sensitive field-effect transistors, Appl. Phys. Lett. 83 (1) (2003) 177–179, https://doi.org/10.1063/1.1589188.
[88] Q.i. Cheng, M. Wang, M. Tao, R. Yin, Y. Li, N. Yang, W. Xu, C. Gao, Y. Hao, Z. Yang, Planar Dual Gate GaN HEMT Cascode Amplifier as a Voltage Readout pH Sensor With High and Tunable Sensitivities, IEEE Electron Device Lett. 41 (3) (2020) 485–488, https://doi.org/10.1109/LED.2020.2967631.
[89] D. Xue, H. Zhang, A. ul Ahmad, H. Liang, J. Liu, X. Xia, W. Guo, H. Huang, N. Xu, Enhancing the sensitivity of the reference electrode free AlGaN/GaN HEMT based pH sensors by controlling the threshold voltage, Sens. Actuators, B 306 (2020) 127609, https://doi.org/10.1016/j.snb.2019.127609.
[90] H. Zhang, J. Tu, S. Yang, K. Sheng, P. Wang, Optimization of gate geometry towards high-sensitivity AlGaN/GaN pH sensor, Talanta 205 (2019) 120134, https://doi.org/10.1016/j.talanta.2019.120134.
[91] X. Liu, L. Zhao, B. Miao, Z. Gu, J. Wang, H. Peng, J. Li, W. Sun, J. Li, Wearable Multiparameter Platform Based on AlGaN/GaN High-electron-mobility Transistors for Real-time Monitoring of pH and Potassium Ions in Sweat, Electroanalysis 32 (2) (2020) 422–428, https://doi.org/10.1002/elan.201900405.
[92] S. Alur, T. Gnanaprakasa, H. Xu, Y. Wang, A.L. Simonian, O.A. Oyarzabal, M. Park, A Biosensor Based on GaN Field Effect Transistor, CS MANTECH Conference (2009) 18–21.
[93] A. Varghese, C. Periasamy, L. Bhargava, Fabrication and Charge Deduction Based Sensitivity Analysis of GaN MOS-HEMT Device for Glucose, MIG, C-erbB-2, KIM-1, and PSA Detection, IEEE Trans. Nanotechnology 18 (2019) 747–755, https://doi.org/10.1109/TNANO.2019.2928308.
[94] J. Liu, H. Zhang, X. Xiaochuan, u.A. Aqrab, D. Xue, H. Huang, N. Xu, Q. Xi, W. Guo, H. Liang, High sensitivity detection of glucose with negatively charged gold nanoparticles functionalized the gate of AlGaN/GaN High Electron Mobility Transistor, Sens. Actuators, A 312 (2020) 112128, https://doi.org/10.1016/j.sna.2020.112128.
[95] J. Liu, H. Zhang, D. Xue, A.u. Ahmad, X. Xia, Y. Liu, H. Huang, W. Guo, H. Liang, An effective hydroxylation route for a highly sensitive glucose sensor using APTES/GOx functionalized AlGaN/GaN high electron mobility transistor, RSC Adv. 10 (19) (2020) 11393–11399, https://doi.org/10.1039/C9RA09446F.
[96] M. Stutzmann, G. Steinhoff, M. Eickhoff, O. Ambacher, C.E. Nebel, J. Schalwig, R. Neuberger, G. Müller, GaN-based heterostructures for sensor applications, Diam. Relat. Mater. 11 (3-6) (2002) 886–891, https://doi.org/10.1016/S0925-9635(02)00026-2.
[97] A.T. Alreshaid, J.G. Hester, W. Su, Y. Fang, M.M. Tentzeris, Review—Ink-Jet Printed Wireless Liquid and Gas Sensors for IoT, SmartAg and Smart City Applications, J. Electrochem. Soc. 165 (10) (2018) B407–B413, https://doi.org/10.1149/2.0341810jes.
[98] P. Ramaswamy, IoT smart parking system for reducing green-house gas emission, In Proceedings of the 2016 International Conference on Recent Trends in Information Technology (ICRTIT), Chennai, India, pp. 1–6, (2016), https://doi.org/10.1109/ICRTIT.2016.7569513.
[99] J.-H. Suh, I. Cho, K. Kang, S.-J. Kweon, M. Lee, H.-J. Yoo, I. Park, Fully integrated and portable semiconductor-type multi-gas sensing module for IoT applications, Sens. Actuators, B 265 (2018) 660–667, https://doi.org/10.1016/j.snb.2018.03.099.
[100] M. Ashok kumar, T. Thirumurugan, Integrated IOT based design and Android operated Multi-purpose Field Surveillance Robot for Military Use, In Advances in Engineering Research, Proceedings of the International Conference for Phoenixes on Emerging Current Trends in Engineering and Management, PECTEAM, (2018), https://doi.org/10.2991/pecteam-18.2018.42.
[101] R. Rushikesh, C.M.R. Sivappagari, Development of IoT based vehicular pollution monitoring system, in: In Proceedings of the 2015 International Conference on Green Computing and Internet of Things (ICGCIoT), IEEE, 2015, pp. 779–783, https://doi.org/10.1109/ICGCIoT.2015.7380568.
[102] Lei Shu, Mithun Mukherjee, Xiaoling Wu, Toxic gas boundary area detection in large-scale petrochemical plants with industrial wireless sensor networks, IEEE Commun. Mag. 54 (10) (2016) 22–28, https://doi.org/10.1109/MCOM.2016.7588225.
[103] G.P. Alcantara, A short review of gas sensors based on interdigital electrode, IEEE ICEMI 12 (2015) 1616–1621, https://doi.org/10.1109/ICEMI.2015.7494489.
[104] Yu-Lin Wang, C.Y. Chang, Wantae Lim, S.J. Pearton, D.P. Norton, B.H. Chu, C. F. Lo, F. Ren, J.W. Johnson, P. Rajagopal, J.C. Roberts, E.L. Piner, K.J. Linthicum, Oxygen gas sensing at low temperature using indium zinc oxide-gated AlGaN/GaN high electron mobility transistors, J. Vacuum Sci. Technol. B, Nanotechnol. Microelectronics: Materials, Processing, Measurement, Phenomena 28 (2) (2010) 376–379.
[105] Junghui Song, Wu Lu, Thermodynamic and Kinetic Analysis of Hydrogen Sensing in Pt/AlGaN/GaN Schottky Diodes at High Temperatures, IEEE Sensors J. 8 (6) (2008) 903–909, https://doi.org/10.1109/JSEN.2008.923938.
[106] H. Kim, W. Lim, J. Lee, S.J. Pearton, F. Ren, S. Jang, Highly sensitive AlGaN/GaN diode-based hydrogen sensors using platinum, Sens. Actuators, B 164 (2012) 64–68, https://doi.org/10.1016/j.snb.2012.01.067.
[107] Hyonwoong Kim, Soohwan Jang, AlGaN/GaN HEMT based hydrogen sensor with platinum nanonetwork gate electrode, Curr. Appl Phys. 13 (8) (2013) 1746–1750, https://doi.org/10.1016/j.cap.2013.07.008.
[108] X.H. Wang, X.L. Wang, C. Feng, C.B. Yang, B.Z. Wang, J.X. Ran, H.L. Xiao, C. M. Wang, J.X. Wang, Hydrogen sensors based on AlGaN/AlN/GaN HEMT, Microelectron. J. 39 (1) (2008) 20–23, https://doi.org/10.1016/j.mejo.2007.10.022.
[109] Zhibo Guo, Lai Wang, Zhibiao Hao, Yi Luo, Modeling and experimental study on sensing response of an AlGaN/GaN HEMT-based hydrogen sensor, Sens. Actuators, B 176 (2013) 241–247, https://doi.org/10.1016/j.snb.2012.09.012.
[110] I. Rýger, G. Vanko, T. Lalinský, Š. Haščík, P. Nemec, A. Benčúrová, M. Tomáška, The GaN/SiC Heterostructure-based Hydrogen SAW Sensor Operating in GHz Range, Procedia Eng. 87 (2014) 260–263, https://doi.org/10.1016/j.proeng.2014.11.657.
[111] K.H. Baik, J. Kim, S. Jang, Improved GaN Based Hydrogen Sensors, ECS Trans. 72 (5) (2016) 23–28, https://doi.org/10.1149/07205.0023ecst.
[112] K.H. Baik, S. Jang, AlGaN/GaN Heterostructure Based Hydrogen Sensor with Temperature Compensation, ECS J. Solid State Sci. Technol. 9 (4) (2020) 045010, https://doi.org/10.1149/2162-8777/ab8b72.
[113] Sunwoo Jung, Kwang Hyeon Baik, Soohwan Jang, GaN Based Hydrogen Sensor in Humid Ambient, ECS Trans. 77 (6) (2017) 33–37, https://doi.org/10.1149/07706.0033ecst.
[114] J.H. Choi, H. Kim, H.K. Sung, H.Y. Cha, Investigation of Stability and Power Consumption of an AlGaN/GaN Heterostructure Hydrogen Gas Sensor Using Different Bias Conditions, Sensors 19 (24) (2019) 5549, https://doi.org/10.3390/s19245549.
[115] G.H. Chung, T.A. Vuong, H. Kim, Demonstration of hydrogen sensing operation of AlGaN/GaN HEMT gas sensors in extreme environment, Results Phys. 12 (2019) 83–84, https://doi.org/10.1016/j.rinp.2018.11.064.
[116] Peter Offermans, Roman Vitushinsky, Mercedes Crego-Calama, Sywert H. Brongersma, Gas Sensing with AlGaN/GaN 2DEG Channels, Procedia Eng. 25 (2011) 1417–1420, https://doi.org/10.1016/j.proeng.2011.12.350.
[117] Y. Halfaya, C. Bishop, A. Soltani, S. Sundaram, V. Aubry, P. Voss, J.P. Salvestrini, A. Ougazzaden, Investigation of the performance of HEMT-based NO, NO_2 and NH_3 exhaust gas sensors for automotive antipollution systems, Sensors 16 (3) (2016) 273, https://doi.org/10.3390/s16030273.
[118] Akhil Ranjan, Manvi Agrawal, K. Radhakrishnan, Nethaji Dharmarasu, AlGaN/GaN HEMT-based high-sensitive NO 2 gas sensors, Jpn. J. Appl. Phys. 58 (SC) (2019) SCCD23, https://doi.org/10.7567/1347-4065/ab1391.
[119] Jianwen Sun, Robert Sokolovskij, Elina Iervolino, Zewen Liu, Pasqualina M. Sarro, Guoqi Zhang, Suspended AlGaN/GaN HEMT NO 2 Gas Sensor Integrated With Micro-heater, J. Microelectromech. Syst. 28 (6) (2019) 997–1004, https://doi.org/10.1109/JMEMS.2019.2943403.
[120] Jianwen Sun, Robert Sokolovskij, Elina Iervolino, Fabio Santagata, Zewen Liu, Pasqualina M. Sarro, Guoqi Zhang, Characterization of an Acetone Detector Based on a Suspended WO 3 -Gate AlGaN/GaN HEMT Integrated With Microheater, IEEE Trans. Electron Devices 66 (10) (2019) 4373–4379, https://doi.org/10.1109/TED.2019.2936912.
[121] Sunghoon Park, Hyunsung Ko, Soohyun Kim, Chongmu Lee, Gas sensing properties of multiple networked GaN/WO_3 core-shell nanowire sensors, Ceram. Int. 40 (6) (2014) 8305–8310, https://doi.org/10.1016/j.ceramint.2014.01.035.
[122] C.V. Nguyen, H. Kim, High Performance NO_2 Gas Sensor Based on Pd-AlGaN/GaN High Electron Mobility Transistors with Thin AlGaN Barrier, Journal of Semiconductor Technology And, Science 20 (2) (2020), https://doi.org/10.5573/JSTS.2020.20.2.170.
[123] Aleksander Gurlo, Nanosensors: towards morphological control of gas sensing activity. SnO 2 , In 2 O 3 , ZnO and WO 3 case studies, Nanoscale 3 (1) (2011) 154–165, https://doi.org/10.1039/c0nr00560f.
[124] G.F. Fine, L.M. Cavanagh, A. Afonja, R. Binions, Metal oxide semiconductor gas sensors in environmental monitoring, Sensors, 10 (6) (2010) 5469, https://doi.org/10.3390/s100605469.
[125] Ananya Dey, Semiconductor metal oxide gas sensors: A review, Mater. Sci. Eng., B 229 (2018) 206–217, https://doi.org/10.1016/j.mseb.2017.12.036.
[126] S.H. Park, S.H. Kim, S.Y. Park, C. Lee, Synthesis and CO gas sensing properties of surface nitrided Ga_2O_3 nanowires, RSC Adv. 4 (108) (2014) 63402, https://doi.org/10.1039/C4RA09538C.
[127] Barrett K. Duan, Paul W. Bohn, Response of nanostructured Pt/GaN Schottky barriers to carbon monoxide, Sens. Actuators, A 194 (2013) 220–227, https://doi.org/10.1016/j.sna.2013.01.026.
[128] E. Cho, D. Pavlidis, G. Zhao, S.M. Hubbard, J. Schwank, Improvement of CO sensitivity in GaN-based gas sensors, IEICE Trans. Electron. 89 (6) (2006) 1047, https://doi.org/10.1093/ietele/e89-c.7.1047.
[129] M Mello, B Potì, A de Risi, A Passaseo, M Lomascolo, M De Vittorio, GaN optical system for CO and NO gas detection in the exhaust manifold of combustion engines, J. Opt. A: Pure Appl. Opt. 8 (7) (2006) S545–S549, https://doi.org/10.1088/1464-4258/8/7/S38.
[130] Monu Mishra, Naman Kumar Bhalla, Ajit Dash, Govind Gupta, Nanostructured GaN and AlGaN/GaN heterostructure for catalyst-free low-temperature CO sensing, Appl. Surf. Sci. 481 (2019) 379–384, https://doi.org/10.1016/j.apsusc.2019.03.125.

[131] R. Sokolovskij, E. Iervolino, C. Zhao, F. Santagata, F. Wang, H. Yu, P.M. Sarro, G. Q. Zhang, Pt-AlGaN/GaN HEMT-sensor for hydrogen sulfide (H_2S) detection, Multidisciplinary Digital Publishing Institute Proceedings 1 (4) (2017) 463, https://doi.org/10.3390/proceedings1040463.
[132] Jian Zhang, Robert Sokolovskij, Ganhui Chen, Yumeng Zhu, Yongle Qi, Xinpeng Lin, Wenmao Li, Guo Qi Zhang, Yu-Long Jiang, Hongyu Yu, Impact of high temperature H2 pre-treatment on Pt-AlGaN/GaN HEMT sensor for H2S detection, Sens. Actuators, B 280 (2019) 138–143, https://doi.org/10.1016/j.snb.2018.10.052.
[133] Jassim Shahbaz, Martin Schneidereit, Klaus Thonke, Ferdinand Scholz, Functionalized GaN/GaInN heterostructures for hydrogen sulfide sensing, Jpn. J. Appl. Phys. 58 (SC) (2019) SC1028, https://doi.org/10.7567/1347-4065/ab112b.
[134] Wei-Jun Luo, Xiao-Juan Chen, Ting-Ting Yuan, Lei Pang, Xin-Yu Liu, AlGaN/GaN Based Diodes for Liquid Sensing, Chinese Phys. Lett. 30 (3) (2013) 037301, https://doi.org/10.1088/0256-307X/30/3/037301.
[135] Nidhi Chaturvedi, Kuldip Singh, Pharyanshu Kachhawa, Richard Lossy, Shivanshu Mishra, Ashok Chauhan, Dheeraj K. Kharbanda, Amber Kumar Jain, Rajiv Ranjan Thakur, Devanshu Saxena, Pramod K. Khanna, Joachim Wuerfl, AlGaN/GaN HEMT based sensor and system for polar liquid detection, Sens. Actuators, A 302 (2020) 111799, https://doi.org/10.1016/j.sna.2019.111799.
[136] Y. Chen, I. Sarangadharan, R. Sukesan, C.-Y. Hseih, G.-Y. Lee, J.-I. Chyi, Y.-L. Wang, High-field modulated ion-selective field-effect-transistor (FET) sensors with sensitivity higher than the ideal Nernst sensitivity, Sci. Rep. 8 (1) (2018) 1–11, https://doi.org/10.1038/s41598-018-26792-9.
[137] Adarsh Nigam, Thirumaleshwara N. Bhat, Vijendra Singh Bhati, Surani Bin Dolmanan, Sudhiranjan Tripathy, Mahesh Kumar, MPA-GSH Functionalized AlGaN/GaN High-Electron Mobility Transistor-Based Sensor for Cadmium Ion Detection, IEEE Sensors J. 19 (8) (2019) 2863–2870, https://doi.org/10.1109/JSEN.2019.2891511.
[138] Xiuling Jia, Dunjun Chen, Liu Bin, Hai Lu, Rong Zhang, Youdou Zheng, Highly selective and sensitive phosphate anion sensors based on AlGaN/GaN high electron mobility transistors functionalized by ion imprinted polymer, Sci Rep 6 (1) (2016), https://doi.org/10.1038/srep27728.
[139] X.L. Jia, X.Y. Huang, Y. Tang, L.H. Yang, D.J. Chen, H. Lu, R. Zhang, Y.D. Zheng, Ultrasensitive Detection of Phosphate Using Ion-Imprinted Polymer Functionalized AlInN/GaN High Electron Mobility Transistors, IEEE Electron Device Lett. 37 (7) (2016) 913–915, https://doi.org/10.1109/LED.2016.2567447.
[140] Mohsen Asadnia, Matthew Myers, N.D. Akhavan, Kane O'Donnell, Gilberto A. Umana-Membreno, U.K. Mishra, Brett Nener, Murray Baker, Giacinta Parish, Mercury(II) selective sensors based on AlGaN/GaN transistors, Anal. Chim. Acta 943 (2016) 1–7, https://doi.org/10.1016/j.aca.2016.08.045.
[141] Taha Ayari, Chris Bishop, Matthew B. Jordan, Suresh Sundaram, Xin Li, Saiful Alam, Youssef ElGmili, Gilles Patriarche, Paul L. Voss, Jean Paul Salvestrini, Abdallah Ougazzaden, Gas sensors boosted by two-dimensional h-BN enabled transfer on thin substrate foils: towards wearable and portable applications, Sci. Rep. 7 (1) (2017), https://doi.org/10.1038/s41598-017-15065-6.
[142] Lei Zhao, Xinsheng Liu, Bin Miao, Zhiqi Gu, Jin Wang, HuoXiang Peng, Jian Zhang, Bin Zeng, Jiadong Li, A differential extended gate-AlGaN/GaN HEMT sensor for real-time detection of ionic pollutants, Anal. Methods 11 (31) (2019) 3981–3986, https://doi.org/10.1039/C9AY01019J.
[143] T. Lalinský, I. Rýger, G. Vanko, M. Tomáška, I. Kostič, S. Haščík, M. Vallo, AlGaN/GaN based SAW-HEMT structures for chemical gas sensors, Procedia Eng. 5 (2010) 152–155, https://doi.org/10.1016/j.proeng.2010.09.402.
[144] Ivan Rýger, Gabriel Vanko, Tibor Lalinský, Martin Vallo, Martin Tomáška, Adrian Ritomský, AlGaN/GaN Based SAW-HEMT Devices for Chemical Gas Sensors Operating in GHz Range, Procedia Eng. 25 (2011) 1101–1104, https://doi.org/10.1016/j.proeng.2011.12.271.
[145] Sunwoo Jung, Kwang Hyeon Baik, Soohwan Jang, GaN Based Ethanol Sensor, ECS Trans. 75 (40) (2017) 9–12, https://doi.org/10.1149/07540.0009ecst.
[146] Minseong Park, Yongmin Baek, Mesgana Dinare, Doeon Lee, Kyung-Ho Park, Jungho Ahn, Dahee Kim, Joseff Medina, Won-Jin Choi, Sihwan Kim, Changjie Zhou, Junseok Heo, Kyusang Lee, Hetero-integration enables fast switching time-of-flight sensors for light detection and ranging, Sci Rep 10 (1) (2020), https://doi.org/10.1038/s41598-020-59677-x.
[147] Patrick Herfurth, David Maier, Yakiv Men, Rudolf Rösch, Lorenzo Lugani, Jean-Francois Carlin, Nicolas Grandjean, Erhard Kohn, GaN-on-insulator technology for high-temperature electronics beyond 400 °C, Semicond. Sci. Technol. 28 (7) (2013) 074026, https://doi.org/10.1088/0268-1242/28/7/074026.
[148] F. Medjdoub, D. Ducatteau, C. Gaquiere, J.F. Carlin, M. Gonschorek, E. Feltin, M. A. Py, N. Grandjean, E. Kohn, Evaluation of AlInN/GaN HEMTs on sapphire substrate in microwave, time and temperature domains, Electron. Lett. 43 (5) (2007) 309–311, https://doi.org/10.1049/el:20073170.
[149] David Maier, Mohammed Alomari, Nicolas Grandjean, Jean-Francois Carlin, Marie-Antoinette Diforte-Poisson, Christian Dua, Andrey Chuvilin, David Troadec, Christophe Gaquiere, Ute Kaiser, Sylvain L. Delage, Erhard Kohn, Testing the Temperature Limits of GaN-Based HEMT Devices, IEEE Trans. Device Mater. Relib. 10 (4) (2010) 427–436, https://doi.org/10.1109/TDMR.2010.2072507.
[150] F. Medjdoub, J.F. Carlin, M. Gonschorek, E. Feltin, M.A. Py, D. Ducatteau, C. Gaquiere, N. Grandjean, E Kohn, Can InAlN/GaN be an alternative to high power/high temperature AlGaN/GaN devices?, Proceedings of the 2006 International Electron Devices Meeting, San Francisco, CA, USA,IEEE, pp. 1–4, (2006), https://doi.org/10.1109/IEDM.2006.346935.
[151] A. Hassan, M. Ali, A. Trigui, Y. Savaria, M. Sawan, A GaN-Based Wireless Monitoring System for High-Temperature Applications, Sensors 19 (8) (2019) 1785, https://doi.org/10.3390/s19081785.
[152] D. Maier, M. Alomari, N. Grandjean, J.-F. Carlin, M.-A. Diforte-Poisson, C. Dua, S. Delage, E. Kohn, InAlN/GaN HEMTs for operation in the 1000◦C regime: A first experiment, IEEE Electron Device Lett. 33 (7) (2012) 985–987, https://doi.org/10.1109/LED.2012.2196972.
[153] L. Bouguen, L. Konczewicz, S. Contreras, B. Jouault, J. Camassel, Y. Cordier, High temperature behaviour of AlGaN/GaN Hall-FET sensors, Mater. Sci. Eng., B 165 (2009) 1–4, https://doi.org/10.1016/j.mseb.2008.11.041.
[154] Abdelkader Abderrahmane, Shota Koide, Shin-Ichiro Sato, Takeshi Ohshima, Adarsh Sandhu, Hiroshi Okada, Robust Hall Effect Magnetic Field Sensors for Operation at High Temperatures and in Harsh Radiation Environments, IEEE Trans. Magn. 48 (11) (2012) 4421–4423, https://doi.org/10.1109/TMAG.2012.2196986.
[155] M.J. Wang, B. Shen, F.J. Xu, Y. Wang, J. Xu, S. Huang, Z.J. Yang, K. Xu, G. Y. Zhang, High temperature dependence of the density of two-dimensional electron gas in $Al_{0.18}Ga_{0.82}N$/GaN heterostructures, Appl. Phys. A 88 (4) (2007) 715–718, https://doi.org/10.1007/s00339-007-4034-5.
[156] M. Mahfoud, Q.-H. Tran, S. Wane, D.-T. Ngo, E.H. Belarbi, A. Boukra, M. Kim, A. Elzwawy, C.G. Kim, G. Reiss, B. Dieny, A. Bousseksou, F. Terki, Reducedthermal dependence on the sensitivity of a planar Hall sensor, Appl. Phys. Lett. 115 (7) (2019), 072402, https://doi.org/10.1063/1.5110671.
[157] Taehyeong Jeon, Jae Hoon Lee, Artem Talantsev, Cheol Gi Kim, Planar Hall Resistance Sensor With Improved Thermal Stability, IEEE Magn. Lett. 10 (2019) 1–5, https://doi.org/10.1109/LMAG.2019.2943054.
[158] D.L. Partin, J.P. Heremans, T. Schroeder, C.M. Thrush, L.A. Flores-Mena, Temperature stable Hall effect sensors, IEEE Sensors J. 6 (1) (2006) 106–110, https://doi.org/10.1109/JSEN.2005.860362.
[159] J. Jankowski, S.E.Ahmar, M. Oszwalkdowski, Hall sensors for extreme temperatures, Sensors, 11 (2011) 876–885, https://doi.org/10.3390/s110100876.
[160] Mohammadreza Sadeghi, James Sexton, Chen-Wei Liang, Mohamed Missous, Highly Sensitive Nanotesla Quantum-Well Hall-Effect Integrated Circuit Using GaAs–InGaAs–AlGaAs 2DEG, IEEE Sensors J. 15 (3) (2015) 1817–1824, https://doi.org/10.1109/JSEN.2014.2368074.
[161] V. Mosser, S. Contreras, S. Aboulhouda, Ph. Lorenzini, F. Kobbi, J.L. Robert, K. Zekentes, High sensitivity hall sensors with low thermal drift using AlGaAs/InGaAs/GaAs heterostructures, Sens. Actuators, A 43 (1-3) (1994) 135–140, https://doi.org/10.1016/0924-4247(93)00680-3.
[162] H.S. Alpert, C.A. Chapin, K.M. Dowling, S.R. Benbrook, H. Köck, U. Ausserlechner, D.G. Senesky, Sensitivity of 2DEG-based Hall-effect sensors at high temperatures, Rev. Sci. Instrum. 91 (2) (2020) 025003, https://doi.org/10.1063/1.5139911.
[163] S. Boppel, M. Ragauskas, A. Hajo, M. Bauer, A. Lisauskas, S. Chevtchenko, A. Rämer, I. Kašalynas, G. Valušis, H.J. Würfl, W. Heinrich, Viktor Krozer GüntherTränkle, Hartmut G. Roskos, 0.25-$muhbox{m}$ GaNTeraFETs Optimized as THz Power Detectors and Intensity-Gradient Sensors, IEEE Transactions on Terahertz, Science and Technology 6 (2) (2016) 348–350, https://doi.org/10.1109/TTHZ.2016.2520202.
[164] Mi.Hou, H. So, A.J. Suria, A.S. Yalamarthyand D.G. Senesky, Suppression of persistent photoconductivity in AlGaN/GaN ultraviolet photodetectors using in situ heating IEEE Electron Device Letters 38 1 2016 56 59 10.1109/LED.2016.2626388.
[165] Kiarash Ahi, Review of GaN-based devices for terahertz operation, Opt. Eng 56 (09) (2017) 1, https://doi.org/10.1117/1.OE.56.9.090901.
[166] Petar Igic, Nebojsa Jankovic, Jon Evans, Matthew Elwin, Stephen Batcup, Soroush Faramehr, Dual-Drain GaN Magnetic Sensor Compatible With GaN RF Power Technology, IEEE Electron Device Lett. 39 (5) (2018) 746–748, https://doi.org/10.1109/LED.2018.2816164.
[167] Chaker Fares, Fan Ren, Stephen J. Pearton, Gwangseok Yang, Jihyun Kim, Chien-Fong Lo, J. Wayne Johnson, Effect of alpha-particle irradiation dose on SiN x /AlGaN/GaN metal–insulator semiconductor high electron mobility transistors, J. Vac. Sci. Technol., B 36 (4) (2018) 041203, https://doi.org/10.1116/1.5042261.
[168] S. Vittoz, L. Rufer, G. Rehder, U. Heinle, P. Benkart, Analytical and numerical modelling of AlGaN/GaN/AlN heterostructure based cantilevers for mechanical sensing in harsh environments, Sensors and Actuators A: Physical 172 (1) (2011) 27–34, https://doi.org/10.1016/j.sna.2011.02.024.
[169] J. Dzuba, G. Vanko, I. Ryger, M. Vallo, V. Kutis, T. Lalinsky, Influence of temperature on the sensitivity of the AlGaN/GaN C-HEMT-based piezoelectric pressure sensor, 10th Int, Conf. on Advanced Semiconductor Devices & Microsystems (ASDAM), IEEE (2014) 1–4, https://doi.org/10.1109/ASDAM.2014.6998633.
[170] B.S. Kang, H.T. Wang, F. Ren, S.J. Pearton, Electrical detection of biomaterials using AlGaN/GaN high electron mobility transistors, J. Appl. Phys. 104 (3) (2008) 031101, https://doi.org/10.1063/1.2959429.
[171] Zhibo Guo, Lai Wang, Zhibiao Hao, Yi Luo, pH sensor based on an AlGaN/GaN HEMT structure, Procedia Eng. 27 (2012) 693–697, https://doi.org/10.1016/j.proeng.2011.12.507.
[172] H. Trevino II, R.Y. Garza, H.F Huq, Smart Detection of MIG Using AlGaN/GaN High Electron Mobility Transistors, ISDRS 2013, (2013).
[173] Chih-Cheng Huang, Geng-Yen Lee, Jen-Inn Chyi, Hui-Teng Cheng, Chen-Pin Hsu, You-Ren Hsu, Chia-Hsien Hsu, Yu-Fen Huang, Yuh-Chang Sun, Chih-Chen Chen, Sheng-Shian Li, J. Andrew Yeh, Da-Jeng Yao, Fan Ren, Yu-Lin Wang, AlGaN/GaN high electron mobility transistors for protein–peptide binding affinity study,

Biosens. Bioelectron. 41 (2013) 717–722, https://doi.org/10.1016/j.bios.2012.09.066.
[174] S. Yang, L. Gu, X. Ding, B. Miao, Z. Gu, L. Yang, J. Li, D. Wu, Disposable Gate AlGaN/GaN High-Electron- Mobility Sensor for Trace-Level Biological Detection, IEEE Electron Device Lett. 39 (10) (2018) 1592–1595, https://doi.org/10.1109/LED.2018.2868433.
[175] A.G. Gudkov, S.V. Agasieva, V.G. Tikhomirov, V.V. Zherdeva, D.V. Klinov, V. D. Shashurin, Perspectives in the Development of Biosensors Based on AlGaN/GaN HEMT, Biomed Eng 53 (3) (2019) 196–200, https://doi.org/10.1007/s10527-019-09908-x.
[176] Jin Wang, Zhiqi Gu, Xinsheng Liu, Lei Zhao, Huoxiang Peng, Jiadong Li, An electronic enzyme-linked immunosorbent assay platform for protein analysis based on magnetic beads and AlGaN/GaN high electron mobility transistors, Analyst 145 (7) (2020) 2725–2730, https://doi.org/10.1039/C9AN01809C.
[177] Wang Soo Jeat, Mastura Shafinaz Zainal Abidin, Abdul Manaf Hashim, Shaharin Fadzli Abd Rahman, Maneea Eizadi Sharifabad, Farahiyah Mustafa, Abdul Rahim Abdul Rahman, Rabia Qindeel, Nurul Afzan Omar, Fabrication and Characterization of GaN-Based Two Terminal Devices for Liquid Sensing, IOP Conf. Ser.: Mater. Sci. Eng. 17 (2011) 012024, https://doi.org/10.1088/1757-899X/17/1/012024.
[178] I. Rýger, G. Vanko, P. Kunzo, T. Lalinský, M. Vallo, A. Plecenik, L. Satrapinský, T. Plecenik, AlGaN/GaN HEMT Based Hydrogen Sensors With Gate Absorption Layers Formed by High Temperature Oxidation, Procedia Eng. 47 (2012) 518–521, https://doi.org/10.1016/j.proeng.2012.09.198.
[179] K. Maier, A. Helwig, G. Müller, P. Becker, P. Hille, J. Schörmann, J. Teubert, M. Eickhoff, Detection of oxidizing gases using an optochemical sensor system based on GaN/InGaN nanowires, Sens. Actuators, B 197 (2014) 87–94, https://doi.org/10.1016/j.snb.2014.02.002.
[180] Ivan Rýger, Gabriel Vanko, Tibor Lalinský, Štefan Haščík, Anna Benčúrová, Pavol Nemec, Robert Andok, Martin Tomáška, GaN/SiC based surface acoustic wave structures for hydrogen sensors with enhanced sensitivity, Sens. Actuators, A 227 (2015) 55–62, https://doi.org/10.1016/j.sna.2015.02.041.
[181] M. Sciullo, M. Choudhury, E. Patrick, M.E. Law, Optimization of GaN-Based HEMTs for Chemical Sensing: A Simulation Study, ECS Trans. 75 (16) (2016) 259–264, https://doi.org/10.1149/07516.0259ecst.
[182] Sunwoo Jung, Kwang Hyeon Baik, Soohwan Jang, GaN Based Carbon Dioxide Sensor, ECS Trans. 77 (6) (2017) 121–125, https://doi.org/10.1149/07706.0121ecst.
[183] Roozbeh Anvari, Dino Spagnoli, Gilberto A. Umana-Membreno, Giacinta Parish, Brett Nener, Theoretical study of the influence of surface effects on GaN-based chemical sensors, Appl. Surf. Sci. 452 (2018) 75–86, https://doi.org/10.1016/j.apsusc.2018.04.250.
[184] Y. Dong , D.H.k Son , Q. Dai , J.H. Lee , C.H. Won ,J.G. Kim, D. Chen , J.H. Lee , H. Lu, R. Zhang and Y. Zheng, High Sensitive pH Sensor Based on AlInN/GaN Heterostructure Transistor, Sensors, 18 (5) (2018) 1314, https://doi.org/10.3390/s18051314.
[185] N. Chaturvedi, R. Lossy, K. Singh, D.K. Kharbanda, S. Mishra, A. Chauhan, K. Kishore, P.K. Khanna, J. Wuerfl, Design and development of gallium nitride HEMTs based liquid sensor 2018 IEEE SENSORS, pp. 1-3, (2018), https://doi.org/10.1109/ICSENS.2018.8589615.
[186] H.O. Chahdi , A. Ougazzaden, J.P. Salvestrini, H. Maher, A. Soltani, O. Helli, N.E. Bourzgui, L. Breuil, D. Danovitch, P. Voss, S. Sundaram, Sensors based on AlGaN/GaN HEMT for fast H2 and O2 detection and measurement at high temperature, 2019 IEEE SENSORS, Montreal, QC, Canada, pp. 1-4, (2019) https://doi.org/10.1109/SENSORS43011.2019.8956568.
[187] Arathy Varghese, Chinnamuthan Periasamy, Lava Bhargava, Surani Bin Dolmanan, Sudhiranjan Tripathy, Linear and Circular AlGaN/AlN/GaN MOS-HEMT-based pH Sensor on Si Substrate: A Comparative Analysis, IEEE Sens. Lett. 3 (4) (2019) 1–4, https://doi.org/10.1109/LSENS.2019.2909291.
[188] Giacinta Parish, Farah Liyana Muhammad Khir, N. Radha Krishnan, Jianan Wang, Jonathan S. Krisjanto, Haoran Li, Gilberto A. Umana-Membreno, Stacia Keller, Umesh K. Mishra, Murray V. Baker, Brett D. Nener, Matthew Myers, Role of GaN cap layer for reference electrode free AlGaN/GaN-based pH sensors, Sens. Actuators, B 287 (2019) 250–257, https://doi.org/10.1016/j.snb.2019.02.039.
[189] Hyeong-Ho Park, Yumin Koh, Chu-Young Cho, Manjeet Kumar, Ju-Hyung Yun, Kyung-Ho Park, Improved Hydrogen Sensing Performance of AlGaN/GaN Based Gas Sensors with Controlled Surface Nanostructures of Platinum Nanoparticulate Films, j nanosci nanotechnol 20 (4) (2020) 2503–2507, https://doi.org/10.1166/jnn.2020.17200.
[190] H. Zhang,Yang K. Sheng ,The leakage mechanism of the package of the AlGaN/GaN liquid sensor, Materials, 13 (8) (2020) 1903, https://doi.org/10.3390/ma13081903.
[191] Saeed S. Ba Hashwan, Mohd Haris Bin Md Khir, Y. Al-Douri, Abdelaziz Yousif Ahmed, Recent Progress in the Development of Biosensors for Chemicals and Pesticides Detection, IEEE Access 8 (2020) 82514–82527, https://doi.org/10.1109/ACCESS.2020.2991380.
[192] K.H. Baik, S. Jang, Chu-Young Cho, Kyung-Ho Park, Fan Ren, S.J. Pearton, Soohwan Jang, AlGaN/GaN heterostructure based Pt nanonetwork Schottky diode with water-blocking layer, Sensors and Actuators B: Chemical 317 (2020) 128234, https://doi.org/10.1016/j.snb.2020.128234, 045010.
[193] F. Cozette, M. Lesecq, A. Cutivet, N. Defrance, M. Rousseau, H. Maher, J.C. D. Jaeger, Resistive nickel temperature sensor integrated into short-gate length AlGaN/GaN HEMT dedicated to RF applications, IEEE Electron Device Lett. 39 (10) (2018) 1560–1563, https://doi.org/10.1109/LED.2018.2864643.
[194] Robert Sokolovskij, Elina Iervolino, Changhui Zhao, Fei Wang, Hongyu Yu, Fabio Santagata, Pasqualina M. Sarro, Guo Zhang, Pt-AlGaN/GaN HEMT-sensor layout optimization for enhancement of hydrogen detection, 2017 IEEE sensors (2017) 1–3, https://doi.org/10.1109/ICSENS.2017.8234419.
[195] Kwang Hyeon Baik, Sunwoo Jung, Fan Ren, S.J. Pearton, Soohwan Jang, Moisture Insensitive PMMA Coated Pt-AlGaN/GaN Diode Hydrogen Sensor and Its Thermal Stability, ECS Journal of Solid State Science and Technology 7 (7) (2018) Q3009–Q3013, https://doi.org/10.1149/2.002107jss.
[196] X. Tan, Y.J. Lv, X.Y. Zhou, Y.G. Wang, X.B. Song, G.D. Gu, P.F. Ji, X.L. Yang, B. Shen, Z.H. Feng, S.J. Cai, AlGaN/GaN pressure sensor with a Wheatstone bridge structure, AIP Advances 8 (8) (2018) 85202, https://doi.org/10.1063/1.4996257.